DOKUZ EYLÜL UNIVERSITY
GRADUATE SCHOOL OF NATURAL AND APPLIED SCIENCES

COMPUTER AIDED DESIGN OF THERMAL SYSTEMS

by

Değer AKIN

November, 2007

İZMİR

COMPUTER AIDED DESIGN OF THERMAL SYSTEMS

A Thesis Submitted to the
Graduate School of Natural and Applied Sciences of
Dokuz Eylül University
In Partial Fulfillment of the Requirements for the Degree of Master of Science in Mechanical Engineering, Energy Program

by
Değer AKIN

November, 2007
İZMİR

M.Sc THESIS EXAMINATION RESULT FORM

We have read the thesis entitled **"COMPUTER AIDED DESIGN OF THERMAL SYSTEMS"** completed by **DEĞER AKIN** under supervision of **ASS. PROF. DR. DİLEK KUMLUTAŞ** and we certify that in our opinion it is fully adequate, in scope and in quality, as a thesis for the degree of Master of Science.

.....

Ass. Prof. Dr. Dilek KUMLUTAŞ

Supervisor

.....

(Jury Member)

.....

(Jury Member)

Prof. Dr. Cahit HELVACI
Director
Graduate School of Natural and Applied Sciences

ACKNOWLEDGEMENTS

First of all, I would like to thank my supervisor, Ass. Prof. Dr. Dilek KUMLUTAŞ, for her support and guidance throughout this thesis study.

I would like to thank Mechanical Engineering Department of Ege University for providing the opportunity of utilization from FLUENT.

I also wish to express my gratitude to my friends at Department of Mechanical Engineering for their endless patience, help and support.

Finally, I would like to thank my parents for their patience and unconditional support. Furthermore, I would like to thank my brother for encouraging and giving advices to feel myself better when I get hopeless.

Değer AKIN

COMPUTER AIDED DESIGN OF THERMAL SYSTEMS

ABSTRACT

In this thesis study, thermal output of a steel panel radiator, in accordance with TS EN442, was numerically specified with the usage of finite volume method. Three-dimensional analysis was implemented to the whole of the radiator by means of forced convection model. Results were compared with the experimental data obtained at CETIAT laboratories in France. Thermal outputs represented a good agreement with experimental data. In the content of this analysis, the effect of variation at ambient convective heat transfer coefficient on the thermal output was also investigated. Furthermore, modifications at convector design were performed to enhance the thermal output of the radiator. In this sense, eight convector designs were designed. Smallest repeated section of radiator (module) was used for computations rather than whole of the radiator. Thermal output was specified for the conditions: fix surface temperature at the inner surface of module and fluid flow existed inside the module. Remarkable thermal output enhancements were obtained for cascade convector design and convector design with three contact faces between panel and convector.

Keywords: radiator, computational fluids dynamic, finite volume method, thermal output, EN442

ISIL SİSTEMLERİN BİLGİSAYAR DESTEKLİ TASARIMI

ÖZ

Bu tez çalışmasında, TS EN442'ye uygun bir çelik panel radyatörun ısıl gücü sonlu hacimler yöntemi ile sayısal olarak belirlenmiştir. Üç boyutlu çözümleme, zorlanmış taşınım modeli yoluyla radyatörün tamamına uygulanmıştır. Sonuçlar, Fransa'daki CETIAT laboratuarlarında elde edilen deneysel veriler ile karşılaştırılmıştır. Isıl güçler, deneysel veriler ile uyumluluk göstermiştir. Bu çalışma kapsamında, ortam taşınım katsayısının değişiminin radyatörün ısıl gücüne olan etkisi de incelenmiştir. Ayrıca, radyatörün ısıl gücünü arttırmak amacıyla konvektor tasarımında modifikasyonlar gerçekleştirilmiştir. Bu bağlamda, sekiz adet konvektor tasarlanmıştır. Radyatörün tamamını modellemek yerine, radyatörün tekrar eden en küçük kısmı (modül) hesaplamalarda kullanılmıştır. Isıl güç, modülün iç yüzeyinde sabit sıcaklık olması ve modülün içinde akış olması durumları için belirlenmiştir. Kayda değer ısıl güç arttırımı, kademeli konvektor tasarımı ve panel ile konvektör arasında üç temas yüzeyi kullanan konvektor tasarımında elde edilmiştir.

Anahtar sözcükler: radyatör, hesaplamalı akışkanlar dinamiği, sonlu hacim yöntemi, ısıl güç, EN442

CONTENTS

Page

M.Sc THESIS EXAMINATION RESULT FORM ii
ACKNOWLEDGEMENTS iii
ABSTRACT iv
ÖZ v

CHAPTER ONE – INTRODUCTION 1
1.1 Panel Radiators 1
1.2 Classification of Panel Radiators 7
1.3 Radiator Standards 8

CHAPTER TWO – EXPERIMENTAL FACILITY 11
2.1 TS EN442-2: Test Methods and Rating 11
2.2 Selection of Heating Appliance for Determining Thermal Output of a Type .. 12
2.3 Experimental System 13
2.3.1 Reference Experimental Facility 13
2.3.2 Sample Radiators 15
2.4 Experimental Methods 17
2.4.1 Weight Method 17
2.4.2 Electrical Method 19
2.5 Standard Thermal Output 20
2.5.1 Air Pressure Correction 20
2.5.2 Characteristic Equation 21
2.6 Test Report of Type 22/600 Radiator 22

CHAPTER THREE – NUMERICAL METHODS 25
3.1 Computational Fluid Dynamics 25
3.1.1 Working Procedure of CFD Code 25
3.2 Governing Equations of Fluid Flow and Heat Transfer 28
3.2.1 Equation of State 30
3.2.2 General Transport Equations 31

3.2.3 Differential and Integral Forms of General Transport Equations 32
3.3 Finite Volume Method for Diffusion 34
3.3.1 One-Dimensional Steady State Diffusion 34
3.3.2 General Form of Discretised Equations for Steady State Diffusion 38
3.4 Finite Volume Method for Convection and Diffusion 39
3.4.1 Steady One-Dimensional Convection and Diffusion 40
3.4.2 Properties of Discretisation Schemes 42
3.4.3 Central Differencing Scheme for Convection and Diffusion 44
3.4.4 Upwind Differencing Scheme for Convection and Diffusion 45
3.5 Solution Algorithms for Pressure-Velocity Coupling in Steady Flows 49
3.5.1 The Staggered Grid 51
3.5.2 The Momentum Equation 54
3.5.3 The "SIMPLE" Algorithm 58
3.5.4 The "SIMPLEC" Algorithm 64

CHAPTER FOUR – NUMERICAL STUDY 65
4.1 Steel Panel Radiator 65
4.1.1 Pre-processing 67
4.1.2 Processing 69
4.2 Convector Designs 71
4.2.1 Pre-processing 75
4.2.2 Processing 79

CHAPTER FIVE – NUMERICAL RESULTS 81
5.1 Effects of Variation at Ambient Convective Heat Transfer Coefficient 81
5.2 Evaluation of Experimental Data with Numerical Data 89
5.3 Evaluation of Thermal Output with New Convector Designs 97
5.3.1 Fix Temperature at Inner Surfaces of Modules 97
5.3.2 Fluid Flow Inside The Modules 101

CHAPTER SIX - CONCLUSION 106

REFERENCES 109

CHAPTER ONE
INTRODUCTION

1.1 Panel Radiators

Panel radiators are the most favored radiator type in Turkey and Europe on account of their compact and stylish design, high thermal output and low water capacity. Though the term "radiator" reminds radiation, most of the thermal output is come true by natural convection (Beck et al., 2004). Generally, steel panel radiators use convection fins (convectors) in order to improve their heat output. Panels are formed by welding two panel leaves symmetrically in order to form a space for water passings through the radiator. Hot water passing through the radiator makes the radiator hotter than air surrounding it. By this way, an amount of heat is transferred to the air from water by means of radiator and this yields water to exist at a lower temperature from the radiator.

Cast iron radiators had been used before panel radiators. Although heat transfer surface area of cast iron radiators are more than steel panel radiators, they are so heavy, expensive, occupy more place and hard to repair. For these reasons, steel and aluminum radiators have superseded cast iron radiators. At the same output rates, they are smaller, lighter and have lower water capacity so they have a faster response than cast iron radiators. Die-cast aluminum radiators are an alternative to steel panel radiators for being lighter and requiring less water. The disadvantage of steel panel radiators is low corrosion resistance according to aluminum radiators. By means of water treatment, this could be overcome (Beck et al., 2001).

The construction of a panel radiator that uses convectors to increase thermal output is shown in Figure 1.1. Generally, a panel radiator is formed by joining two panels with T-Fittings and placing a convector or convectors to the gap between panels depending on heat demand. In addition to these components; left side, right side and top covers are used except for panel radiators that are formed by only a panel or a panel and convector.

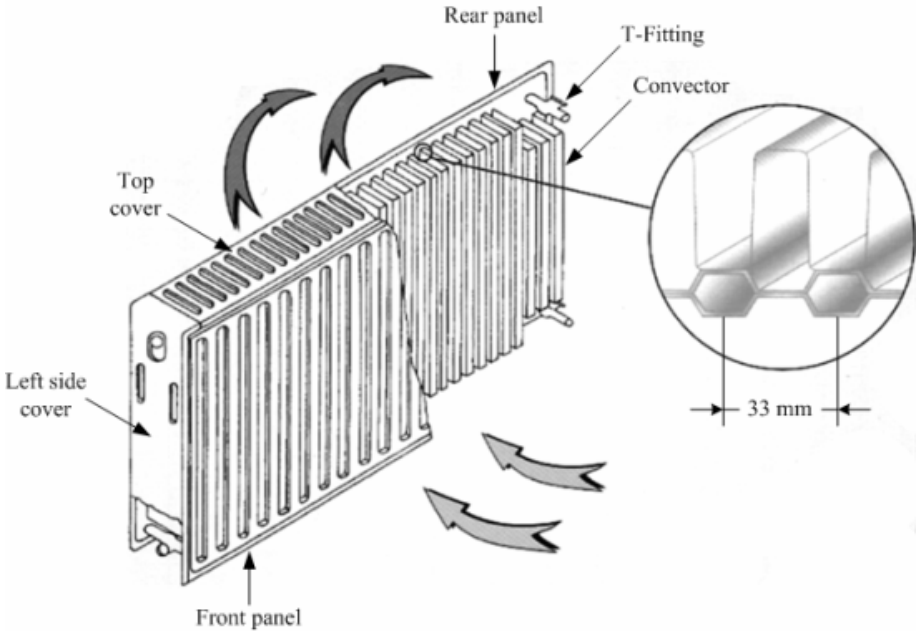


Figure 1.1 Construction of steel panel radiator

The amount of heat transfer from the radiator depends on the water temperature, size and the design of the radiator. Several studies and designs were made to enhance the heat capacity of the radiator and convector. Gregory (1986) made a research to acquaint contractors with deciding whether or not specify aluminum radiators rather than steel radiators. The constructional differences between die cast aluminum radiator and aluminum radiators were presented in his study. For the same heat output rate, aluminum radiators were found to be more expensive (30% - 100%) than conventional steel radiators. But they provided %30 to 300% more heat output per unit frontal area and were more lightweight than steel radiators. Probert et al. (1989) installed a suitably designed horizontal shelf between the radiator and the window against the usage of double glazing to reduce the heat losses from the window. By this way, the heat loss from the window was decreased at a rate of %14.

Chen (1990) determined the energy consumption of an office room with three different heating systems; a ceiling radiant heating system, radiator heating system and warm air heating system by using airflow program PHOENICS-84. Radiator heating system supplied the best comfortable environment in comparison to other systems. Energy consumption rate of radiant heating system was %17 more than the

energy consumption rates of radiator heating and warm air heating systems that were nearly the same except energy used for the ventilators.

Grétarsson et al. (1991) prepared a program by means of Turbo Pascal to present return temperature and thermal output of the radiator against the variation of mass flow rates according to design conditions. The study was concentrated on two design conditions: 90/70 standard design of Denmark (fossil fuel) and 80/40 design used in Iceland (geothermal). Results of 90/70 system were compared with experimental data. By means of results for 80/40 system, the accuracy of German standard DIN 4703 was evaluated for Icelandic geothermal district heating. Ward (1991) investigated the thermal output of the domestic radiators at the conditions of low mass flow rate or higher temperature differences along the radiator. The study also came out the problems that occurred at mass flow rates less than 20% of design conditions.

Harris (1995) made experiments to measure the effect of metal foils behind radiators on heat losses. Installing foil behind a radiator made a reduction of up to 6% in the overall energy consumption of the room and heat loss through the wall fell to less than 30%. Lu et al. (1997) investigated the airflow and temperature field in a heated room by using a CFD simulation. The study includes the usage of CFD code, CFDS-FLOW3D to predict three dimensional airflow field and temperature distribution in a full-scale enclosure with a radiator. The predicted airflow pattern and temperature field were validated with the measured data carried out by Lebrun and Marret (1976).

Inard et al. (1998) carried out a model to investigate the thermal behavior of dwelling cells and evaluate the performance of two types of heat source that were localized (a hot water radiator and electrical convector) and distributed (a hot water heated floor and electrical heated ceiling). According to the criteria of energy consumption and thermal comfort, distributed heat sources were showed a slightly advantage over the localized sources because of distributed system not having a thermal coupling between the heat source and the heat losing walls.

Beck et al. (2001) researched the effect of the wall emissivity behind the radiator on heat output of radiator. The effects were investigated both numerically and experimentally. The presence of high emissivity wall behind the radiator led 20% increase at heat output than reflective material. Compared heat outputs were computed by considering the gap between the radiator and wall. By means of an extrapolation, results would be applicable to a normal radiator so the output of single bank and double bank radiators were respectively increased by 10% and 5%. The data obtained from the experimental study was used as boundary conditions for CFD program in order to represent fluid flow and thermal flow process at the gap.

Wallentén (2001) measured the convective heat transfer coefficient at an outer ambient wall with window exposed to natural climate to provide data for building simulation programs. Three different experiments were made to specify convective heat transfer coefficients: radiator at the back wall and no ventilation, radiator at the back wall and ventilation from window at 0.1 ach (air circulation per hour), radiator below window and ventilation from window at 0.6 ach in case of room furnished.

Beck et al. (2004) computed the total heat transfer from a radiator by using high emissivity sheets placed in the gap between two flat panel radiators. These sheets should heat up by radiation and then transfer this heat to the air. The novel design was using sheets against fins. With the usage of two sheets, the thermal out put of the novel design was ranged from 71% to 88% of a finned double radiator depending on the fouling occurred during experiments. The novel design is easier to be cleaned and cheaper to manufacture according to a finned double radiator.

Zhai et al. (2005) utilized the integration of building energy simulation (ES) and computational fluid dynamics (CFD) programs to provide more accurate prediction of building energy use and indoor environment due to complementary information provided by the two programs. The results of coupled program were compared with four sets of experimental data from literature. Validations of coupled program consisted of natural convection in a room without a radiator, with a radiator, convective heat transfer coefficients in a room with a radiator and mixed convection

in a glazed atrium. Witry et al. (2005) used the CFD code FLUENT to investigate the thermal performance of an automotive aluminum plate radiator manufactured by aluminum roll-bonding technique. The addition of some form of airside turbulators should immensely improve heat transfer level. Arslantürk (2006) investigated the heat pipe/fin space radiators having fins temperature-dependent thermal conductivity. The non-linear fin equation was solved by using Adomian decomposition method that provides an infinite series converging very rapidly. The efficiency of fin was expressed in terms of thermo geometric fin parameter for making optimization calculations easily.

Arslantürk et al. (2006) evaluated the optimum dimensions of a central heating radiator by means of an approximate analytical model. Optimization procedure was formed with the utilization of radiator's volume fraction (ratio of radiator cross-section area to area occupied by the radiator) depending on tube radius. The temperature distribution within the fins and the tube wall was represented in order to show analytically obtained temperature values of a given thermal and geometrical parameters. Heat transfer rates were investigated for the fix volume fraction against the variation at mass flow rate of inner fluid velocity. The effects of inner fluid temperature and the room temperature on optimum dimensions and maximum heat transfer rate were investigated for a given radiator volume.

Oliet et al. (2007) performed a set of parametric studies on automotive radiators by means of CHESS (Compact Heat Exchanger Simulation Software) developed by the authors. The influence of air and liquid side conditions (mass flow, inlet temperatures and selected coolant fluid) on overall performance was investigated. In addition to these parameters, the influences of some geometrical parameters (fin spacing, louver angle, coolant flow lay-out) on overall performance were also analyzed. The overall behavior of an automobile radiator working at usual range of operating conditions was represented by means of parametric studies in a detailed way.

In this study, thermal output of a type-22 (panel-convector-convector-panel) steel panel radiator was specified with the usage of CFD code FLUENT. The radiator was manufactured in accordance with TS EN442. Entire of the radiator was modeled to compare results with experimental data. Compared data were obtained at an experimental facility in France. Thermal output was specified for three different excess temperatures (difference between mean water temperature in the radiator and ambient air temperature). Thermal output at 60°C excess temperature (design condition) represented a good agreement with the experimental data. 2% discrepancy was occurred between numerical and experimental data.

Thermal output of the radiator was tried to be enhanced by changing convector design. In this sense, eight convectors were created by changing form of cross-section area, using pops at surfaces and increasing number of contact faces between panel and convector. Instead of modeling entire radiator, modules (smallest repeated section of the radiator) were used for computations. Depending on the boundary conditions, this study consisted of two different analyses: fix temperature at the inner surface of module and fluid flow existed in the module. Six modules were used for fix surface temperature analysis. One of them was the module with original convector design to compare thermal outputs. Maximum increase at thermal output was gained for the module with cascade convector design. In spite of 30% increase at the heat transfer surface area, the increase at the thermal output was specified as 11%. Five modules were used for the analysis fluid flow existed in the module. Two of them were the modules with original and cascade convector design. Maximum increase at thermal output was gained for the module with three contact faces. In spite of 75% increase at the heat transfer surface area, the increase at the thermal output was specified as 35%. Cascade convector system used in the content of this analysis represented 9% increase at thermal output rather than 11% increase obtained in the event of fix temperature at the inner surface of the module.

1.2 Classification of Panel Radiators

Radiators are classified depending on the number of panels and convectors used to form the radiator. In this sense, two digits are used to specify the type of the radiator. The first digit refers to number of panel and the second one refers to number of convectors. Panels and convectors are respectively abbreviated as "P" and "C".

- P (one panel and no convector) Type-10
- PC (one panel and one convector) Type-11
- PP (two panels and no convector) Type-20
- PCP (two panels and one convector) Type-21
- PCCP (two panels and two convectors) Type-22
- PCCPCP (three panels and three convectors) Type-33

Any kind of a radiator is named by specifying its panel-convector arrangement, type, height and length. Radiator types are shown in Figure 1.2

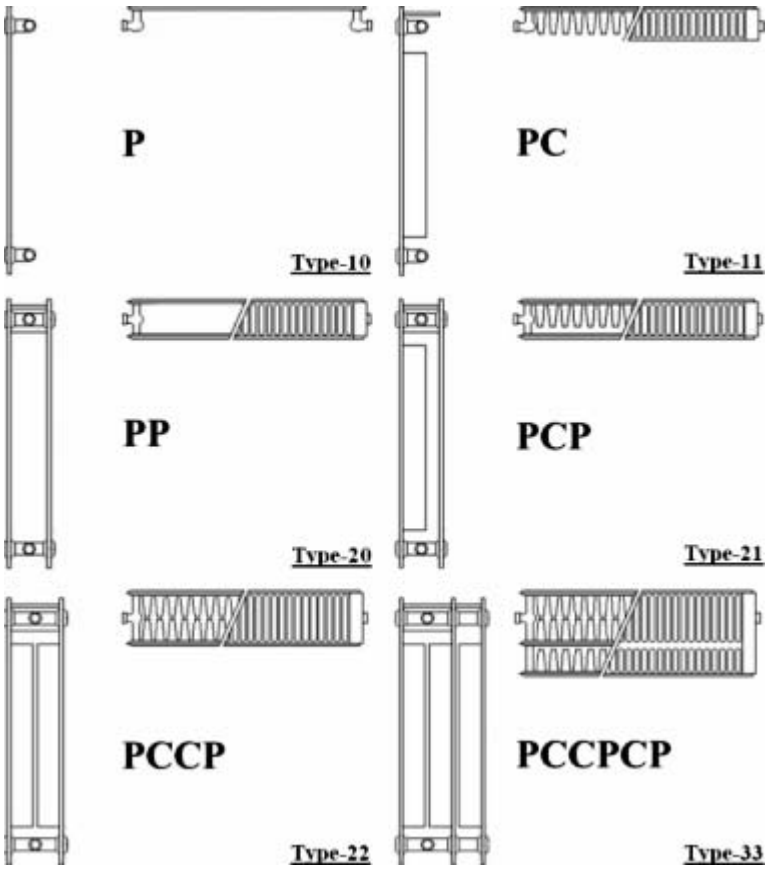


Figure 1.2 Types of radiator arrangements

1.3 Radiator Standards

In central heating systems, the proper radiator type is chosen from catalogs after the computation of the heat losses from volumes. Heat capacity values in catalogs are determined with the method reported in TS EN442-2. Before EN442, TS6554 in Turkey, BS3528 in England and DIN4703 in German had been used for this computation.

By means of an initial French request, a Technical Committee consisted of representatives from the 18 National Standards bodies, test institutes and user associations was established to draft a new European Standard. Such a Standard has to comply with an agreed framework, taking into account such topics as safety in use, marketing and labeling, manufacturing quality and performance rating (Radiator standard BSEN442, n.d.).

Heat output performance is obviously the main requirement for radiators but there are several other important aspects covered by the new standard that were either not covered by previous standards or are now covered with greater precision (Radiator standard BSEN442, n.d.):

- Minimum material thickness for all wet surfaces
- A detailed table of manufacturing tolerances
- Periodic burst pressure tests to supplement the 100% leak pressure tests
- Pre-treatment and paint quality requirements for corrosion protection and resistance to impact damage
- Requirements for product marking, labeling and catalogue data

It is in the area of heat output performance. However, the new standard will have the greatest immediate impact. 1997 outputs reduced by 11% because the test methods, accuracy of testing and design of the new test rooms were changed from the previous BS 3528 test criteria (Radiator standard BSEN442, n.d.). The Technical Committee drew up a very tight specification for a new standardized test room,

which coupled with changes to test methods and rating procedures, resulted in remarkable accurate and consistent results. There are currently four such test rooms, at BSRIA in Bracknell England, at Lyon, Stuttgart and Milan. These have reported repeatable results with an accuracy of ±1%. Radiators are tested at a lower temperature difference than old national standards. The comparison between BS 3528 and BS EN442 is listed in Table 1.1.

Table 1.1 Comparison between BS 3528 and BS EN442

Standard	Inlet Water Temp. (°C)	Outlet Water Temp. (°C)	Mean Water Temp. (°C)	Air Temp. (°C)	Excess Temp. (ΔT) (°C)
BS 3528	90	70	80	20	60
BS EN 442	75	65	70	20	50

This excess temperature (ΔT), the difference between the mean water temperature in the radiator and ambient air temperature in the test chambers, was previously 60°C, now it is 50°C. While this may not sound significant, outputs at excess temperature of 50°C is over 20% lower than at excess temperature of 60°C (Radiator standard BSEN442, n.d.). Other changes included testing with Top Bottom Same End (TBSE) connections rather than the old, Top Bottom Opposite End (TBOE). Connections are shown in Figure 1.3. The new design of test room, particularly the elimination of water-cooling to the rear wall of the test booth itself, resulted in outputs. They are lower and regardless of the used excess temperature (ΔT).

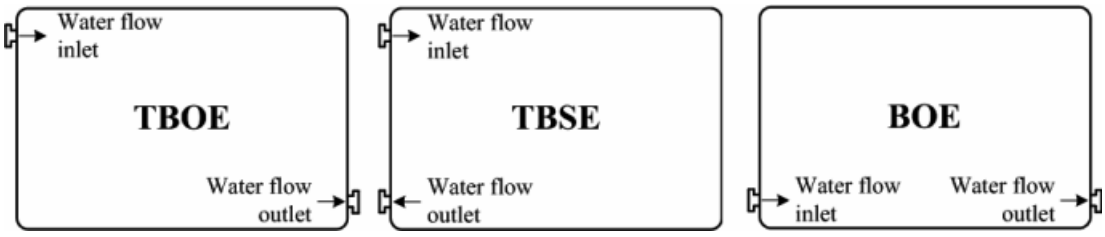


Figure 1.3 Radiator connections

Other standards related with radiator are; EN573-3 "Wrought aluminum alloys-Chemical composition and forms of products Part 3: Chemical composition", EN10310 "Cold rolled low carbon steel flat products for cold forming: Technical

delivery conditions", EN10130 "Cold rolled uncoated low carbon and high yield strength steel flat products for cold forming on dimensions shape" related with TS3519, EN45001 "General criteria for the operation of testing laboratories" related with TS EN 45001, ISO31-4 1978 "Quantities and units-part: Heat" related with TS 297, ISO185 "Grey cast iron-Classification" related with TS204 and ISO2409 1992 (EN ISO2409) "Paints and varnishes cross – cut test" related with TS4313.

CHAPTER TWO
EXPERIMENTAL FACILITY

2.1 TS EN442-2: Test Methods and Rating

TS EN442 (radiators and convectors) standard was accepted to publish by TSE Technical Committee in 1998. It is based on EN442 which was already accepted by CEN (European Committee for Standardization) in 1996. TS EN442 consists of these parts:

- TS EN442-1: Technical specifications and requirements
- TS EN442-2: Test methods and rating
- TS EN442-3: Evaluation of conformity

TS EN442-1 defines the technical specifications and requirements of radiators and convectors to be installed in central heating systems in residential buildings.

TS EN442-2 defines procedures for determining the standard thermal output of the heating appliances fed with water or steam at temperatures below 120°C, supplied by a remote heat source. This standard specifies criteria for arrangements of laboratory and suitable experimental methods, acceptable tolerances and models that are used at initial experiments and are going to be used for confirmation of conformity of general production. TS EN442-2 also defines additional information that is necessary to be assured by manufacturer company in order to guarantee that end product is suitably used along its purpose in an appositely way. This standard is not applied to independent heating appliances.

TS EN442-3 specifies the procedures for evaluating the conformity of radiators/convectors according to EN442-1. It specifies the procedures and methods for the initial evaluation and the controls required to maintain conformity.

2.2 Selection of Heating Appliance for Determining Thermal Output of a Type

According to TS EN442-2, heating appliances must be grouped as families and types. A family can be divided into specific number of distinct types for the purpose of determination of thermal output at technical documents. For a type that includes 300 mm and further height models, the numbers of test models are listed in Table 2.1:

Table 2.1 Minimum number of models going to be tested

Height Range (H_r) (m)	Height Number
≤ 1	3
1 >	4

Models must be 1m long or at length nearest to 1m. For sliced radiators, slice number must be 10 and minimum length must be 0.6m. In case of $H_r \leq 1$, test models must be at maximum and minimum value of height range and nearest to intermediate height (H_{int}) that is given below:

$$H_{\text{int}} = H_{\max} - \frac{1}{2} H_r \tag{2.1}$$

H_{max} is the maximum height of the type. In case of 1m < H_r < 2.5m, test models must be must be at maximum and minimum height of height range and nearest to lengths given below:

$$H_{\text{int}1} = H_{\max} - \frac{1}{3} H_r \quad \text{and} \quad H_{\text{int}2} = H_{\max} - \frac{2}{3} H_r \tag{2.2}$$

If height of the type includes heights less than 300mm, the minimum height less than 300mm must be tested in addition to given heights above. In case of all heights of a type are less than 300mm, models at maximum and minimum heights must be tested.

2.3 Experimental System

According to TS EN442-2, experimental system must include:

- An experimental facility
- Three pieces of sample radiator set

According to TS EN442-2, experimental facility is classified as reference and approved.

2.3.1 Reference Experimental Facility

Reference experimental facility comprises:

- A room suitable for experiments inside which heating appliance going to be tested is assembled, is independent from outer ambient, is surrounded with water cooled surfaces to sustain special heating conditions, is closed and is not ventilated.
- Equipments necessary for circulation of cooling water inside the walls of closed room.
- Primer heating circuit feeding to the test equipment according to the experimental method.
- Measuring and control equipments.

Dimensions of test room are:

Length : 4±0.02m
Width : 4±0.02m
Height : 3±0.02m

Test room must be constructed with water-cooled sandwich panels as shown in Figure 2.1. Inner surfaces of the test room must be smooth and made of flat steel sheet. Sandwich panels must be formed as specified below:

- Water cooled steel panel
- Steel panels and exterior steel sheets between which insulation foam is injected in order to form a construction that prop up itself
- Exterior sheet with 0.6mm sheet thickness

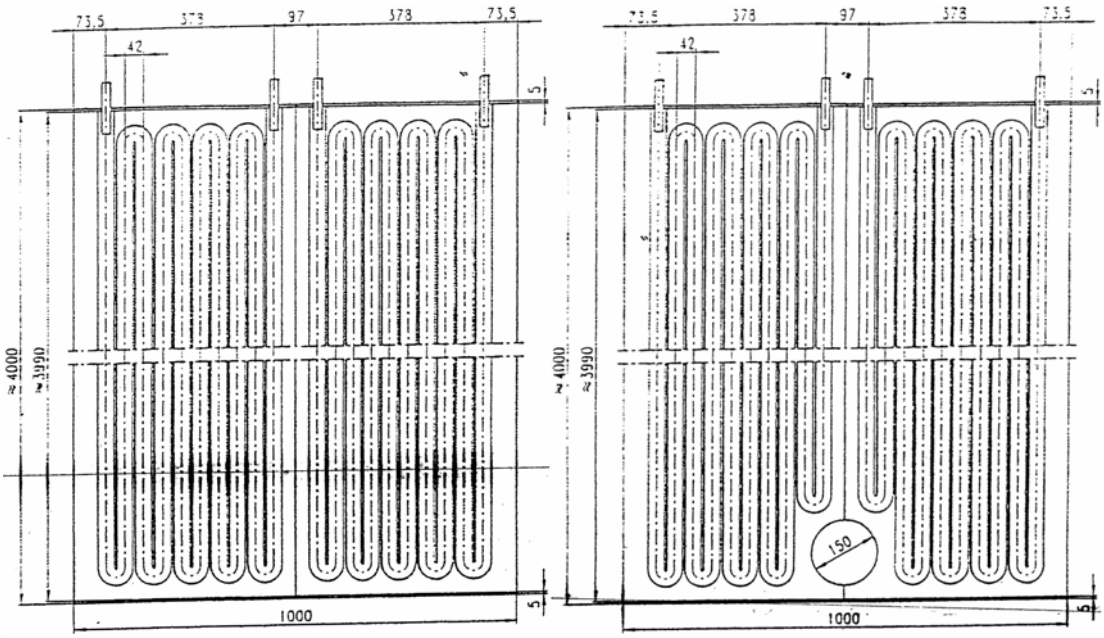


Figure 2.1 Water-cooled sandwich panel and panel with hole for exterior connections

Water-cooled panels are formed by welding two steel sheets as shown in Figure 2.2. The properties of steel sheets are:

- Steel sheet with 2mm sheet thickness
- Steel sheet with 1mm sheet thickness and in form of undulation to form water passing duct (width cross-section area of 150mm^2)

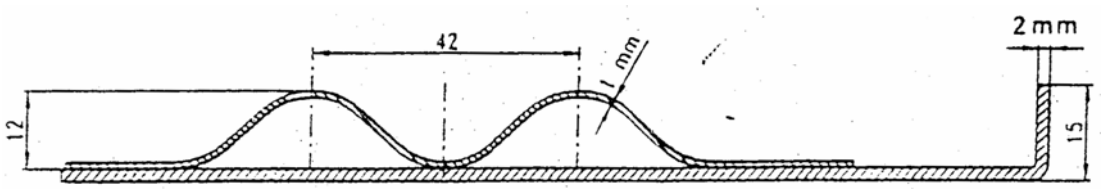


Figure 2.2 Width cross-section view of water-cooled panel

The thickness of insulation foam must be 80mm. Minimum total thermal resistance of each wall, floor and ceiling must be 2.5m^2K/W. The wall behind the test model must be made of same sandwich panel but its connection to the cooling system must be demounted (no water circulation in panels). Interior faces of the test room must be painted with a dull color which has minimum radiation emissivity of 0.9. During experiments, average temperature of the cooled interior faces must be suitable for steady state condition and reference air temperature must be adjusted to 20±0.5°C. Average temperature of interior face is the average of the inlet and outlet water temperatures for related face.

Temperatures in the test room must be measured to specify reference room temperature and observe the thermal condition of experimental facility. Temperature measurements performed along the vertical axis of test room are:

- At reference air temperature point: 0.75m above from the floor
- Additional points: 0.05m above from the floor
  1.50m above from the floor
  0.05m below from the ceiling

Temperature measurements are also performed 0.5m above from floor on interior faces. Surface temperatures, except for wall behind the heating appliance, must be in tolerance of ±0.3K.

2.3.2 Sample Radiators

Functions of sample radiators:

- confirm that test data of experimental facility can be re-obtained according to adjusted tolerances in accordance with TS EN442-2
- confirm that reference and approved experimental facilities are giving results according to adjusted tolerances in accordance with TS EN442-2

- form a general basis for each experimental facility in order to confirm the repeatability of test data according to adjusted tolerances in accordance with TS EN442-2

Only a sample radiator set is manufactured for experimental facility constructed according to TS EN442-2 in order to confirm reproducibility of experimental facility. This set is sent to all of the reference experimental facilities in accordance with TS EN442-2 in order to specify "$Ø_o$" (reference value of a sample radiator) and "$Ø_M$" (reference value of a sample radiator to evaluate equivalency of a reference experimental facility). This single sample radiator set is named as "primer set". All laboratories equipped with approved sample radiators. This set is named as "secondary set" and used for confirmation of repeatability at experimental facility. Secondary set of reference experimental facility is used to confirm the reproducibility of approved experimental facility.

The confirmation of experimental facilities is based on two criteria: Sensibility and Equivalency. Sensibility of reference experimental facility is specified by means of its secondary set. By this way, "S_o" repeatability tolerance of experimental facility is specified. The results of 10 experiments that are arbitrary performed must show 1% discrepancy according to "S_o" repeatability tolerance. Equivalency of reference experimental facility must be confirmed by means of its primer sample radiator set. Experimental results of each sample radiator must be in ±1% tolerance of "$Ø_M$". Confirmation process of approved experimental facilities is performed by reference experimental facilities on the condition that approved experimental facilities are not only used for designs in accordance with TS EN442-2. Thermal output of the other designs can be computed in approved experimental facilities. Sensibility of approved experimental facility is specified by means of its secondary sample radiator set as done in reference experimental facility. Equivalency of approved experimental facility must be confirmed by the usage of the secondary sample radiator set of a reference experimental facility. "$Ø_o$" reference value from approved experimental facility must be ±1% of sensibility tolerance of each sample radiator that is tested in a confirmed reference experimental facility.

2.4 Experimental Methods

Heating appliance that is going to be tested must be assembled according to conditions that are given below:

- Heating appliance must be placed parallel to the back wall and symmetric to the vertical axis of the back wall.
- The gap between nearest thermal diffusion surface of heating appliance and back wall must be 0.05±0.002m
- The gap between bottom of the heating appliance and floor must be 0.11±0.005m
- Absence of air accumulations that cause air tampons at connection pipes of the primer flow circuit must be provided.

Thermal output of the heating appliance can be specified in two ways:

- *Weight Method*: by measuring water flow rate passing through heating appliance and specifying enthalpy differences at inlet and return connections
- *Electrical Method*: by measuring energy input rate to water circuit.

2.4.1 Weight Method

Thermal output of the heating appliance is computed by means of measuring water flow rate passing through heating appliance and enthalpy measurements at the inlet and return connections to specify enthalpy difference.

Experimental arrangement for weight method is shown in Figure 2.3. Great amount of water circulated through electrical heater (3) and mixing valve (4) is pumped to the overflowing mouth (5) by means of circulation pump. Water coming from the overflowing mouth (5) passes through test radiator (7) and then water flows to the measuring case (14). In order to specify water flow rate, water at the measurement case (14) is used.

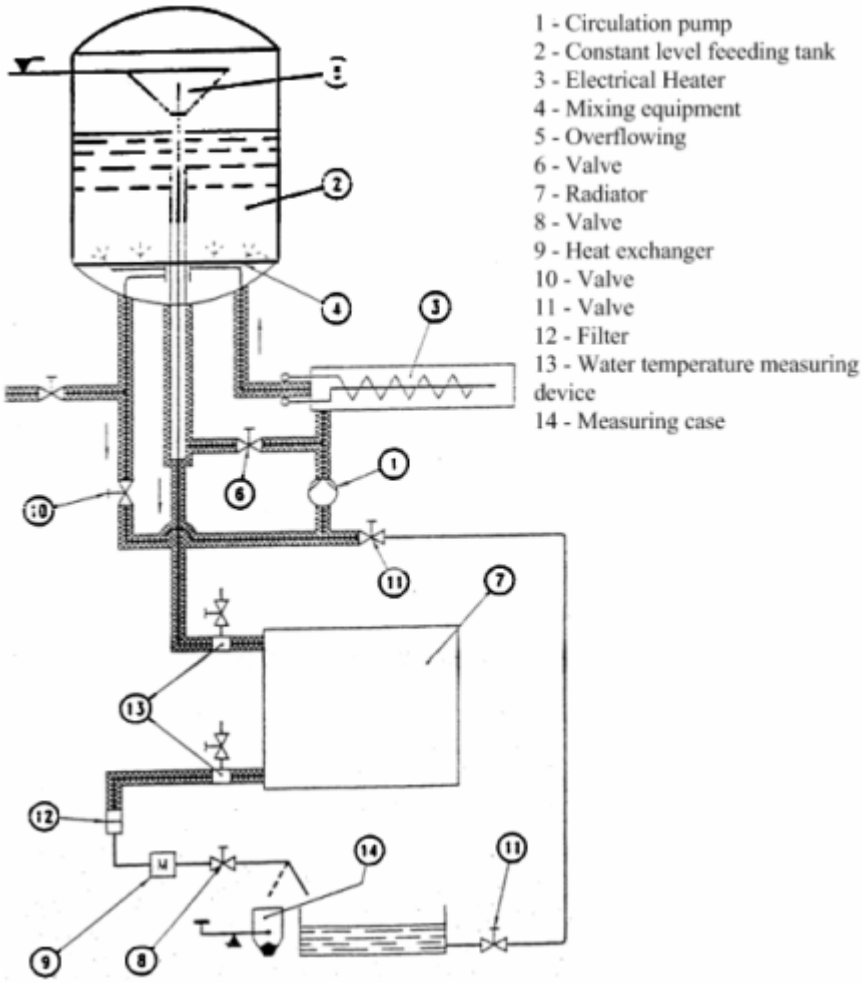


Figure 2.3 Experimental arrangement of weight method

Thermal output ($Ø_{me}$) is computed by means of water flow rate (q_m), measured t_1 and t_2 temperatures. These measured temperatures are used to compute specific enthalpies.

$$\phi_{me} = q_m(h_1 - h_2) \tag{2.3}$$

Water flow rate is computed by means of collected water at measuring case (m) and total time (τ) that is the passing time during collection of water in the measuring case.

$$q_m = \frac{m}{\tau} \tag{2.4}$$

2.4.2 Electrical Method

Thermal output of the heating appliance is computed by measuring energy input rate to water circuit. Experimental arrangement of electrical method is shown in Figure 2.4. Water is pumped to the test radiator (4) after passed through an electrical heating case (1). Energy input rate to the water circuit is specified by subtracting heat losses ($Ø_v$) that are occurred at electrical heating case (1) and pipes from electrical power supplied to electrical heating case (1) with considering the pump (9) power. Heat loss at the observed temperature differences is specified by means of a short-circuit experiment (usage of an insulated pipe, of which thermal lost is known, instead of radiator). Temperature measuring points (5) are directly placed inlet and outlet connections of electrical heating case (1) in order to measure the thermal loss at electrical heating case (1).

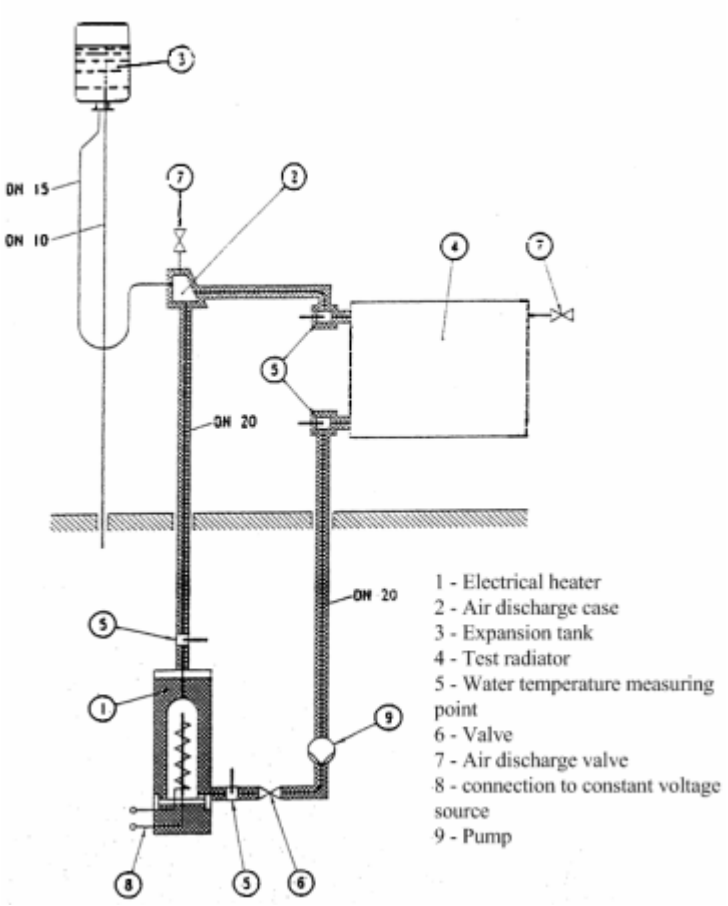


Figure 2.4 Experimental arrangement of electrical method

Thermal output ($Ø_{me}$) is equal to the difference between electrical power used for heater (P_{el}) and heat losses ($Ø_v$) at heater and pipes.

$$\phi_{me} = P_{el} - \phi_v \tag{2.5}$$

Water flow rate is obtained by means of thermal output ($Ø_{me}$) and the difference between specific enthalpies.

$$q_m = \frac{\phi_{me}}{(h_1 - h_2)} \tag{2.6}$$

2.5 Standard Thermal Output

Standard thermal output is computed from the characteristic equation of the appliance. Features of standard thermal output:

- Standard thermal output must represent the real thermal output of the appliance.
- Equivalency must be in accordance with TS EN442 at the same time considering the measurement techniques.
- Standard thermal output must represent obtainable thermal output of a sample that is taken from production line against same experimental conditions.

2.5.1 Air Pressure Correction

Depending on the discrepancy at the air pressure in the test room according to atmospheric air pressure (101.3 kPa), pressure correction is applied to the measured thermal output ($Ø_{me}$) of the heating appliance in order to obtain standard thermal output of heating appliance:

$$\phi = \phi_{me}\left[S_k + (1 - S_k) f_p\right] \tag{2.7}$$

Correction factor (f_p) is computed as,

$$f_p = \left(\frac{P_0}{p} \right)^{n_p} \tag{2.8}$$

(p) is the barometric pressure measured during experiment. (n_p) and (S_k) are taken from Table 4 of TS EN442-2.

2.5.2 Characteristic Equation

Characteristic equation is specified with constant water flow rate and excess temperatures (ΔT) at least three points. These excess temperatures (ΔT) are: 30±2.5K, 50±2.5K, 60±2.5K.

In the course of specifying characteristic equation, reference air temperature should not change more than 1K from one measurement to another. In the course of experiment, water flow rate must not make deviation more than ±0.5%. Standard characteristic equation obtained from the test of a model is,

$$\phi = K_M . \Delta T^n \tag{2.9}$$

where "K_M" is the model constant. Logarithmic model of characteristic equation is used to obtain "K_M" and "n". By means of least squares method, "log K_M" and "n" are:

$$log\, K_M = \frac{\sum (log\, \phi) . \sum \left[(log\, \Delta T)^2 \right] - \sum (log\, \Delta T - log\, \phi) . \sum (log\, \Delta T)}{N \sum \left[(log\, \Delta T)^2 \right] - \left(\sum log\, \Delta T \right)^2} \tag{2.10}$$

$$n = \frac{N \sum \left[(log\, \Delta T .\ log\, \phi) \right] - \sum (log\, \Delta T) . \sum (log\, \phi)}{N \sum \left[(log\, \Delta T)^2 \right] - \left(\sum log\, \Delta T \right)^2} \tag{2.11}$$

where N = number of test point

2.6 Test Report of Type 22/600 Radiator

Rapport d'essai / Prüfbericht /Test report N° 2005-001
Donneur d'ordres / Applicant / Antragsteller : ELBA

CETIAT

26/01/2005

6. VALEURS MESUREES ET RESULTATS
MEASURED VALUES AND RESULTS
MESSGRÖSSEN UND ERGEBNISSE

	Symbole Symbol Symbol	Unité Unit Einheit	Point de mesure Measuring Mebpunkt 1	2	3
Débit d'eau Water flow rate Wasserstrom	q_m	kg/h	146.7	146.6	146.7
Température d'entrée d'eau Inlet water temperature Vorlauftemperatur	t_1	°C	75.0	86.3	52.6
Enthalpie d'entrée d'eau Inlet water enthalpy Enthalpie im Vorlauf	h_1	KJ/kg	314.0	361.4	220.4
Température de sortie d'eau Outlet water temperature Rücklauftemperatur	t_2	°C	65.0	73.7	47.5
Enthalpie de sortie d'eau Outlet water enthalpy Enthalpie im Rücklauf	h_2	KJ/kg	272.3	308.5	198.9
Chute de température Temperature drop Temperaturunterschied	t_1-t_2	K	10.0	12.6	5.1
Différence d'enthalpie Enthalpy difference Enthalpiedifferenz	Δh	KJ/kg	41.7	52.9	21.5
Température de référence de l'air Reference air temperature Bezugs-Lufttemperatur	t_r	°C	20.0	20.1	19.9
Température moyenne d'eau Mean water temperature Mittlere Wassertemperatur	t_m	°C	70.0	80.0	50.1
Différence de température eau-air Excess temperature (tm-tr) Übertemperatur	ΔT	K	50.0	59.9	30.1
Puissance thermique (mesurée) Thermal output (measured) Wärmeleistung (gemessen)	Φ_{me}	W	1699.4	2156.0	876.3
Pression atmosphérique Air pressure Luftdruck	p	kPa	100.6	100.6	100.6
Puissance thermique ramené à la pression atmosphérique normale de 101.325 kPa Thermal output corrected for barometric pressure influence Wärmeleistung mit Luftdruck-Korrektur	Φ	W	1705.8	2164.0	879.5

Figure 2.5 Measured values and results from test report of type 22/600 radiator

Rapport d'essai / Prüfbericht /Test report N° 2005-001
Donneur d'ordres / Applicant / Antragsteller : ELBA

CETIAT

26/01/2005

La correction des puissances thermiques due à la pression de l'air a été effectuée selon 6.4.4.4 en applicant les valeurs suivantes :

The correction of thermal output values due to the airpressure has been done according to 6.4.4.4 using the following values :

Die Luftdruck-Korrektur der Wärmeleistungen nach 6.4.4.4 wurde unter Anwendung folgender Werte durchgeführt :

S_k	0.20	n_p	0.70

7. RESULTATS / RESULTS / ERGEBNISSE :

$$\Phi = K_m \cdot \Delta T^n$$

Equation caractéristique du modèle essayé
(la valeur K_m et l'exposant n sont déterminés par régression selon l'Annexe C de EN 442-2)

Characteristic equation of the tested model
(the value K_m and the exponent n shall established by regression according to Annex C of EN 442-2)

Kennlinien des Prüflings
(der Wert K_m und der Exponent n sind durch Regressionsrechnung nach Anhang C von EN 442-2 zu ermitteln)

$$\Phi = 10.1350 \cdot \Delta T^{1.3105}$$

Puissance thermique nominale Φs en W pour ΔT = 50 K
Standard thermal output Φs in W for ΔT = 50 K
Norm-Wärmeleistung Φs in W für ΔT = 50 K

$$\Phi_s = 1707 \text{ W}$$

Figure 2.6 Characteristic equation, standard thermal output and pressure correction components from test report of type 22/600 radiator

Rapport d'essai / Prüfbericht /Test report N° 2005-001
Donneur d'ordres / Applicant / Antragsteller : ELBA `

CETIAT

26/01/2005

8. TEMPERATURES DANS LA CELLULE D'ESSAIS
TEMPERATURES IN TEST BOOTH
TEMPERATUREN IN DER PRÜFKABINE

(en °C) Essai / Measuring / Mebpunkt	1	2	3
Axe vertical central Central vertical axis Senkrechten Mittelachse			
0.05 m du plancher / from the floor / über dem Boden	18.5	18.2	19.1
0.75 m du plancher / from the floor / über dem Boden	20.0	20.1	19.9
1.50 m du plancher / from the floor / über dem Boden	21.0	21.3	20.5
0.05 m du plafond / from the ceiling / unter der Decke	23.7	24.4	22.1
Températures moyennes des parois Mean temperatures of the walls Mitteltemperaturen der Wände			
Sud / South / Süden	16.9	16.2	18.2
Est / East / Ost	16.9	16.2	18.2
Ouest / West / West	16.9	16.2	18.2
Plafond / Ceiling / Decke	17.1	16.4	18.3
Plancher / Floor / Boden	17.4	16.7	18.5
Températures sur la paroi au dos du radiateur Temperatures on the back wall behind the radiator Temperaturen aud der Rückwand hinter den Heizkörper			
0.5 m du plancher / from the floor / über dem Boden	43.6	48.6	34.8
Point central / Central point / Mittelpunkt	28.1	30.0	25.0

Figure 2.7 Temperatures in test booth from test report of type 22/600 radiator

CHAPTER THREE
NUMERICAL METHODS

3.1 Computational Fluid Dynamics

Computational fluid dynamics or CFD is the analysis of systems comprising fluid flow, heat transfer and related events. Computational fluid dynamics technique is very satisfying and powerful. In this sense, technique spans a wide range of industrial and non-industrial application areas. Usage of CFD technique leads reduction of time and costs. The cost of an experiment is proportional to the variations at the number of data points and configurations. This may lead increase or decrease at the expense. CFD codes can produce large volumes of results depending on hardware configuration with no added expense. Whilst optimizing an equipment performance in other words performing a parametric study, CFD code is very cheap according to experiments.

3.1.1 Working Procedure of CFD Code

CFD codes can cope with fluid flow problems by the help of embedded numerical algorithms. All codes contain three main elements: a pre-processor, a solver and a post-processor.

Pre-processing is the basic of solving a fluid flow problem. At this step, main aim is to prepare the problem for solver and transformation of this input into a form suitable for use by the solver. Activities carried out at the pre-processing stage (Versteeg & Malalasekera, 1995, p. 3):

- Definition of the geometry of the region of interest.
- Grid generation, division of the domain into smaller parts so that a grid of cells is obtained
- Definition of the physical and chemical properties of the model.

- Definition of fluid properties.
- Specifications of appropriate boundary conditions for cells that is suitable for the domain.

There are three different type of numerical solution technique: finite difference, finite element and spectral methods. Solution procedure of these methods is (Versteeg & Malalasekera, 1995, p. 3):

- Approximation of unknown flow variables by means of simple functions.
- Discretisation by substitution of the approximations into the governing flow equations and subsequent mathematical manipulations.
- Solution of the algebraic equations.

These methods differ from each other by the way approximation and discretisation process of the flow variables.

Finite Difference Method. Finite difference method uses point samples at node points of a grid of coordinate lines to determine the unknowns Ø of the flow problem. Truncated Taylor series are often used to generate finite difference approximations of derivates of Ø in terms of point samples of Ø at each grid point and its immediate neighbours. Finite differences yielding an algebraic equation for the values of Ø at each grid point replaces those derivates appearing in the governing equations (Versteeg & Malalasekera, 1995, p. 4).

Finite Element Method. Finite element method determines the local variations of unknown flow variables Ø by means of simple piecewise functions valid on elements. The exact solution of Ø precisely satisfies the governing equation. Substitution of the piecewise approximation functions for Ø into the equation will not hold exactly and residual is defined to measure the errors. Multiplication of these residuals with a set of weighting functions and integration minimizes errors. Finally a set of algebraic equations for the unknown coefficients of the approximation

functions are obtained. This method has been developed initially for structural stress analysis (Versteeg & Malalasekera, 1995, p. 4).

Spectral Method. Truncated Fourier series or Chebyshev polynomials are used to approximate the unknown Ø. The approximations are not local but valid for the entire computational fluid domain. Truncated series is used to replace the unknowns in the governing equations. A weighted residuals concept similar to the finite element method or making the approximate function coincide with at a number of grid points provides the residual to the algebraic equations for the coefficients of the Fourier and Chebyshev series (Versteeg & Malalasekera, 1995, p. 4).

Finite Volume Method. The finite volume method is a special finite difference formulation. This method is central to FLUENT that is commercially available CFD code. PHOENICS, FLOW3D and STAR-CD also use finite volume method. The numerical algorithm of finite volume method consists of the following steps (Versteeg & Malalasekera, 1995, p. 4):

- Formal integration of the governing equations of fluid flow over all the (finite) control volumes of the solution domain.
- Substitution of a variety of finite difference type approximations for the terms in the integrated equation representing flow process (Discretisation). By this way, integral equations are converted into a system of algebraic equations.
- Solution of algebraic equations by means of an iterative method.

Integration of the governing equations of fluid flow over all the control volume provides the conservation of relevant properties for each finite size cells so that this makes the finite volume method distinguish from all other CFD techniques. Owing to the clear relationship between the numerical algorithm and the embedded physical conservation principle, concepts of finite volume method are simpler to understand according to finite element and spectral method. Conservation of a general flow variable Ø within a finite control volume can be expressed:

$$\begin{bmatrix}\text{Rate of change of } Ø\\ \text{in the control volume}\\ \text{with respect to time}\end{bmatrix} = \begin{bmatrix}\text{Net flux of } Ø\\ \text{due to convection}\\ \text{into the control volume}\end{bmatrix} + \begin{bmatrix}\text{Net flux of } Ø\\ \text{due to diffusion}\\ \text{into the control volume}\end{bmatrix} + \begin{bmatrix}\text{Net rate of creation}\\ \text{of } Ø \text{ inside the}\\ \text{control volume}\end{bmatrix}$$

CFD codes contain discretisation techniques suitable for the treatment of convection and diffusion as well as source terms and the rate of change with respect to time. Iterative solution approach is required owing to the underlying physical procedure's being complex and non-linear.

The third main element of a CFD code is post-processor. Post-processing has been developing as the pre-processors. Most CFD packages are now equipped with versatile data visualization tools owing to the increase at the demand of CFD codes. Post-processing includes; geometry and grid display, vector plots, line and shaded contour plots, 2D and 3D surface plots, particle tracking, color postscript output and dynamic result display. In addition to these, all codes produce trusty alphanumeric output and have data export facilities for further usage of the obtained data by means of another program.

3.2 Governing Equations of Fluid Flow and Heat Transfer

Governing equations of a fluid flow can be expressed by means of conservation laws of physics (Versteeg & Malalasekera, 1995, p. 10):

- Conservation of mass.
- Newton's Second Law: the rate of change of momentum equals to the sum of the forces on a fluid particle.
- First Law of Thermodynamics: the rate of change of energy is equal to the sum of the rate of heat addition to and the rate of work done on fluid particle.

Mass balance of the fluid element is the first step in the derivation of the mass conservation equation. Mass balance can be expressed as; rate of increase of mass in fluid element is equal to the net rate of flow of mass into fluid element. The rate of change of momentum of a fluid particle equals the sum of the forces acting on the particle. Forces acting on the fluid particle comprise surface forces and body forces. Surface forces consist of pressure forces and viscous forces.

Surface forces are used as separate terms in momentum equation. In spite of this, body forces are used as source terms in momentum equation. Body forces consist of (Versteeg & Malalasekera, 1995, p. 15):

- Gravity force
- Centrifugal force
- Coriolis force
- Electromagnetic forces

The energy (E) of a fluid is defined as the sum of internal energy i, kinetic energy $\frac{1}{2}$ ($u^2 + v^2 + w^2$) and gravitational potential energy. Gravitational potential energy is formed by gravitational force. Gravitational force acts as a body force so the effects of the gravitational potential energy changes is included as source term to the energy equation. In order to provide conservation of energy of the fluid particle, the sum of the net rate of heat addition to the fluid, net rate of work done on the fluid particle and the rate of increase of energy due to sources are equated to the rate of change of energy of the fluid particle.

An equation for the changes of the kinetic energy can be obtained by multiplying x-, y- and z- components of the momentum equations with their related velocity components. The multiplied sum of the momentum components provides the change of kinetic energy. By this way, an equation for internal energy i or temperature T can be obtained.

$$\underbrace{E}_{\substack{\text{SPECIFIC}\\ \text{ENERGY}}} = \underbrace{i}_{\substack{\text{INTERNAL}\\ \text{ENERGY}}} + \underbrace{1/2\left(u^2+v^2+w^2\right)}_{\substack{\text{KINETIC}\\ \text{ENERGY}}} \tag{3.1}$$

3.2.1 Equation of State

A system of five partial differential equations (mass conversation, *x*-, *y*-, *z*-momentum and energy equations) describes the motion of a fluid in three dimensions. There are four thermodynamic variables among the unknowns: *ρ, p, i, and T.* Thermodynamic equilibrium assumptions forms an opportunity to provide a relationship between the thermodynamic variables. Assumptions are valid except for certain flows with strong shockwaves. The state of a substance in thermodynamic equilibrium can be described by two state variables. The major aim is to relate the other variables to the two state variables. The state equations for pressure p and specific internal energy *i* can be obtained by the usage of density ρ and temperature *T* as state variables:

$$p = p\left(\rho, T\right) \quad \text{and} \quad i = i\left(\rho, T\right) \tag{3.2}$$

Equations of state for perfect gases (Versteeg & Malalasekera, 1995, p. 21):

$$p = \rho RT \qquad \text{and} \qquad i = C_v\, T \tag{3.3}$$

For compressible flows, the linkage of energy equation to the mass conservation and momentum equations is provided by means of the assumptions of thermodynamic equilibrium owing to density variations in the flow field. As a result of density variations, pressure and temperature variations occur in the flow field.

For incompressible flows (liquids and gases at low speeds), only the consideration of mass conversation and momentum equations solves the flow field owing to flows not including density variations. If the problem involves heat transfer energy equation is solved by means of data obtained from mass conversation and momentum equation.

3.2.2 General Transport Equations

Table 3.1 summarizes the governing equations of a time dependent, three dimensional and compressible Newtonian fluid flow. (Versteeg & Malalasekera, 1995, p. 24) By means of Newtonian model, the viscous stresses are expressed in terms of gradients of velocity components.

Table 3.1 Governing equations of a compressible fluid flow

Mass	$\frac{\partial \rho}{\partial t} + div(\rho\, \mathbf{u}) = 0$	(3.4)
x-momentum	$\frac{\partial \rho u}{\partial t} + div(\rho u\, \mathbf{u}) = -\frac{\partial p}{\partial x} + div(\mu\, grad\, u) + S_{Mx}$	(3.5)
y-momentum	$\frac{\partial \rho v}{\partial t} + div(\rho v\, \mathbf{u}) = -\frac{\partial p}{\partial y} + div(\mu\, grad\, v) + S_{My}$	(3.6)
z-momentum	$\frac{\partial \rho w}{\partial t} + div(\rho w\, \mathbf{u}) = -\frac{\partial p}{\partial z} + div(\mu\, grad\, w) + S_{Mz}$	(3.7)
Internal energy	$\frac{\partial \rho i}{\partial t} + div(\rho i\, \mathbf{u}) = -p\, div\, \mathbf{u} + div(k\, grad\, T) + \mathbf{\Phi} + S_i$	(3.8)
Equations of state	$p = p(\rho, T)$ and $i = i(\rho, T)$	(3.9)
	For perfect gas $\rightarrow p = \rho RT$ and $i = C_v T$	(3.10)

The dissipation function $\mathbf{\Phi}$ describes all effects arisen from viscous stresses in the internal energy equation (3.8) (Versteeg & Malalasekera, 1995, p. 15):

$$\mathbf{\Phi} = \mu\left\{2\left[\left(\frac{\partial u}{\partial x}\right)^2 + \left(\frac{\partial v}{\partial y}\right)^2 + \left(\frac{\partial w}{\partial z}\right)^2\right] + \left(\frac{\partial u}{\partial y} + \frac{\partial v}{\partial x}\right)^2 + \left(\frac{\partial u}{\partial z} + \frac{\partial w}{\partial x}\right)^2 + \left(\frac{\partial v}{\partial z} + \frac{\partial w}{\partial y}\right)^2\right\} + \lambda(div\, \mathbf{u})^2 \tag{3.11}$$

Equations of state is added two algebraic equations to the five partial differential equations. After obtaining Newtonian model, a system of seven equations with seven unknowns is formed. By this way, system is mathematically closed. This system can be solved by means of supplementation of suitable auxiliary conditions (initial and boundary conditions).

3.2.3 Differential and Integral Forms of General Transport Equations

Table 3.1 shows that partial differential conservation equations are generally similar. For a general variable *Ø*, conservative form of all fluid flow equations can be written as (Versteeg & Malalasekera, 1995, p. 25):

$$\frac{\partial(\rho\phi)}{\partial t} + div(\rho\phi\,\mathbf{u}) = div(\Gamma\ grad\ \phi) + S_\phi \tag{3.12}$$

Equation (3.12) means,

$$\begin{bmatrix}\text{Rate of increase of}\\ \phi \text{ of fluid elemet}\end{bmatrix} + \begin{bmatrix}\text{Net rate of flow of}\\ \phi \text{ out of fluid element}\end{bmatrix} = \begin{bmatrix}\text{Rate of increase of}\\ \phi \text{ due to diffusion}\end{bmatrix} + \begin{bmatrix}\text{Rate of increase of}\\ \phi \text{ due to sources}\end{bmatrix}$$

Equation (3.12) is the general transport equation for property *Ø* and includes various transport process. On the left hand side, the rate of change term and convective term exist. On the right hand side, the diffusive term (Γ = diffusion coefficient) and source term exist.

Equation (3.12) is the initial point for computational procedures in the finite element method. Special forms of Table 3.1 can be obtained by setting *Ø* equal to *u, v, w, i, T* or h_0 and defining appropriate values for diffusion coefficient Γ and source terms. The integration of Equation (3.12) over a three-dimensional control volume *CV* is the key step of finite volume method (Versteeg & Malalasekera, 1995, p. 25):

$$\int_{CV} \frac{\partial(\rho\phi)}{\partial t} dV + \int_{CV} div(\rho\phi\,\mathbf{u})\,dV = \int_{CV} div(\Gamma\ grad\ \phi)\,dV + \int_{CV} S_\phi dV \tag{3.13}$$

By using Gauss' divergence term, the volume integral in the second term on the left hand side (convective term) and in the first term on the right hand side (diffusive term) are re-written as integrals over the entire bounding surface of the control volume (Versteeg & Malalasekera, 1995, p. 25):

$$\int_{CV} div\ \mathbf{a} dV = \int_{A} \mathbf{n} \,.\, \mathbf{a} dA \tag{3.14}$$

n.a → the component of vector **a** in the direction of the vector **n** normal to surface element *dA*

Equation (3.14) shows that the integral of divergence of a vector **a** over a volume is equal to the component of **a** in the direction normal to the surface over the entire bounding surface *A*. Application of Gauss' divergence theorem to Equation (3.13) (Versteeg & Malalasekera, 1995, p. 26):

$$\frac{\partial}{\partial t}\left(\int_{CV} \rho\phi\, dV\right) + \int_{A} \mathbf{n} \,.\, (\rho\phi\, \mathbf{u}) dA = \int_{A} \mathbf{n} \,.\, (\Gamma\, grad\phi) dA + \int_{CV} S_{\phi} dV \tag{3.15}$$

Equation (3.15) can be expressed in words as:

$$\begin{bmatrix} \text{Rate of} \\ \text{increase} \\ \text{of } \phi \end{bmatrix} + \begin{bmatrix} \text{Net rate of decrease of} \\ \phi \text{ due to convection} \\ \text{across the boundries} \end{bmatrix} = \begin{bmatrix} \text{Rate of increase of} \\ \phi \text{ due to diffusion} \\ \text{across the boundries} \end{bmatrix} + \begin{bmatrix} \text{Net Rate} \\ \text{of creation} \\ \text{of } \phi \end{bmatrix}$$

The rate of increase term of equation (3.15) is equal to zero in steady state problems. The integrated form of steady transport equation is (Versteeg & Malalasekera, 1995, p. 26):

$$\int_{A} \mathbf{n} \,.\, (\rho\phi\, \mathbf{u}) dA = \int_{A} \mathbf{n} \,.\, (\Gamma\, grad\phi) dA + \int_{CV} S_{\phi} dV \tag{3.16}$$

For the time dependent problems, equation (3.15) is integrated with respect to time t over a small interval Δt from t until $t+\Delta t$. So the most general integrated form of the transport equation is (Versteeg & Malalasekera, 1995, p. 27):

$$\int_{\Delta t}\frac{\partial}{\partial t}\left(\int_{CV}(\rho\phi)\,dV\right)dt+\int_{\Delta t}\int_{A}\mathbf{n}.(\rho\phi\,\mathbf{u})\,dA\,dt=\int_{\Delta t}\int_{A}\mathbf{n}.(\Gamma_{\phi}\,grad\phi)\,dA\,dt+\int_{\Delta t}\int_{CV}S_{\phi}dV\,dt \tag{3.17}$$

3.3 Finite Volume Method for Diffusion

By removing the transient and convective terms from the general transport equation (3.12), governing equation of steady diffusion can be obtained (Versteeg & Malalasekera, 1995, p. 85):

$$div(\Gamma\,grad\,\phi)+S_{\phi}=0 \tag{3.18}$$

The key step of the finite volume method is the control volume integration as described before. The control volume integration of equation (3.18) is (Versteeg & Malalasekera, 1995, p. 85):

$$\int_{CV}div(\Gamma\,grad\,\phi)\,dV+\int_{CV}S_{\phi}dV=\int_{A}\mathbf{n}.(\Gamma\,grad\phi)\,dA+\int_{CV}S_{\phi}dV \tag{3.19}$$

3.3.1 One-Dimensional Steady State Diffusion

For one-dimensional steady state diffusion, general transport equation becomes (Versteeg & Malalasekera, 1995, p. 86):

$$\frac{d}{dx}\left(\Gamma\frac{d\phi}{dx}\right)+S=0 \tag{3.20}$$

This diffusion process can be illustrated as shown in Figure 3.1. Γ is the diffusion coefficient and *S* is the source term. Boundary values of *Ø* at point A and B are constant. The first step is to divide the domain into discrete control volumes. A number of nodal points are placed to the space between A and B. the faces of control volumes are positioned midway between adjacent nodes. By this way, each node is surrounded by a control volume or cell. In order to provide that the physical boundaries coincide with the control volume boundaries, control volumes in relation with domain boundaries are placed near the edge of the domain.

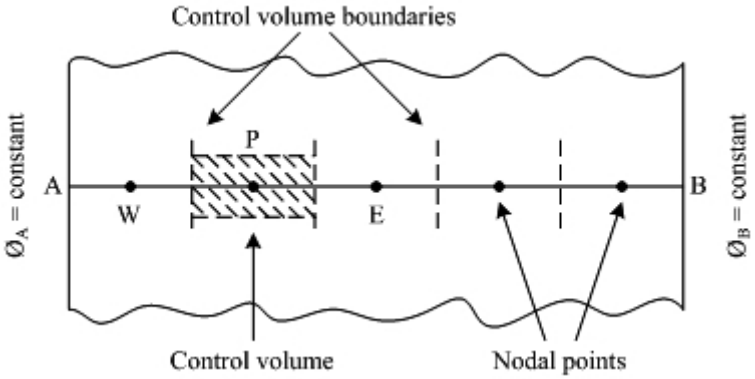


Figure 3.1 One-dimensional diffusion

A system of notation can be used to obtain diffusion equations. The usual convention of CFD method is shown in Figure 3.2. The nodal point is shown as *P* and its neighbours west by *W* and east by *E* are shown. The west side face of the control volume is referred to by "*w*" and the east side is referred to by "*e*". The distance between the node *W* and *P*, and nodes *P* and *E* are respectively shown as δx_{WP} and δx_{PE}. The distances between face "*w*" and point *P*, and point *P* and face "*e*" are respectively shown as δx_{wP} and δx_{Pe}. Control volume width is $\Delta x = \delta x_{we}$.

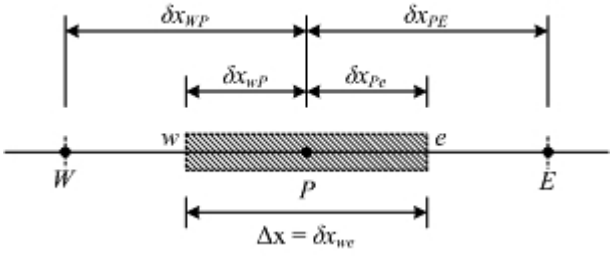


Figure 3.2 Notation of nodal points and boundary faces

The integration of the governing equation over a control volume yields a discretised equation at nodal point *P* of the control volume shown in Figure 3.2 (Versteeg & Malalasekera, 1995, p. 86):

$$\int_{\Delta V}\frac{d}{dx}\left(\Gamma\frac{d\phi}{dx}\right)dV+\int_{\Delta V}SdV=\left(\Gamma A\frac{d\phi}{dx}\right)_e-\left(\Gamma A\frac{d\phi}{dx}\right)_w+\overline{S}\Delta V \tag{3.21}$$

where A $\Rightarrow$ Cross - sectional area
ΔV $\Rightarrow$ Control volume
$\overline{\text{S}}$ $\Rightarrow$ Average value of S over the control volume

Equation (3.21) states that the diffusive flux of *Ø* leaving the east face minus the diffusive flux of *Ø* entering the west face is equal to the generation of *Ø*. By this way, a balance equation for *Ø* is formed over the control volume. The interface diffusion coefficient Γ and the gradient *dØ*/*dx* at east "e" and west "w" are needed to develop useful forms of the discretised equations. An approximate distribution of properties between nodal points is used to determine gradients at control volume faces. Linear approximation is the simplest way of calculating interface values and gradients. This is so-called **central differencing scheme**. In a uniform grid, linearly interpolated values of Γe and Γ_w are (Versteeg & Malalasekera, 1995, p. 87):

$$\Gamma_w=\frac{\Gamma_W+\Gamma_P}{2} \tag{3.22a}$$

$$\Gamma_e=\frac{\Gamma_P+\Gamma_E}{2} \tag{3.22b}$$

Diffusive flux terms are (Versteeg & Malalasekera, 1995, p. 87),

$$\left(\Gamma A\frac{d\phi}{dx}\right)_e=\Gamma_e A_e\left(\frac{\phi_E-\phi_P}{\delta x_{PE}}\right) \tag{3.23}$$

$$\left(\Gamma A\frac{d\phi}{dx}\right)_w=\Gamma_w A_w\left(\frac{\phi_P-\phi_W}{\delta x_{WP}}\right) \tag{3.24}$$

The source term S may be a function of the dependent variable. For this reason, the finite volume method approximates the source term by means of a linear form (Versteeg & Malalasekera, 1995, p. 87):

$$\overline{S}\Delta V = S_u + S_P\phi_P \tag{3.25}$$

By means of equations (3.23), (3.24) and (3.25), equation (3.21) becomes (Versteeg & Malalasekera, 1995, p. 87):

$$\Gamma_e A_e\left(\frac{\phi_E - \phi_P}{\delta x_{PE}}\right) - \Gamma_w A_w\left(\frac{\phi_P - \phi_w}{\delta x_{WP}}\right) + \left(S_u + S_P\phi_P\right) = 0 \tag{3.26}$$

Equation (3.26) can be written as below to emphasize the nodal points (Versteeg & Malalasekera, 1995, p. 87):

$$\left(\frac{\Gamma_e}{\delta x_{PE}}A_e + \frac{\Gamma_w}{\delta x_{WP}}A_w - S_P\right)\phi_P = \left(\frac{\Gamma_w}{\delta x_{WP}}A_w\right)\phi_W + \left(\frac{\Gamma_e}{\delta x_{PE}}A_e\right)\phi_E + S_u \tag{3.27}$$

Using a_W and a_E for the coefficients of $\emptyset_W$ and $\emptyset_E$, a_P for the coefficient of $\emptyset_P$; equation (3.27) can also be written as (Versteeg & Malalasekera, 1995, p. 87):

$$a_P\phi_P = a_W\phi_W + a_E\phi_E + S_u \tag{3.28}$$

Where,

a_W	a_E	a_P
$\frac{\Gamma_w}{\delta x_{WP}}A_w$	$\frac{\Gamma_e}{\delta x_{PE}}A_e$	$a_W + a_E - S_P$

The values of S_u and S_p can be obtained from source model, equation (3.25). In order to solve the problem, discretised equations must be formed at each of the nodal points. General discretised equation (3.28) is modified to incorporate boundary conditions at control volumes that are adjacent to domain boundaries. The

distribution of property $\emptyset$ at nodal points can be obtained by solving resulting system of linear algebraic equations by means of any suitable matrix solution technique.

3.3.2 General Form of Discretised Equations for Steady State Diffusion

The methodology used in deriving discretised equations in the one-dimensional case can be easily extended to two- and three-dimensional problems. The general form of discretised equations for one-, two- and three-dimensional problems is (Versteeg & Malalasekera, 1995, p. 102):

$$a_P \phi_P = \sum a_{nb} \phi_{nb} + S_u \tag{3.29}$$

where $\sum$ indicates summation over all neighbouring nodes (nb), $\emptyset_{nb}$ are the values of property $\emptyset$ at the neighbouring nodes and (S_u + $S_P \emptyset_P$) is the linearised source term. In all cases the coefficients around node P that are listed in Table 3.2 satisfy the following relation (Versteeg & Malalasekera, 1995, p. 102):

$$a_P = \sum a_{nb} - S_P \tag{3.30}$$

Table 3.2 Neighbour coefficients for one-, two- and three-dimensional diffusion problems

	a_W	a_E	a_S	a_N	a_B	a_T
1D	$\frac{\Gamma_w A_w}{\delta x_{WP}}$	$\frac{\Gamma_e A_e}{\delta x_{PE}}$	–	–	–	–
2D	$\frac{\Gamma_w A_w}{\delta x_{WP}}$	$\frac{\Gamma_e A_e}{\delta x_{PE}}$	$\frac{\Gamma_s A_s}{\delta y_{SP}}$	$\frac{\Gamma_n A_n}{\delta y_{PN}}$	–	–
3D	$\frac{\Gamma_w A_w}{\delta x_{WP}}$	$\frac{\Gamma_e A_e}{\delta x_{PE}}$	$\frac{\Gamma_s A_s}{\delta y_{SP}}$	$\frac{\Gamma_n A_n}{\delta y_{PN}}$	$\frac{\Gamma_b A_b}{\delta z_{BP}}$	$\frac{\Gamma_t A_t}{\delta z_{PT}}$

Boundary conditions are incorporated by cutting the link to the boundary side and introducing the boundary side flux through additional source terms S_u and S_P. For one-dimensional control volume of width $\Delta\zeta$ with a boundary B, link cutting is performed by setting coefficient a_B equal to zero. Source contributions for fixed value of $\emptyset_B$ are (Versteeg & Malalasekera, 1995, p. 102):

$$S_u = \frac{2k_B A_B}{\Delta\zeta}\phi_B \quad \text{and} \quad S_P = -\frac{2k_B A_B}{\Delta\zeta} \tag{3.31}$$

Source contributions for fixed flux q_B are (Versteeg & Malalasekera, 1995, p. 102):

$$S_u + S_P\phi_P = q_B \tag{3.32}$$

3.4 Finite Volume Method for Convection and Diffusion

The effects of convection must be accounted when fluid flow plays a significant role. Diffusion always occurs with convection in nature so the steady state convection-diffusion equation is obtained from general transport equation (3.12) for a general property Ø by deleting the transient term (Versteeg & Malalasekera, 1995, p. 103):

$$div(\rho\phi\,\mathbf{u}) = div(\Gamma\, grad\ \phi) + S_\phi \tag{3.33}$$

The integration of equation (3.33) over a control volume (Versteeg & Malalasekera, 1995, p. 103):

$$\int_A \mathbf{n}\,.\,(\rho\phi\,\mathbf{u})\,dA = \int_A \mathbf{n}\,.\,(\Gamma\, grad\phi)\,dA + \int_{CV} S_\phi dV \tag{3.34}$$

The left hand side of equation (3.34) gives the net convective flux and the right hand side consists of net diffusive flux and generation or destruction of the property Ø with in the control volume. The distribution of a transported quantity along its gradients is affected in all directions at the diffusion process. On the other hand, the distribution of this quantity is only affected along the flow direction at the convection process. So the main problem in the discretisation of the convective terms is the calculation of the value of transported property Ø at control volume faces and its convective flux across these boundaries. The velocities going to be used in the computation of convective fluxes are assumed to be somehow known.

3.4.1 Steady One-Dimensional Convection and Diffusion

The steady convection-diffusion of a property *Ø* in a given one-dimensional flow field ***u*** without source term is governed by (Versteeg & Malalasekera, 1995, p. 104),

$$\frac{\partial}{\partial x}(\rho u\phi) = \frac{\partial}{\partial x}\left(\Gamma \frac{\partial \phi}{\partial x}\right) \tag{3.35}$$

In convection and diffusion problems, flow must satisfy continuity (Versteeg & Malalasekera, 1995, p. 104),

$$\frac{\partial(\rho u)}{\partial x} = 0 \tag{3.36}$$

One-dimensional control volume is shown in Figure 3.3 and the notations for the computation are same as the notations used in the diffusion.

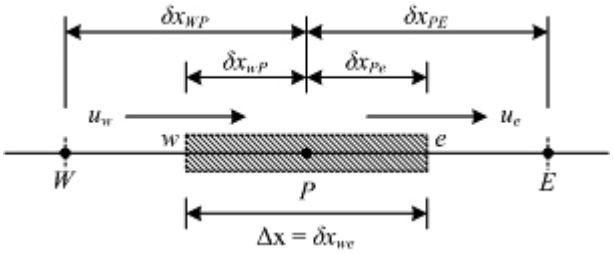


Figure 3.3 One-dimensional control volume around node *P*.

Integration of equation (3.35) over the control volume is (Versteeg & Malalasekera, 1995, p. 104),

$$(\rho uA\phi)_e - (\rho uA\phi)_w = \left(\Gamma A \frac{\partial \phi}{\partial x}\right)_e - \left(\Gamma A \frac{\partial \phi}{\partial x}\right)_w \tag{3.37}$$

And the integration of continuity equation is (Versteeg & Malalasekera, 1995, p. 104):

$$(\rho u A)_e - (\rho u A)_w = 0 \tag{3.38}$$

The terms in equation (3.37) must be approximated in order to obtain discretised equations. It is useful to represent convective mass flux per unit area as *F* and diffusion conductance at cell faces as *D* (Versteeg & Malalasekera, 1995, p. 104):

$$F = \rho u \qquad \text{and} \qquad D = \frac{\Gamma}{\delta x} \tag{3.39}$$

Cell values of the variables *F* and *D* are,

$$F = (\rho u)_w,\ D_w = \frac{\Gamma_w}{\delta x_{WP}} \qquad \text{and} \qquad F = (\rho u)_e,\ D_e = \frac{\Gamma_e}{\delta x_{PE}} \tag{3.40}$$

By the usage of **central differencing approach** for the diffusion terms on the right hand side of the equation (3.37) and assuming that A_w=A_e=A, the integrated convection-diffusion equation becomes as (Versteeg & Malalasekera, 1995, p. 105),

$$F_e\phi_e - F_w\phi_w = D_e(\phi_E - \phi_P) - D_w(\phi_P - \phi_W) \tag{3.41}$$

and the integrated continuity equation can be written as (Versteeg & Malalasekera, 1995, p. 105),

$$F_e - F_w = 0 \tag{3.42}$$

By means of an approximation scheme, equation (3.41) can be solved to obtain the transported property *Ø* at the e and w faces of the control volume.

3.4.2 Properties of Discretisation Schemes

The more cell is formed the more realistic numerical result, that are indistinguishable from exact solution of transport equation, may be obtained in theory. A finite number of cells are used for practical calculations so the realism of the numerical result depends on the fundamental properties of the discretisation scheme (Versteeg & Malalasekera, 1995, p. 105):

- Conservativeness
- Boundedness
- Transportiveness

Conservativeness. A set of discretised conservation equations including fluxes of the transported property $\emptyset$ through control volume faces occurs as a consequence of the integration of the convection-diffusion equation over a finite number of control volumes. By equaling the fluxes of $\emptyset$ that are leaving a control volume a cross certain face and entering the adjacent control volume through the same face, conservation of $\emptyset$ for the whole solution domain can be ensured.

Boundedness. The set of algebraic equations that is obtained from the discretised equation at each nodal point forms a matrix of coefficients. The resulting matrix must be diagonally dominant in order to satisfy the boundedness (Scarborough, 1958). This yields the internal nodal values of the property $\emptyset$ being bounded by its boundary values in the absence of source terms. This can be thought of a steady state conduction condition without sources and with boundary temperatures of T_1 and T_2 where $T_1 > T_2$. All interior nodal values of temperature T must be between T_2 and T_1. All coefficients of the discretised equations must also have the same sign in order to supply the boundedness condition. By this way, an increase in the variable $\emptyset$ at one node makes an increase in $\emptyset$ at neighbouring nodes. If these two main conditions for boundedness are not satisfied, the solution doesn't converge or if it converges, it contains wiggles.

Transportiveness. Figure 3.4 can be used to illustrate the transportiveness condition of a fluid flow. In order to show a measure of the relative strengths of convection and diffusion, the non-dimensional cell Peclet number is defined as (Versteeg & Malalasekera, 1995, p. 112):

$$Pe = \frac{F}{D} = \frac{\rho u}{\Gamma/\delta x} \qquad \text{where } \delta x = \text{cell width (characteristic lenght)} \tag{3.43}$$

The lines in Figure 3.4 show the general shape of contours of a constant *Ø* for different values of *Pe*. In order to define the size of the influence of the upstream node *P* at the downstream node *E*, there are two extreme cases:

- $Pe = 0 \rightarrow$ no convection pure diffusion
- $Pe = \infty \rightarrow$ no diffusion pure convection

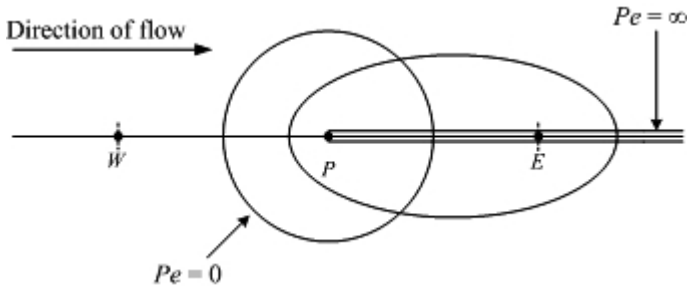


Figure 3.4 Distribution of *Ø* at different cell Peclet numbers

In the situation of pure diffusion (ρu=0), no fluid flow occurs and the fluid is stagnant so the diffusion process yields distribution of *Ø* equally in all direction and the contours of constant *Ø* forms concentric circles with *P* at their center. Condition at the east node is influenced by both upstream node P and other downstream node in an equivalent manner. As *Pe* increases, the node *E* is strongly influenced by conditions at *P* and conditions at *P* are weakly influenced or are not influenced by conditions at *E*. The contours of constant *Ø* form elliptical shape rather than circular shape. In the situation of pure convection ($\Gamma/\delta x$=0), all property of *Ø* spreading from the node *P* is immediately transported to downstream *E*. For this reason, the value of *Ø* at *E* is only affected by upstream conditions. As a consequence of no diffusion, $Ø_E$

is equal to $\emptyset_P$. The relationship between the magnitude of Peclet number and the directionality of influencing of the discretisation scheme is very important.

3.4.3 Central Differencing Scheme for Convection and Diffusion

The cell values for the convective terms on the left hand side of equation (3.41) can be computed by means of linear interpolation. For the right hand side of this equation (diffusion term), the cell face values are computed by means of **central differencing scheme**. The cell values of property $\emptyset$ are (Versteeg & Malalasekera, 1995, p. 105),

$$\phi_e = \frac{(\phi_P + \phi_E)}{2} \tag{3.44a}$$

$$\phi_w = \frac{(\phi_W + \phi_P)}{2} \tag{3.44b}$$

The usage of above terms for convection terms of equation (3.41),

$$\frac{F_e}{2}(\phi_P + \phi_W) - \frac{F_w}{2}(\phi_W + \phi_P) = D_e(\phi_E - \phi_P) - D_w(\phi_P - \phi_W) \tag{3.45}$$

This can be written as (Versteeg & Malalasekera, 1995, p. 105),

$$\left[\left(D_w + \frac{F_w}{2}\right) + \left(D_e - \frac{F_e}{2}\right) + (F_e - F_w)\right]\phi_P = \left(D_w + \frac{F_w}{2}\right)\phi_W + \left(D_e - \frac{F_e}{2}\right)\phi_E \tag{3.46}$$

The central differencing expressions for the discretised convection-diffusion equation are (Versteeg & Malalasekera, 1995, p. 105),

$$a_P\phi_P = a_W\phi_W + a_E\phi_E \tag{3.47}$$

Where,

a_W	a_E	a_P
$\left(D_w + \frac{F_w}{2}\right)$	$\left(D_e - \frac{F_e}{2}\right)$	$a_W + a_E + (F_e - F_w)$

The central differencing scheme uses consistent expressions in order to evaluate convective and diffusive fluxes at the control volume faces. This shows that scheme is conservative. The internal coefficients of discretised scalar transport equation (3.47) are shown above. The flow field is also governed by the discretised continuity equation (3.42). If the flow field satisfies continuity, (F_e-F_w) is equal to zero. For this reason, a_p is equal to the (a_w+a_e). This makes the coefficients of the central differencing scheme form diagonally dominant matrix. East coefficients a_E of the discretised convection diffusion equation can be negative if the convection dominates (a_E=D_e-F_e/2). In order to supply positive a_E values for a unidirectional flow, De and Fe must satisfy (Versteeg & Malalasekera, 1995, p. 114),

$$\frac{F_e}{D_e} = Pe_e < 2 \tag{3.48}$$

If *Pe* is greater than 2, the east coefficient will be negative. By this way, one of the requirements for boundedness is violated so physically impossible solutions may be obtained. The node *P* is influenced from the directions of all its neighbours. The direction of the flow or the strength of convection relative to diffusion is not recognized by the scheme so it does not agree with transportiveness condition at high *Pe*. The scheme will be stable and accurate only if *Pe* < 2. This states that the scheme can be used if the velocity is small for the given flow conditions or if the grid spacing is small (diffusion-dominated low Reynolds number flows). On the other hand, the Taylor series truncation error of the central differencing scheme is second order. Because of the limitations described above, central differencing scheme is not a suitable discretisation scheme for general purpose flow calculations.

3.4.4 Upwind Differencing Scheme for Convection and Diffusion

Central differencing scheme is unsuitable in a strongly convective flow from west to east because node *W* should have more influence on the west cell face than node *P*. In order to supply this influence, the convected value of *Ø* at a cell face is taken to be equal to the value at the upstream node at the upwind differencing scheme.

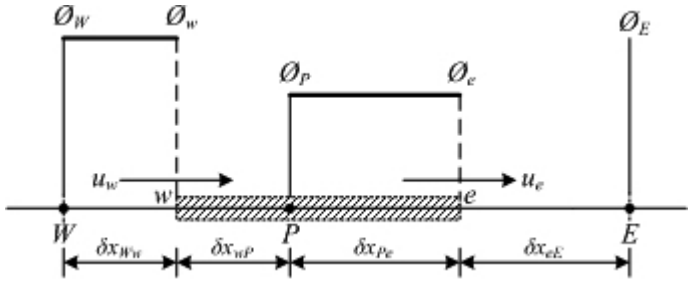


Figure 3.5 Upwind differencing scheme for positive direction

When the flow is in the positive direction as shown in Figure 3.5, upwind scheme sets (Versteeg & Malalasekera, 1995, p. 115),

$$\emptyset_w = \emptyset_W \quad \text{and} \quad \emptyset_e = \emptyset_P \tag{3.49}$$

The discretised equation (3.41) becomes

$$F_e\phi_P - F_w\phi_W = D_e(\phi_E - \phi_P) - D_w(\phi_P - \phi_W) \tag{3.50}$$

This can be written as (Versteeg & Malalasekera, 1995, p. 115)

$$\left[(D_w + F_w) + D_e + (F_e - F_w)\right]\phi_P = (D_w + F_w)\phi_W + D_e\phi_E \tag{3.51}$$

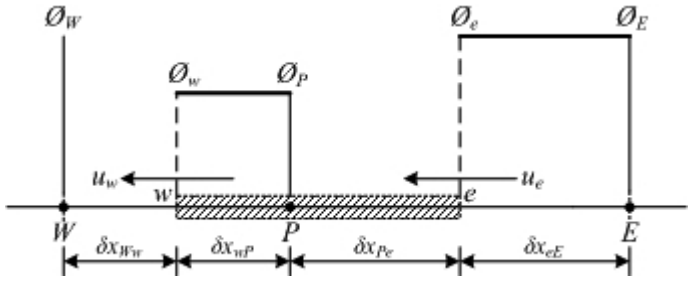


Figure 3.6 Upwind differencing scheme for negative direction

If the flow is in the negative direction as shown in Figure 3.14, upwind scheme sets (Versteeg & Malalasekera, 1995, p. 115),

$$\emptyset_w = \emptyset_P \quad \text{and} \quad \emptyset_e = \emptyset_E \tag{3.52}$$

The discretised equation (3.41) becomes (Versteeg & Malalasekera, 1995, p. 115)

$$F_e\phi_E - F_w\phi_P = D_e(\phi_E - \phi_P) - D_w(\phi_P - \phi_W) \tag{3.53}$$

This can be also written as,

$$[D_w + (D_e - F_e) + (F_e - F_w)]\phi_P = D_w\phi_W + (D_e - F_e)\phi_E \tag{3.54}$$

Equations (3.51) and (3.54) can be written in general form as (Versteeg & Malalasekera, 1995, p. 116)

$$a_P\phi_P = a_W\phi_W + a_E\phi_E \quad \text{where} \quad a_P = a_W + a_E + (F_e - F_w) \tag{3.55}$$

and neighbour coefficients are

For $F_w > 0$ and $F_e > 0$	For $F_w < 0$ and $F_e < 0$
$a_W = D_w + F_w$	$a_W = D_w$
$a_E = D_e$	$a_E = D_e - F_e$

Another form of notation for the neighbour coefficients that covers both directions is (Versteeg & Malalasekera, 1995, p. 116):

a_W	a_E
$D_w + \max(F_w, 0)$	$D_e + \max(0, -F_e)$

The upwind differencing scheme uses consistent expressions to calculate fluxes through the cell faces. By this way, the scheme is conservative. The coefficients of the discretised equation are positive and the coefficient matrix is diagonally dominant so no “wiggles” occurs in the solution. In addition to these, the scheme accounts for the direction of the flow. By this way, the scheme satisfies the requirements for boundedness and the transportiveness. The scheme is based on the backward differencing formula so the accuracy of the scheme is only first order on the basis of the Taylor series truncation error. On the other hand, the scheme

produces in accurate results when the flow is not aligned with the grid lines and makes the distribution of the transported property become smeared in such problems (Leschziner, 1980; Huang *et al*, 1985).

In addition to central and upwind differencing schemes, the **hybrid differencing scheme** of Spalding (1972) combines central and upwind differencing schemes. The central differencing scheme, which is accurate to second order, is employed for small Peclet number ($Pe < 2$) and the upwind scheme, which is accurate to first order but accounts for transportiveness, is employed for large Peclet number ($Pe \geq 2$). The scheme is fully conservative and unconditionally bounded since the coefficients are always positive. It also satisfies the transportiveness by means of upwind formulation for large values of Peclet number. The disadvantage is that the accuracy in terms of Taylor series truncation error is only first order. The **power-law differencing scheme** of Patankar (1980) produces better results than hybrid scheme in case of one-dimensional problems. In this scheme, diffusion is set to zero when cell Peclet number exceeds 10. If $0 < Pe < 10$, the flux is evaluated by using a polynomial expression. Properties of scheme are similar to those of the hybrid scheme. The power-law scheme is more accurate for one-dimensional problems since it attempts to represent the exact solution more closely.

The **quadratic upstream interpolation for convective kinetics** (QUICK) scheme of Leonard (1979) uses a three point upstream-weighted interpolation for cell face values. The scheme is conservative in order to the usage of consistent quadratic profiles for the cell face values of fluxes. The accuracy in terms of the Taylor series truncation error is third order on a uniform mesh since scheme is based on a quadratic function. The transportiveness property is built into the scheme as the quadratic function is based on two upstream and one downstream nodal values. If the flow field satisfies continuity, the coefficient a_P equals to the sum of all neighbouring coefficients which is desirable for boundedness. The main coefficients (E and W) are not guaranteed to be positive and additional coefficients (WW and EE) are negative. Main coefficients become negative at relatively modest cell Peclet numbers ($Pe > 8/3$). This gives rise to stability problems and unbounded solutions under

certain flow conditions. The QUICK scheme is therefore conditionally stable. Matrix solution methods valid for other schemes are not directly applicable due to the usage of additional coefficients.

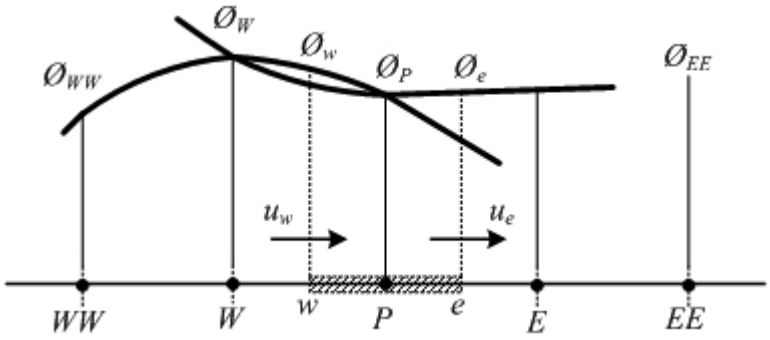


Figure 3.7 Quadratic profiles used in QUICK scheme

The QUICK scheme has been re-formulated in different ways in order to alleviate stability problems arisen from the appearance of negative main coefficients. These formulations all involve placing troublesome negative coefficients in the source term so as to retain positive main coefficients (Hayase *et al*, 1990).

3.5 Solution Algorithms for Pressure-Velocity Coupling in Steady Flows

In the previous sections, the velocity field was somehow known and the convection of a scalar variable $\emptyset$ depends on the magnitude and direction of the local velocity field. In general the velocity field is not known and emerges as part of the overall solution process along with all other flow variables. In order to obtain transport equations for each velocity components (momentum equations), equation (3.12) is used by means of the variable $\emptyset$ that is respectively used as u, v and w. The velocity field must also satisfy the continuity equation. So these equations are (Versteeg & Malalasekera, 1995, p. 135),

x-momentum equation,

$$\frac{\partial}{\partial x}(\rho uu)+\frac{\partial}{\partial y}(\rho vu)=\frac{\partial}{\partial x}\left(\mu\frac{\partial u}{\partial x}\right)+\frac{\partial}{\partial y}\left(\mu\frac{\partial u}{\partial y}\right)-\frac{\partial P}{\partial x}+S_u \tag{3.56}$$

y-momentum equation,

$$\frac{\partial}{\partial x}(\rho uv)+\frac{\partial}{\partial y}(\rho vv)=\frac{\partial}{\partial x}\left(\mu\frac{\partial v}{\partial x}\right)+\frac{\partial}{\partial y}\left(\mu\frac{\partial v}{\partial y}\right)-\frac{\partial P}{\partial y}+S_v \tag{3.57}$$

continuity equation,

$$\frac{\partial}{\partial x}(\rho u)+\frac{\partial}{\partial y}(\rho v)=0 \tag{3.58}$$

The solution of equation set (3.56-58) yields two new problems (Versteeg & Malalasekera, 1995, p. 135):

- The convective terms of momentum equation contain non-linear quantities. For example the first term of equation (3.56) is the x-derivative of ρu^2.
- The existence of every velocity component in each momentum and the continuity equation makes all three equations coupled. On the other hand, pressure term appears in both momentum equations and there is evidently no transport or other equation for pressure. In this sense, the most complex issue to resolve is the role played by pressure.

If the pressure gradient is known, schemes based on obtaining discretised equations explained previous section are applicable for the process of obtaining discretised equations for velocities from momentum equations. But in general purpose flow calculations, the pressure field is wished to be calculated as part of solution. By this way, its gradient is not normally known beforehand. If the flow is compressible, the continuity equation is used as transport equation for density and energy equation is also used as transport equation for temperature in order to obtain pressure from the density and temperature by means of the equation of state $p = p(\rho,T)$. If the flow is incompressible, the density is constant and there is no linkage to the pressure by means of density. In this case, coupling between pressure and velocity yields a constraint on the solution of flow field. If the correct pressure field

is applied in momentum equation, the resulting velocity field should satisfy continuity. The pressure-velocity linkage can be resolved by adopting an iterative solution strategy such as SIMPLE algorithm of Patankar and Spalding (1972). In this algorithm, the convective fluxes per unit mass F through cell faces are evaluated from so-called guessed velocity components. In addition to this, a guessed pressure field is used to solve the momentum equations and a pressure correction equation is solved to obtain a pressure correction field that is in turn used to update the velocity and pressure fields. Initial guesses for velocity and pressure fields are used in order to start the iteration process. The process is iterated until convergence of the velocity and pressure fields.

3.5.1 The Staggered Grid

The finite volume method starts with the discretisation of the relevant transport equations (3.56-58). Attention must be given to decide where velocities are stored. Defining velocities at the same locations as the scalar variables such as pressure, temperature etc. can be logical but this may lead a highly non-uniform pressure field to act like a uniform field in the discretised momentum equations. This can be illustrated with Figure 3.8 that is about the simple two-dimensional situation with a highly irregular "checker-board" pressure field.

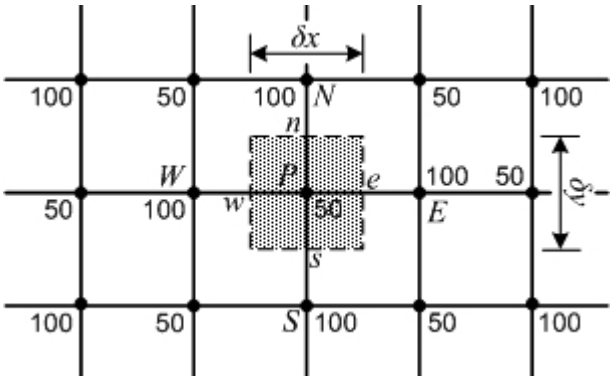


Figure 3.8 "checker-board" pressure field

If the pressure at "*e*" and "*w*" are obtained by linear interpolation, the pressure gradient term $\partial p/\partial x$ in the *u*-momentum equation is given by (Versteeg & Malalasekera, 1995, p. 137),

$$\frac{\partial p}{\partial x} = \frac{p_e - p_w}{\delta x} = \frac{\frac{(p_E + p_P)}{2} - \frac{(p_P + p_W)}{2}}{\delta x} = \frac{p_E - p_W}{2\delta x} \tag{3.59}$$

$\partial p/\partial y$ in the *v*-momentum equation is also given by,

$$\frac{\partial p}{\partial y} = \frac{p_N - p_S}{2\delta y} \tag{3.60}$$

According to Figure 3.8, equations (3.59-60) shows that all the discretised gradients of pressure are zero at nodal points although the pressure field exhibits spatial oscillations in both directions. As a result of this pressure field would give the zero momentum source in the discretised equations as a uniform pressure field. This situation is non-physical. The influence of pressure is not properly represented in the discretised momentum equations if the velocities are defined at scalar grid nodes. A remedy for this problem is to use a staggered grid for the velocity components (Harlow and Welch, 1965). The aim is to evaluate scalar variables at ordinary nodal points and to calculate velocity components on staggered grids centered around the cell faces. The arrangement for a two dimensional flow is shown in Figure 3.9.

The scalar variables are stored at the nodes marked (•). Velocities are defined at the scalar cell faces in between nodes and are indicated by arrows. Figure 3.9 also introduces a new system of notation based on a numbering of grid lines and cell faces. The unbroken grid lines are numbered by means of capital letters (…, *I*-1, *I*, *I*+1,..., *J*-1, *J*,*J*+1,…etc.) and the dashed lines that construct cell faces are denoted by lower case letters (…, *i*-1, *i*, *i*+1,..., *j*-1, *j*, *j*+1,…etc.). There is also a notation system to define the locations of grid nodes and cell faces with precision. Scalar nodes are defined by two capital letters like point *P* denoted by (*I*,*J*). The u-velocities are stored at the east and west cell faces of a scalar control volume. These are located at

the intersection of a line defining a cell boundary and a grid line and are defined by a combination of a lower case letter and a capital like the west face of the cell around point *P* denoted by (*i,J*). The *u*-velocities are stored at scalar cell faces "*e*" and "*w*" and the *v*-velocities at faces "*n*" and "*s*". The control volumes for *u* and *v* are different from the scalar control volumes and each other as shown in Figure 3.9.

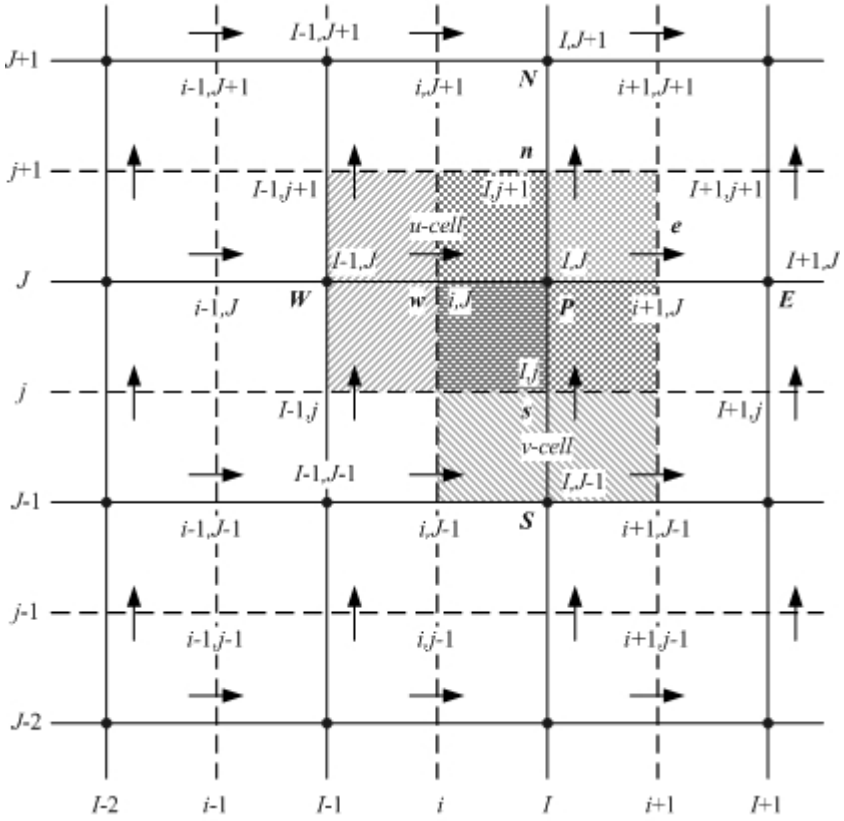


Figure 3.9 Staggered grid arrangement

The pressure nodes coincide with the cell face faces of the *u*-control volume in the staggered grid arrangement. The pressure gradient term $\partial p/\partial x$ is given by (Versteeg & Malalasekera, 1995, p. 138),

$$\frac{\partial p}{\partial x} = \frac{p_P - p_W}{\delta x_u} \tag{3.61}$$

where δx_u is the width of *u*-control volume.

$\partial p/\partial y$ for the *v*-control volume is also given by (Versteeg & Malalasekera, 1995, p. 138),

$$\frac{\partial p}{\partial y} = \frac{p_P - p_S}{\delta y_v} \tag{3.62}$$

where δy_v is the width of *v*-control volume. Substitution of the appropriate nodal pressure values into equations (3.61) and (3.62) now yields very significant non-zero pressure gradient terms according to the checker board pressure field at scalar control volume. Addition to this, staggered grid arrangement also generates velocities at exactly the locations where they are required for the scalar transport convection-diffusion equation. By this way, no interpolation is needed to calculate velocities at scalar faces.

3.5.2 The Momentum Equation

Forward or backward staggered velocity grids may be used for computations. In this case, the uniform grids in Figure 3.9 are backward staggered since the *i*-location for the *u*-velocity $u_{i,J}$ is at a distance of $1/2\delta x_u$ from the scalar node (*I,J*) and the *j*-location for the *v*-velocity $v_{I,j}$ is at a distance of $1/2\ \delta y_v$ from the scalar node (*I,J*). The discretised *u*-momentum equation for velocity at location (*i,J*) is given by (Versteeg & Malalasekera, 1995, p. 139),

$$a_{i,J}u_{i,J} = \sum a_{nb}u_{nb} - \frac{\left(p_{I,J} - p_{I-1,J}\right)}{\delta x_u}\Delta V_u + \bar{S}\Delta V_u$$

or

$$a_{i,J}u_{i,J} = \sum a_{nb}u_{nb} + \left(p_{I-1,J} - p_{I,J}\right)A_{i,J} + b_{i,J} \tag{3.63}$$

where ΔV_u is the volume of *u*-cell, $b_{i,J} = \bar{S}\Delta V_u$ is the momentum source term and $A_{i,J}$ is the cell face area of the *u*-control volume. The pressure gradient source term is now discretised by means of a linear interpolation between the pressure nodes

located at the *u*-control volume boundaries. The neighbours involved in the summation $\sum a_{nb}u_{nb}$ and prevailing velocities are as shown in Figure 3.10.

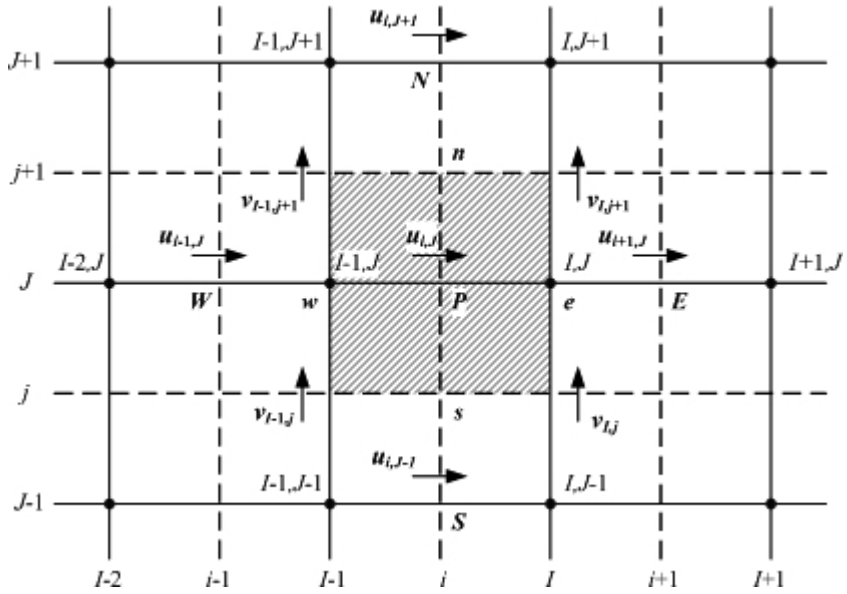


Figure 3.10 *u*-control volume and neighbouring velocity components

The values of coefficients $a_{i,J}$ and a_{nb} may be calculated with any of the differencing methods (upwind, hybrid, QUICK) suitable for convection and diffusion problems. The coefficients contain combinations of the convective flux per unit mass *F* and the diffusive conductance *D* at the *u*-control volume cell faces. By the usage of the new notation system, the values of F and D for each faces e, w, n and s of the u-control volume are (Versteeg & Malalasekera, 1995, p. 140):

$$F_w = (\rho u)_w = \frac{F_{i,J} + F_{i-1,J}}{2} = \frac{1}{2}\left[\left(\frac{\rho_{I,J} + \rho_{I-1,J}}{2}\right)u_{i,J} + \left(\frac{\rho_{I-1,J} + \rho_{I-2,J}}{2}\right)u_{i-1,J}\right] \quad (3.64a)$$

$$F_e = (\rho u)_e = \frac{F_{i+1,J} + F_{i,J}}{2} = \frac{1}{2}\left[\left(\frac{\rho_{I+1,J} + \rho_{I,J}}{2}\right)u_{i+1,J} + \left(\frac{\rho_{I,J} + \rho_{I-1,J}}{2}\right)u_{i,J}\right] \quad (3.64b)$$

$$F_s = (\rho v)_s = \frac{F_{I,j} + F_{I-1,j}}{2} = \frac{1}{2}\left[\left(\frac{\rho_{I,J} + \rho_{I,J-1}}{2}\right)v_{I,j} + \left(\frac{\rho_{I-1,J} + \rho_{I-1,J-1}}{2}\right)v_{I-1,j}\right] \quad (3.64c)$$

$$F_n = (\rho v)_n = \frac{F_{I,j+1} + F_{I-1,j+1}}{2} = \frac{1}{2}\left[\left(\frac{\rho_{I,J+1} + \rho_{I,J}}{2}\right)v_{I,j+1} + \left(\frac{\rho_{I-1,J+1} + \rho_{I-1,J}}{2}\right)v_{I-1,j+1}\right] \quad (3.64d)$$

$$D_w = \frac{\Gamma_{I-1,J}}{x_i - x_{i-1}} \tag{3.64e}$$

$$D_e = \frac{\Gamma_{I,J}}{x_{i+1} - x_i} \tag{3.64f}$$

$$D_s = \frac{\Gamma_{I-1,J} + \Gamma_{I,J} + \Gamma_{I-1,J-1} + \Gamma_{I,J-1}}{4\left(y_J - y_{J-1}\right)} \tag{3.64g}$$

$$D_n = \frac{\Gamma_{I-1,J+1} + \Gamma_{I,J+1} + \Gamma_{I-1,J} + \Gamma_{I,J}}{4\left(y_{J+1} - y_J\right)} \tag{3.64h}$$

A suitable two or four point average is formed over the nearest points where scalar variables or velocity components are not available at a *u*-control volume cell face. The *u*- and *v*-velocity components are used to evaluate above expressions during any iteration. These are obtained as the outcome of the previous iteration. These known *u*- and *v*-values contribute to the coefficients *a* in equation (3.63) and are distinct from $u_{i,J}$ and u_{nb} in this equation which denote the unknown scalars.

The discretised *v*-momentum equation for velocity at location (*I,j*) is given by (Versteeg & Malalasekera, 1995, p. 140),

$$a_{I,j} v_{I,j} = \sum a_{nb} v_{nb} + \left(p_{I,J-1} - p_{I,J}\right) A_{I,j} + b_{I,j} \tag{3.65}$$

The neighbours involved in the summation $\sum a_{nb} v_{nb}$ and prevailing velocities are as shown in Figure 3.11. The coefficients $a_{I,j}$ and a_{nb} also contain combinations of the convective flux per unit mass *F* and the diffusive conductance *D* at the *v*-control volume cell faces. Their values are (Versteeg & Malalasekera, 1995, p. 140):

$$F_w = (\rho u)_w = \frac{F_{i,J} + F_{i,J-1}}{2} = \frac{1}{2}\left[\left(\frac{\rho_{I,J} + \rho_{I-1,J}}{2}\right) u_{i,J} + \left(\frac{\rho_{I-1,J-1} + \rho_{I,J-1}}{2}\right) u_{i,J-1}\right] \tag{3.66a}$$

$$F_e = (\rho u)_e = \frac{F_{i+1,J} + F_{i+1,J-1}}{2} = \frac{1}{2}\left[\left(\frac{\rho_{I+1,J} + \rho_{I,J}}{2}\right) u_{i+1,J} + \left(\frac{\rho_{I,J-1} + \rho_{I+1,J+1}}{2}\right) u_{i+1,J-1}\right] \tag{3.66b}$$

$$F_s = (\rho v)_s = \frac{F_{I,j-1} + F_{I,j}}{2} = \frac{1}{2}\left[\left(\frac{\rho_{I,J-1} + \rho_{I,J-2}}{2}\right)v_{I,j-1} + \left(\frac{\rho_{I,J} + \rho_{I,J-1}}{2}\right)v_{I,J}\right] \tag{3.66c}$$

$$F_n = (\rho v)_n = \frac{F_{I,j} + F_{I,j+1}}{2} = \frac{1}{2}\left[\left(\frac{\rho_{I,J} + \rho_{I,J-1}}{2}\right)v_{I,j} + \left(\frac{\rho_{I,J+1} + \rho_{I,J}}{2}\right)v_{I,j+1}\right] \tag{3.66d}$$

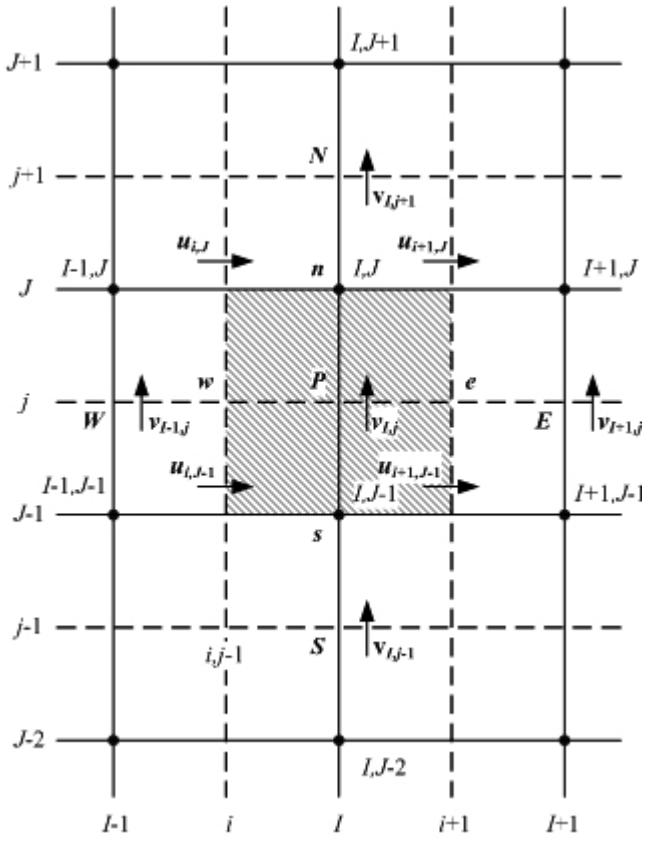


Figure 3.11 *v*-control volume and neighbouring velocity components

$$D_w = \frac{\Gamma_{I-1,J-1} + \Gamma_{I,J-1} + \Gamma_{I-1,J} + \Gamma_{I,J}}{4(x_I - x_{I-1})} \tag{3.66e}$$

$$D_e = \frac{\Gamma_{I,J-1} + \Gamma_{I+1,J-1} + \Gamma_{I,J} + \Gamma_{I+1,J}}{4(x_{I+1} - x_I)} \tag{3.66f}$$

$$D_s = \frac{\Gamma_{I,J-1}}{y_j - y_{j-1}} \tag{3.66g}$$

$$D_n = \frac{\Gamma_{I,J}}{y_{j+1} - y_j} \tag{3.66h}$$

Discretised momentum equations of the form (3.63) and (3.65) can be written for each *u*-and *v*-control volume for the given pressure field and then solved to obtain the velocity fields. If the pressure field is correct, the resulting velocity field satisfies continuity. A method is needed for calculating pressure as the pressure field is unknown.

3.5.3 The "SIMPLE" *Algorithm*

Expansion of SIMPLE is Semi-Implicit Method for Pressure-Linked Equations. The algorithm was originally put forward by Patankar and Spalding (1972) and is essentially a guess and correct procedure for the calculation of pressure on staggered grid arrangement. The method is illustrated by considering the two dimensional laminar steady flow equations in Cartesian coordinates. In order to initiate the SIMPLE calculation process, a pressure field *p** is guessed. Discretised momentum equations (3.63) and (3.65) are solved using the guessed pressure field to yield velocity components u* and v* as follows (Versteeg & Malalasekera, 1995, p. 142)

$$a_{i,J}u^*_{i,J} = \sum a_{nb}u^*_{nb} + \left(p^*_{I-1,J} - p^*_{I,J}\right)A_{i,J} + b_{i,J} \tag{3.67}$$

$$a_{I,j}v^*_{I,j} = \sum a_{nb}v^*_{nb} + \left(p^*_{I,J-1} - p^*_{I,J}\right)A_{I,j} + b_{I,j} \tag{3.68}$$

The correction *p*' is defined as the difference between the correct pressure field *p* and the guessed pressure field *p** (Versteeg & Malalasekera, 1995, p. 143):

$$p = p^* + p' \tag{3.69}$$

u' and *v*' velocity corrections are also defined in order to relate the correct velocities *u* and *v* to the guessed velocities *u** and *v** (Versteeg & Malalasekera, 1995, p. 143):

$$u = u^* + u' \tag{3.70}$$

$$v = v^* + v' \tag{3.71}$$

The correct velocity field (u,v) can be obtained by means of substitution of the correct pressure field p into the momentum equations. Discretised equations (3.63) and (3.65) links the correct velocity fields with the correct pressure field. Subtraction of (3.67) and (3.68) from (3.63) and (3.65) gives (Versteeg & Malalasekera, 1995, p. 143):

$$a_{i,J}\left(u_{i,J}-u^{*}_{i,J}\right)=\sum a_{nb}\left(u_{nb}-u^{*}_{nb}\right)+\left[\left(p_{I-1,J}-p^{*}_{I-1,J}\right)-\left(p_{I,J}-p^{*}_{I,J}\right)\right]A_{i,J} \tag{3.72}$$

$$a_{I,j}\left(v_{I,j}-v^{*}_{I,j}\right)=\sum a_{nb}\left(v_{nb}-v^{*}_{nb}\right)+\left[\left(p_{I,J-1}-p^{*}_{I,J-1}\right)-\left(p_{I,J}-p^{*}_{I,J}\right)\right]A_{I,j} \tag{3.73}$$

Substitution of equations (3.69-71) into equations (3.72-73) yields,

$$a_{i,J}u'_{i,J}=\sum a_{nb}u'_{nb}+\left(p'_{I-1,J}-p'_{I,J}\right)A_{i,J} \tag{3.74}$$

$$a_{I,j}v'_{I,j}=\sum a_{nb}v'_{nb}+\left(p'_{I,J-1}-p'_{I,J}\right)A_{I,j} \tag{3.75}$$

In order to simplify equations 3.74 and 3.75 for velocity corrections, $\sum a_{nb}u'_{nb}$ and $\sum a_{nb}u'_{nb}$ are dropped. Omission of these terms is the main approximation of the SIMPLE algorithm (Versteeg & Malalasekera, 1995, p. 143):

$$u'_{i,J}=d_{i,J}\left(p'_{I-1,J}-p'_{I,J}\right) \qquad \text{where} \qquad d_{i,J}=\frac{A_{i,J}}{a_{i,J}} \tag{3.76}$$

$$v'_{I,j}=d_{I,j}\left(p'_{I,J-1}-p'_{I,J}\right) \qquad \text{where} \qquad d_{I,j}=\frac{A_{I,j}}{a_{I,j}} \tag{3.77}$$

Similar expressions exist for $u_{i+1,J}$ and $v_{I,j+1}$:

$$u_{i+1,J}=u^{*}_{i+1,J}+d_{i+1,J}\left(p'_{I,J}-p'_{I+1,J}\right) \qquad \text{where} \qquad d_{i+1,J}=\frac{A_{i+1,J}}{a_{i+1,J}} \tag{3.78}$$

$$v_{I,j+1}=v^{*}_{I,j+1}+d_{I,j+1}\left(p'_{I,J}-p'_{I,J+1}\right) \qquad \text{where} \qquad d_{I,j+1}=\frac{A_{I,j+1}}{a_{I,j+1}} \tag{3.79}$$

Thus far, only the momentum equations are considered but the velocity field is also subject to the constraint that it should satisfy the continuity equation (3.58). Continuity is satisfied in the discretised form for the scalar volume as shown in Figure 3.12.

$$\left[(\rho uA)_{i+1,J} - (\rho uA)_{i,J}\right] + \left[(\rho vA)_{I,j+1} - (\rho vA)_{I,j}\right] = 0 \tag{3.81}$$

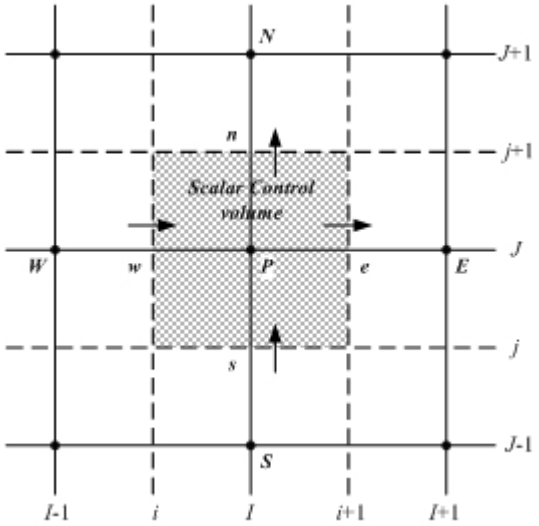


Figure 3.12 the scalar control volume used for the discretisation of the continuity equation

Substitution of the correct velocities of equations (3.78-79) into discretised continuity equation (3.81) and some arrangements yield (Versteeg & Malalasekera, 1995, p. 144),

$$\left[(\rho dA)_{i+1,J} + (\rho dA)_{i,J} + (\rho dA)_{I,j+1} + (\rho dA)_{I,j}\right] p'_{I,J}$$

$$= (\rho dA)_{i+1,J}\, p'_{I+1,J} + (\rho dA)_{i,J}\, p'_{I-1,J} + (\rho dA)_{I,j+1}\, p'_{I,J+1} + (\rho dA)_{I,j}\, p'_{I,J-1}$$

$$+ \left[(\rho u^* A)_{i,J} - (\rho u^* A)_{i+1,J} - (\rho v^* A)_{I,j} - (\rho v^* A)_{I,j+1}\right] \tag{3.81}$$

The coefficients of p' may be written as (Versteeg & Malalasekera, 1995, p. 145),

$$a_{I,J}p'_{I,J} = a_{I+1,J}p'_{I+1,J} + a_{I-1,J}p'_{I-1,J} + a_{I,J+1}p'_{I,J+1} + a_{I,J-1}p'_{I,J-1} + b'_{I,J} \tag{3.82}$$

where $a_{I,J} = a_{I+1,J} + a_{I-1,J} + a_{I,J+1} + a_{I,J-1}$

and the coefficients are ,

$a_{I+1,J}$	$a_{I-1,J}$	$a_{I,J+1}$	$a_{I,J-1}$	$b'_{I,J}$
$(\rho dA)_{i+1,J}$	$(\rho dA)_{i,J}$	$(\rho dA)_{I,j+1}$	$(\rho dA)_{I,j}$	$(\rho u^* A)_{i,J} - (\rho u^* A)_{i+1,J} + (\rho v^* A)_{I,j} - (\rho v^* A)_{I,j+1}$

The discretised continuity equation (3.82) is used as an equation for pressure correction p'. The source term b' in the equation is the continuity imbalance arising from the incorrect velocity field u^*, v^*. The pressure correction field p' can be obtained at all points by solving equation (3.82). By this way the correct pressure field may be obtained using formula (3.69) and velocity components through correction formula (3.78-79). The final solution is not affected by the omission of terms in equations (3.74) and (3.75) at derivation in order that the pressure and velocity corrections will all be zero in a converged solution giving $p^* = p$, $u^* = u$ and $v^* = v$. In addition to pressure correction equation, some **under relaxation** is used during the iterative process because of its being susceptible to divergence. New, improved, pressures p^{new} are obtained with (Versteeg & Malalasekera, 1995, p. 145),

$$p^{new} = p^* + \alpha_p p' \tag{3.83}$$

where α_p is the pressure under-relaxation factor. Taking α_p between 0 and 1 yields to add to guessed field p^* a fraction of the correction field p' that is large enough to move iterative improvement process forward but small enough to ensure stable computation.

The velocities are also under-relaxed. The iteratively improved velocity components u^{new} and v^{new} are obtained from (Versteeg & Malalasekera, 1995, p. 145):

$$u^{new} = \alpha_u u + (1-\alpha_u)u^{(n-1)} \tag{3.84}$$

$$v^{new} = \alpha_v v + (1-\alpha_v)v^{(n-1)} \tag{3.85}$$

where α_u *and* α_v are the *u*- and *v*-velocity under-relaxation factors with values between 0 and 1. *u* and *v* are the corrected velocity components without relaxation and $u^{(n-1)}$ and $v^{(n-1)}$ represent their values obtained in the previous iteration. After some substitution and arrangement, the discretised *u*-momentum equation with under-relaxation takes the form of (Versteeg & Malalasekera, 1995, p. 145),

$$\frac{a_{i,J}}{\alpha_u}u_{i,J} = \sum a_{nb}u_{nb} + (p_{I-1,J} - p_{I,J})A_{i,J} + b_{i,J} + \left[(1-\alpha_u)\frac{a_{i,J}}{\alpha_u}\right]u_{i,J}^{(n-1)} \tag{3.86}$$

and the discretised *v*-momentum equation is,

$$\frac{a_{I,j}}{\alpha_v}v_{I,j} = \sum a_{nb}v_{nb} + (p_{I,J-1} - p_{I,J})A_{I,j} + b_{I,j} + \left[(1-\alpha_v)\frac{a_{I,j}}{\alpha_v}\right]v_{I,j}^{(n-1)} \tag{3.87}$$

The pressure correction equation is also affected by velocity under relaxation and the d-terms of pressure correction equation become (Versteeg & Malalasekera, 1995, p. 146):

$$d_{i,J} = \frac{A_{i,J}\alpha_u}{a_{i,J}}, \quad d_{i+1,J} = \frac{A_{i+1,J}\alpha_u}{a_{i+1,J}}, \quad d_{I,j} = \frac{A_{I,j}\alpha_v}{a_{I,j}} \quad \text{and} \quad d_{I,j+1} = \frac{A_{I,j+1}\alpha_v}{a_{I,j+1}}$$

A correct choice of under relaxation factors α is essential for cost-effective simulations. Too large value of α may lead to oscillatory or even divergent iterative solutions and a value that is too small will cause extremely slow convergence. The optimum values of under-relaxation factors are flow dependent and must be sought

on a case-by-case basis. The SIMPLE algorithm gives a method of calculating pressure and velocities. The method is iterative the calculation needs to be done sequentially when other scalars are coupled to the momentum equation. The sequence of operations in a CFD procedure which employs the SIMPLE algorithm is shown in Figure 3.13.

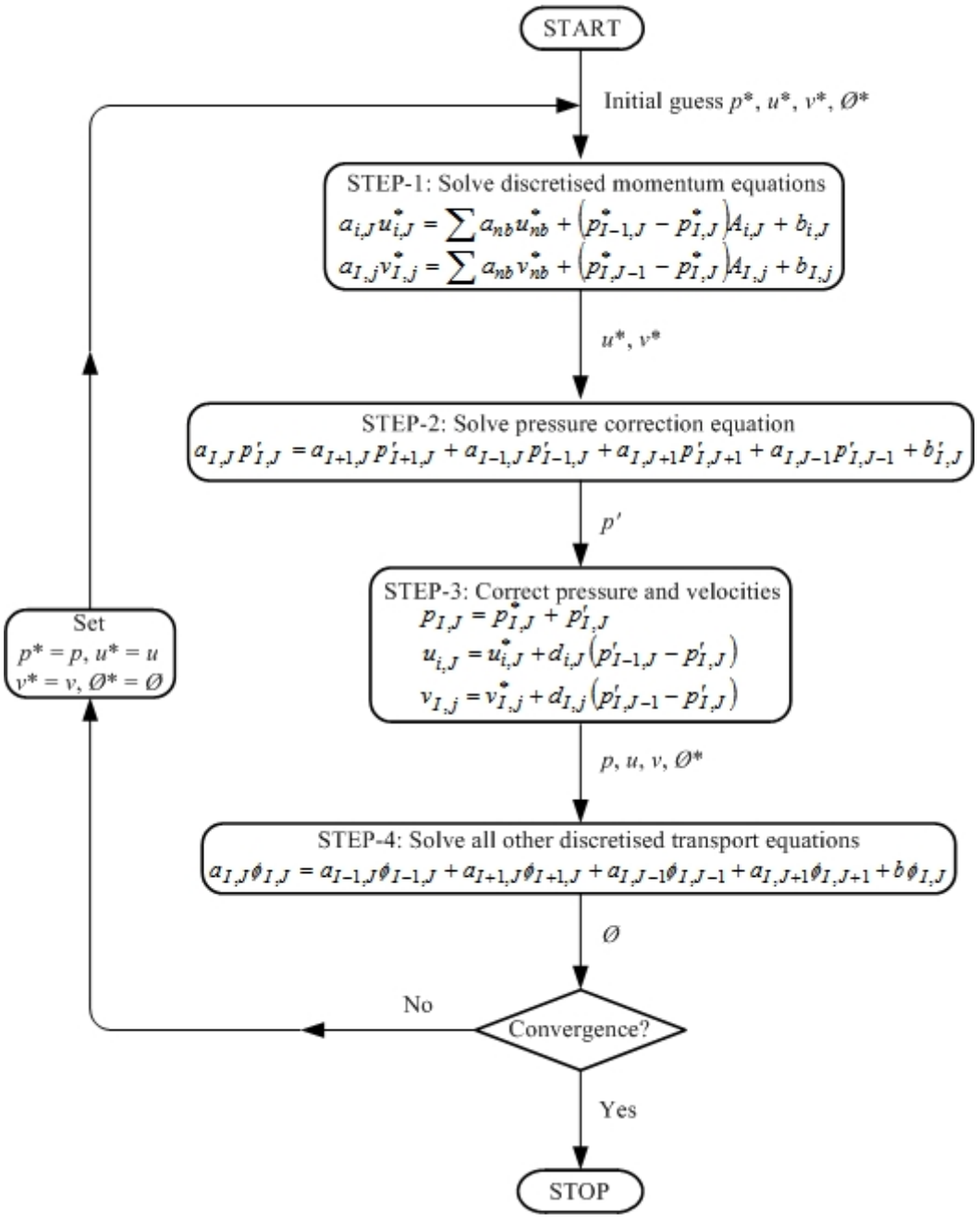


Figure 3.13 The "SIMPLE" algorithm

3.5.4 The "SIMPLEC" *Algorithm*

The SIMPLEC (SIMPLE-Consistent) algorithm of Van Doormal and Raithby (1984) follows the same steps as the SIMPLE algorithm with the difference that the momentum equations are manipulated so that the SIMPLEC velocity correction equations omit terms that are less significant than those omitted in SIMPLE. The *u*-velocity correction equation of SIMPLEC is given by (Versteeg & Malalasekera, 1995, p. 148),

$$u'_{i,J} = d_{i,J}\left(p'_{I-1,J} - p'_{I,J}\right) \qquad \text{where} \qquad d_{i,J} = \frac{A_{i,J}}{a_{i,J} - \sum a_{nb}} \tag{3.88}$$

Similarly the modified *v*-velocity correction equation is,

$$v'_{I,j} = d_{I,j}\left(p'_{I,J-1} - p'_{I,J}\right) \qquad \text{where} \qquad d_{I,j} = \frac{A_{I,j}}{a_{I,j} - \sum a_{nb}} \tag{3.89}$$

The discretised pressure correction equation is the same as in SIMPLE, except that the *d*-terms are calculated from equations (3.88) and (3.89). The sequence of operations of the SIMPLEC algorithm is identical to that of SIMPLE shown in Figure 3.13.

Another improved version of SIMPLE algorithm is SIMPLER (SIMPLE Revised) algorithm that was developed by Patankar (1980). In this algorithm, the discretised continuity equation (3.80) is used to derive a **discretised equation of pressure** in stead of a pressure correction equation as in SIMPLE. In addition to these algorithms, Issa (1986) developed the PISO (Pressure Implicit with Splitting of Operators) algorithm originally for non-iterative computation of unsteady compressible flows. The PISO algorithm has been adapted successfully for iterative solution of steady state problems. PISO involves one predictor step and two corrector steps and can be thought to be an extension of SIMPLE with a **further corrector step** to enhance it.

CHAPTER FOUR
NUMERICAL STUDY

4.1 Steel Panel Radiator

The numerical study is based on a domestic radiator that is in accordance with the standard TS EN442. The radiator is in PCCP (panel-convector-convector-panel) arrangement. In order to show the details of the radiator more exactly, radiator is divided into two parts from the middle of its fittings. For this radiator, the installation of the fitting is in TBOE (top-bottom-opposite-end) arrangement. A panel consists of two panel leaves and these leaves are formed by means of pressing steel sheets. Two panel leaves are assembled by means of welding them along their perimeter. Panels are made of steel sheet with thickness of 1.15 mm in accordance with DIN EN 10130. The module length of the radiator is 33.33 mm long. Panel section and module length of the radiator are shown in Figure 4.1.

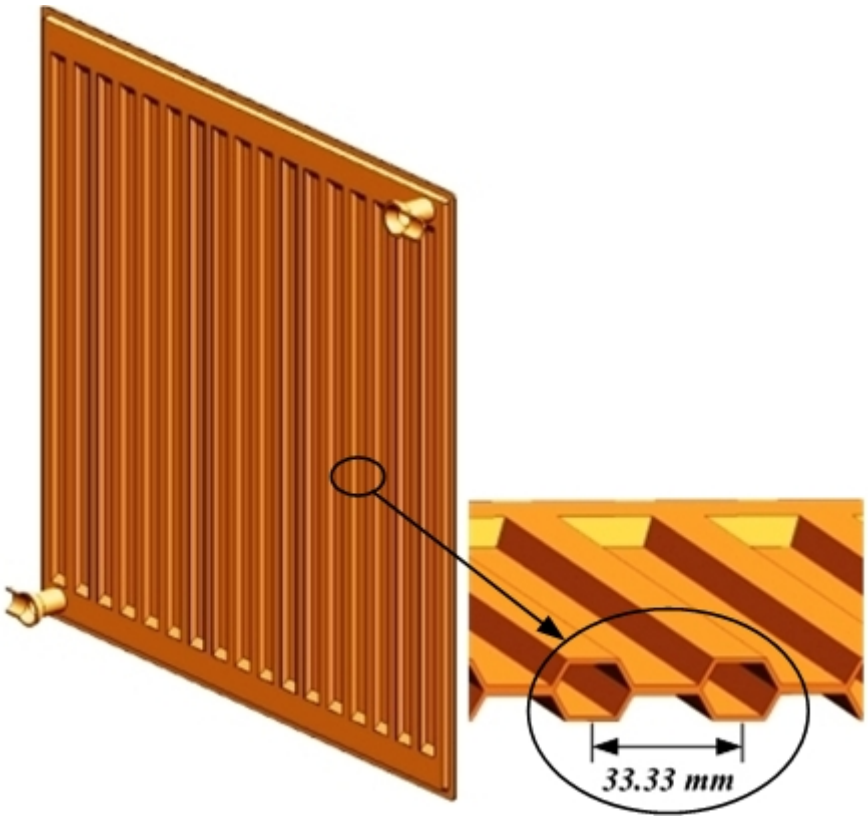


Figure 4.1 Panel section of a half radiator and its module length

The size of the panel radiator used for numerical study is H×L×W = 600×600×104 mm. The convector form of the panel radiator is shown in Figure 4.2. Convectors are made of steel sheet with thickness of 0.7 mm in accordance with DIN EN10130 and are formed by means of pressing steel sheets. As seen in Figure 4.2, the height of the convector is not uniform. In order to increase the heat transfer area of the convector, the height of the convector is higher than usual convectors nearly as high as the height of panel radiator. On the other hand, this leads problems at the installation of T-Fittings. In order to prevent the difficulties at the installation of T-Fittings, the height of the convector is reduced around the installation regions or the corners of the panel radiator. Panels and convector are assembled each other by means of centre welding. The assembly of panel and convector seen in Figure 4.2 is a half part of the whole panel radiator. By taking the symmetry of the panel and convector assembly and combining them each other, numerical model (PCCP type radiator) can be formed.

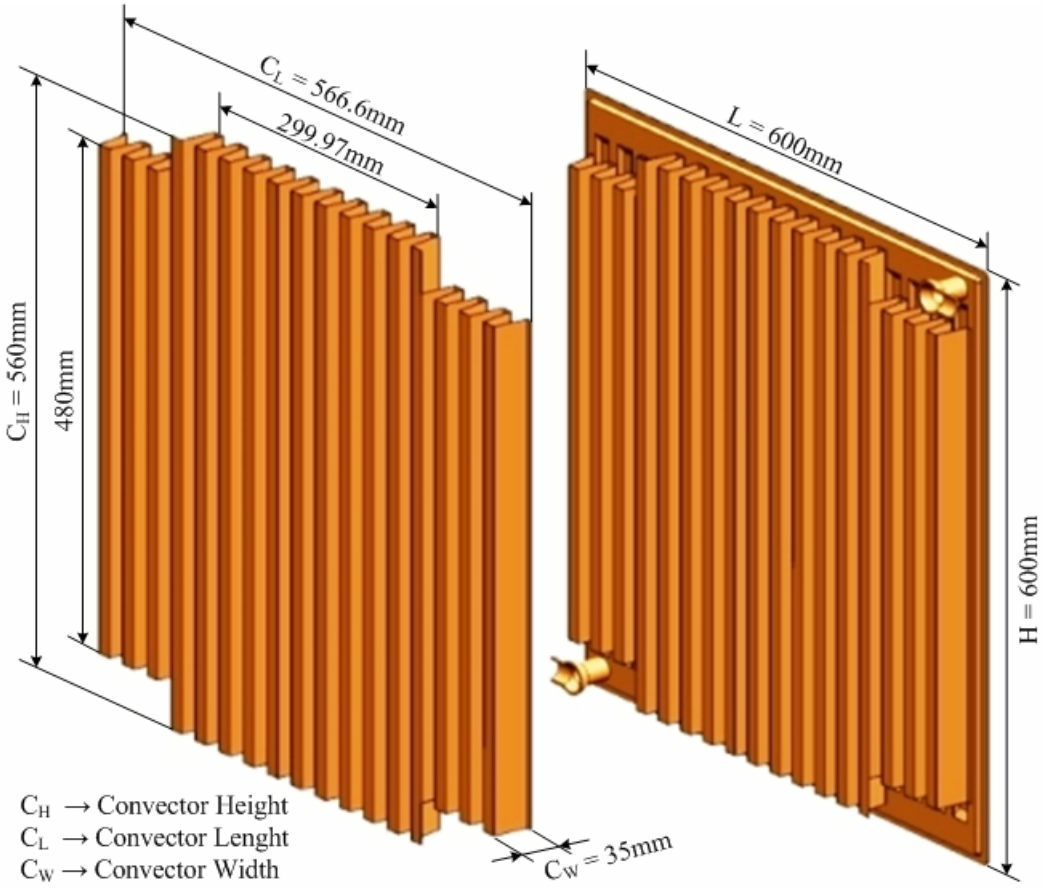


Figure 4.2 Convector section of a half radiator and its assembly with panel

4.1.1 Pre-processing

Pre-processing of the numerical study was performed at GAMBIT (default pre-processing unit of FLUENT). The model meshed on pre-processing section was prepared by the means of a computer aided design program (UniGraphics) and imported as parasolid into the GAMBIT. Model consists of four volumes. These are respectively panel (shell side), water (tube side) and two convectors assembled on panel. The meshing scheme used for the model is tetrahedral meshing scheme. The complexity of the model yields the usage of this meshing scheme. Two types of volume element can be generated by means of tetrahedral volume meshing scheme depending on the number of nodes used. Four or ten nodes can be used at this kind of volume meshing scheme. Tetrahedral volume meshing scheme with four nodes was used for volume meshing. By the help of these four nodes, pyramids are obtained as the volume element. Panel section of the radiator was meshed with interval size of 4.18. As a consequence of this, the volume "panel" including 208896 nodes was obtained. A part of the meshed volume is shown in Figure 4.3 in order to show the mesh density and volume meshing scheme. The fin bases can be easily seen as rectangles at the inner surface of the panel. Continuum (volume) type is specified as solid for the panel and two boundary conditions are specified as wall for the panel.

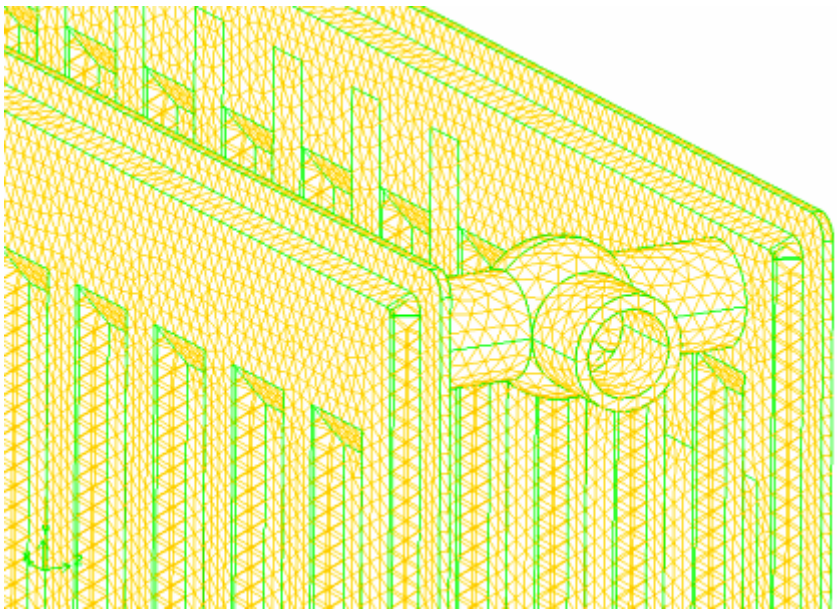


Figure 4.3 Partial view of shell side mesh

Two boundary faces were specified at inlet and outlet of the T-Fittings and were aligned with the inlet and outlet faces of fluid flow. The fluid flow region was modeled as a solid. Figure 4.4 shows the mesh type and the mesh density of the fluid flow region. The fluid flow region was meshed with four nodes tetrahedral volume meshing scheme as done for the panel. The interval size of the tetrahedral meshing scheme is same as the panel. By this type of volume meshing, the continuum was formed with 101045 nodes. The continuum type was specified as fluid. Two boundary face conditions were also specified for the fluid. These boundary face conditions are respectively mass flow inlet and outflow. Mass flow inlet was specified for the inlet T-fitting as fluid flow condition and outflow was specified for the outlet T-Fitting as fluid outflow condition.

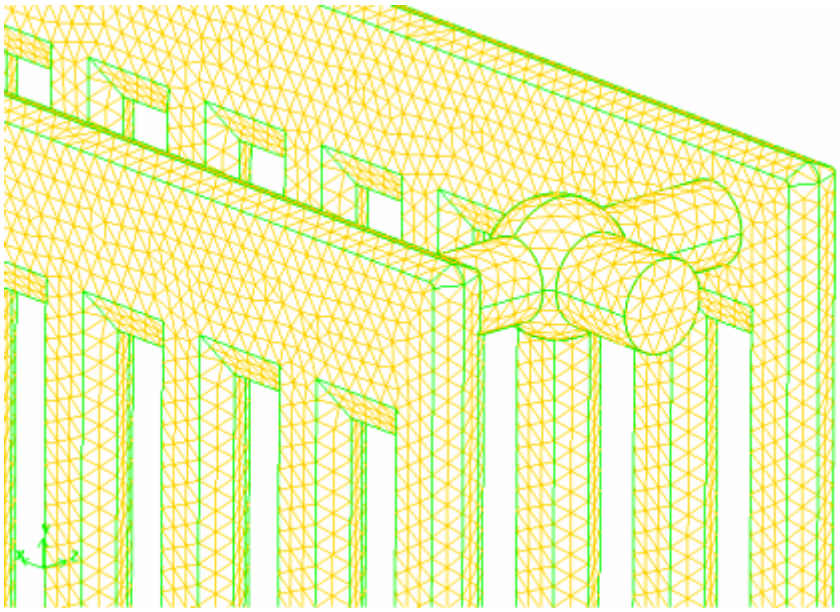


Figure 4.4 Partial view of tube side mesh

Convectors were separately modeled from panel in order to reach the data at fin bases. By this way, fin heat capacity can be obtained separately from panel. Convectors were also meshed with four nodes tetrahedral volume meshing scheme and with interval size of 4.18 as specified in panel and fluid section. The continuums were formed with an average node number of 110858 nodes. The continuum type was specified as solid.

There are no boundary conditions specified for convectors. Convectors were separately modeled from panel but they are in face contact with panel by the help of panel faces at fin bases. The meshing scheme and the density are shown in Figure 4.5.

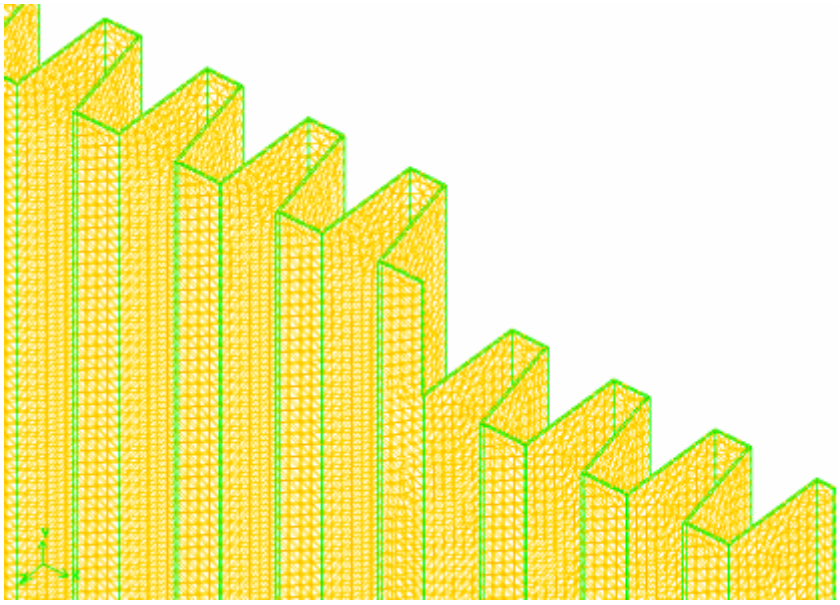


Figure 4.5 Partial view of convector mesh

Outer faces of the continuums were not specified at the pre-processing section. The processor automatically analyses the contact regions.

4.1.2 Processing

Numerical model described in previous section is now used for processing in order to obtain the effects of variation at the ambient convective heat transfer coefficient on the thermal output of the radiator. Computational fluid dynamics program FLUENT was used as processing. FLUENT uses finite volume method in order to obtain numerical solutions. Thermal output of the radiator was measured at inlet and outlet temperatures respectively, 75ºC and 65ºC in accordance with TS EN 442. During this numerical study, inlet water temperature and mass flow rate were fixed. Inlet water temperature was specified as 75ºC as described in TS EN 442. The mass flow rate was obtained from the experimental thermal output of the radiator by

using the energy balance equation. In order to obtain the effects of variation at ambient heat transfer coefficient on the thermal output of the radiator, ambient heat transfer coefficient was respectively specified as 10 W/m^{2}K, 9 W/m^{2}K, 8 W/m^{2}K and 6 W/m^{2}K.

The grid used for numerical study is composed of 1686929 cells, 3872387 faces and 522428 nodes. 3D, segregated, implicit, steady solver was used with laminar viscous model. Energy equation was turned on because of the thermal analysis. The outer surface region of the panel and convectors was in contact with an ambient at 20ºC. During the calculation, forced convection model was used to obtain the heat fluxes from the surfaces that are in contact with the ambient. By means of forced convection model, outlet water temperature was specified according to the fixed inlet temperature. Depending on this, thermal output was also specified. Boundary condition types and inputs are listed in Table 4.1.

Table 4.1 Boundary conditions

Zone	Type	Properties	Inputs
Inlet	Mass Flow Inlet	Mass flow rate	0.0245 kg/s
		Total temperature	75ºC
		Direction type	normal to the boundary
Outlet	Outflow	----------	No input
Adiabatic	Wall	Heat flux	0
		Material	steel
		Position	inlet and outlet T-Fittings
Outer surface of Water	Wall	Thermal condition	coupled
		Material	liquid water
Outer surface of Panel	Wall	Thermal condition	convection
		Heat transfer coefficient	6 W/m^{2}K
		Free stream temperature	20ºC
		Material	steel
Outer surface of convectors	Wall	Thermal condition	convection
		Heat transfer coefficient	6 W/m^{2}K
		Free stream temperature	20ºC
		Material	steel

Material properties are listed in Table 4.2 and taken from the database of processing program FLUENT.

Table 4.2 Material properties

Material Type	Density (kg/m^3)	Specific Heat Capacity (J/kg K)	Thermal Conductivity (W/m K)	Viscosity (kg/m s)
Water	998.2	4182	0.6	0.001003
Steel	8030	502.48	16.27	-

4.2 Convector Designs

The radiator panels and convectors are manufactured by means of pressing steel sheets. The formed whole radiator consists of repeated sections. These sections are called as "radiator module". In order to investigate the thermal output of the radiator against the implementation of new convector designs, a radiator module was used for numerical study instead of the whole radiator. Radiator module dimensions and half of the PCCP type radiator are shown in Figure 4.6. Radiator module and convector are respectively abbreviated as "M" and "C". Subscripts are related with dimensions.

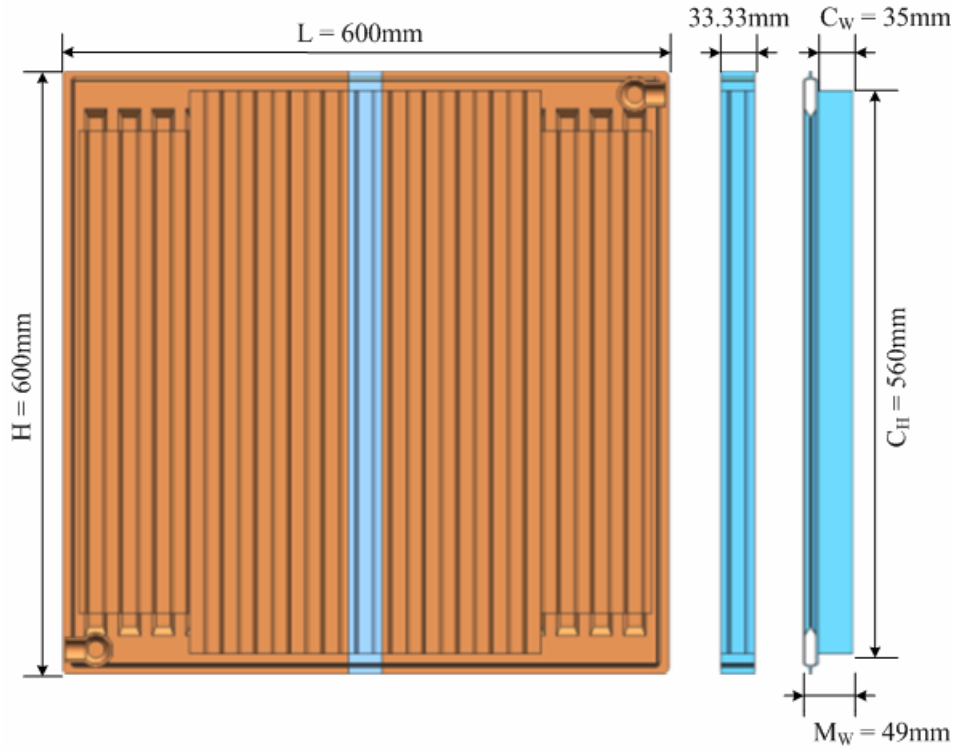


Figure 4.6 Dimensions of radiator module (M_W → Module width)

Dimensions of a module is H×L×W = 600×33.33×49 mm. According to this module length, a PCCP type radiator that is used for the numerical study consists of 36 modules. 18 modules form the half of the whole radiator as shown in Figure 4.6. A module is formed by two parts. These parts are panel section and convector section. The material for the panel section is steel sheet with thickness of 1.15 mm in accordance with DIN EN10130. Dimensions for the panel section is H×L×W = 600×33.33×14 mm. The material of the convector section is steel sheet with thickness of 0.7 mm in accordance with DIN EN10130. Dimensions of the convector section is H×L×W = 560×33.33×35 mm.

The thermal output of a module is computed from the heat transfer rates from panel section and convector section. In order to increase thermal output, the design of the panel section was fixed and convector designs were created. During creation of convector designs, convector material, height, length and width were not changed. According to the fix values of original design, the major changes were taken place at the cross-sectional area of the convector section. Original design and other convector designs are shown in Figure 4.7-4.11.

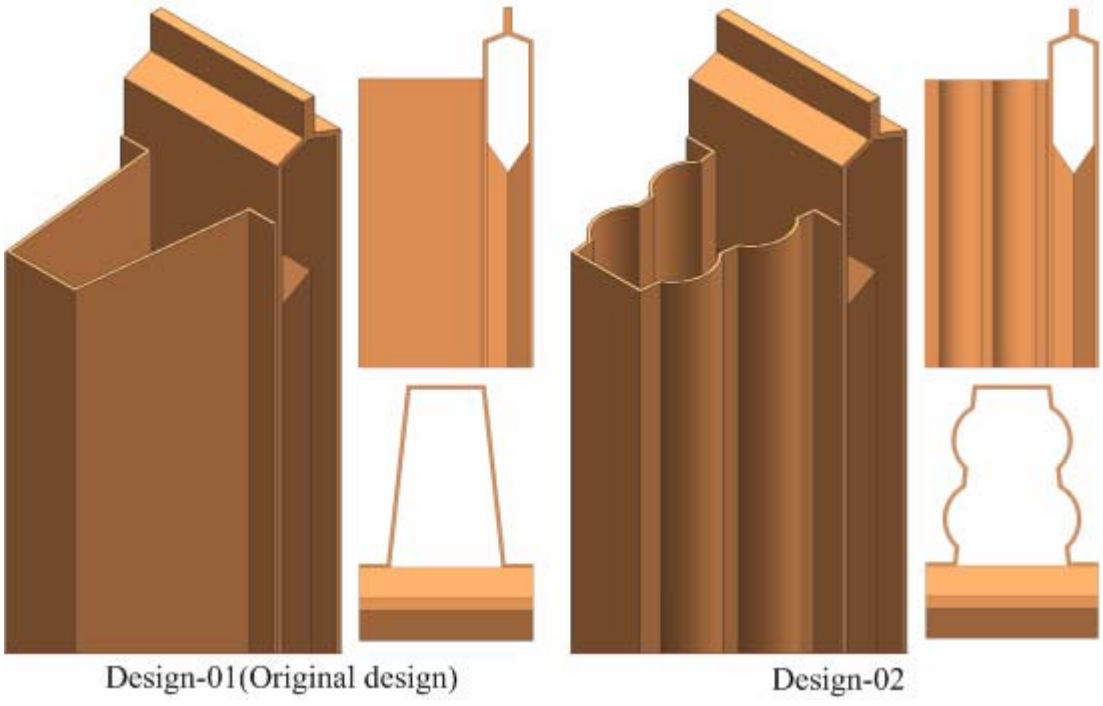


Figure 4.7 Partial views of Design-01(original design) and Design-02

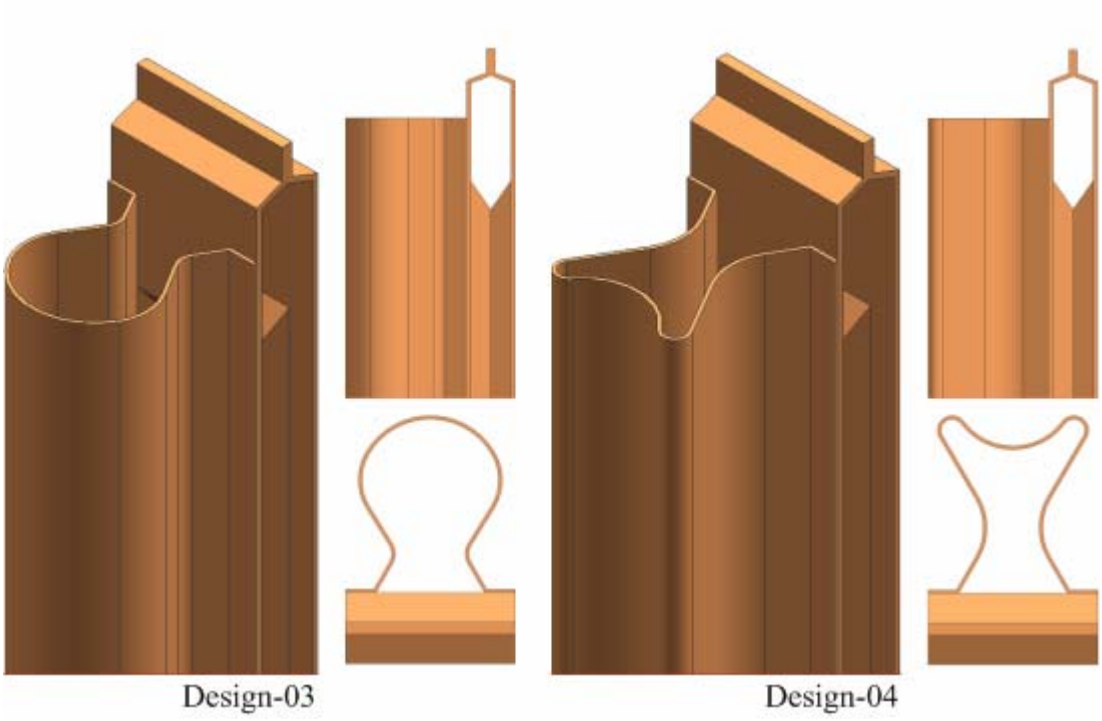


Figure 4.8 Partial views of Design-03 and Design-04

The contact faces (fin base areas) between convector and panel are in same dimensions at all designs except for Design-09.

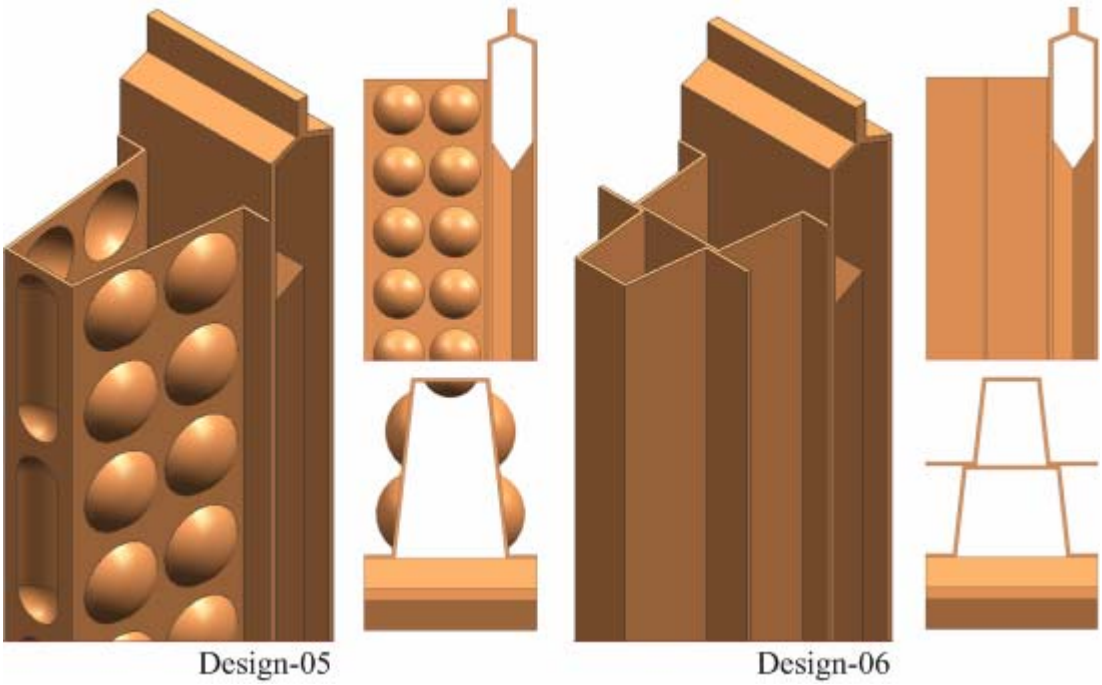


Figure 4.9 Partial views of Design-05 and Design-06

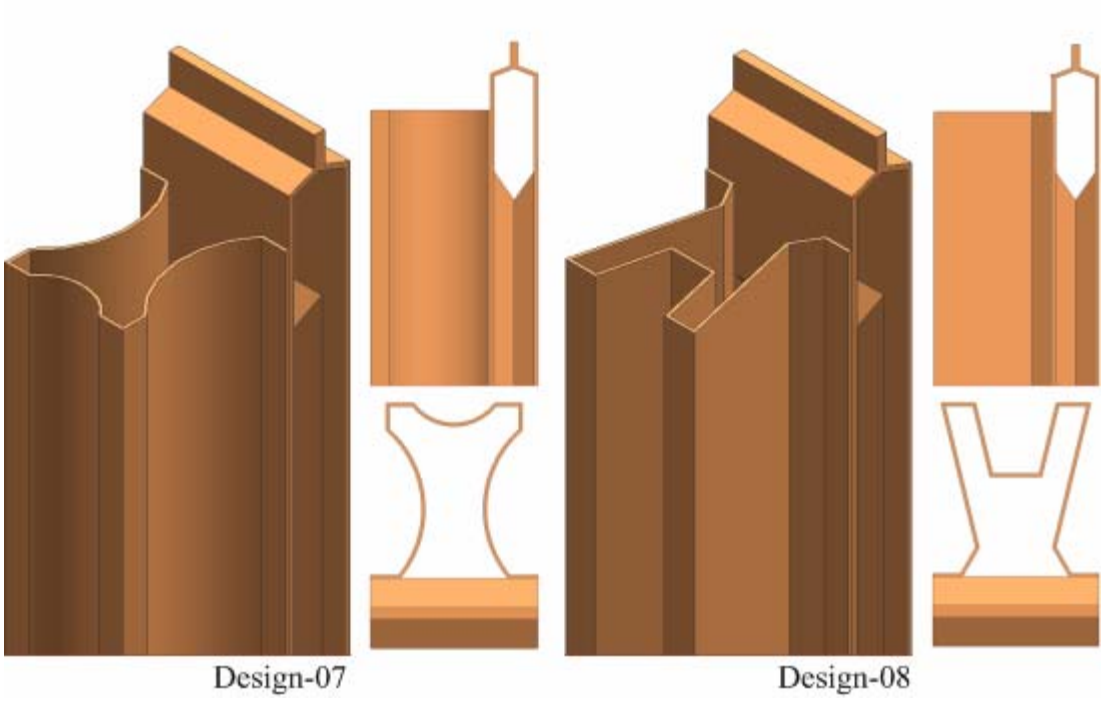


Figure 4.10 Partial views of Design-07 and Design-08

Design-09 differs from other designs due to the height of the convector and the contact faces that were formed between panel and convector as shown in Figure 4.11. Three contact faces were formed rather than two contact faces at other designs.

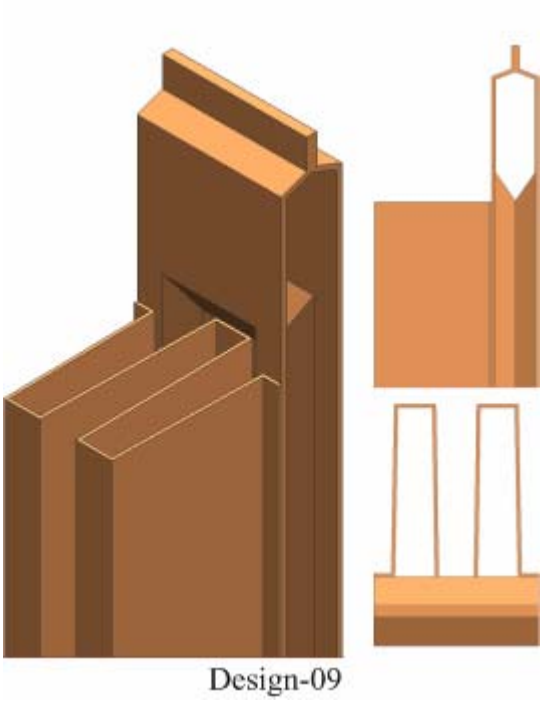


Figure 4.11 Partial view of Design-09

Generally, changes at the new convector designs are at the cross-section area. In addition to changes at the cross-sectional area, the changes at the design-05 and -06 differ from other convector designs. In order to see the effect of pops on the convector surface to the thermal output of the module, Design-05 was created by fixing the cross-sectional area whilst making modifications on the surface of the convector section. A cascade convector form was used for the Design-06. Convector consisted of two similar parts. The major aim was to obtain a flat surface between two convectors. By means of base section of the upper convector part, a flat surface could be obtained between two convectors.

4.2.1 Pre-processing

Pre-processing process was performed with GAMBIT. The models used for pre-processing was created by means of a computer aided design program and imported as parasolid into the GAMBIT. Two different numerical models were formed for processing section due to the investigation of thermal output of a module against fix temperature at the inner surface of the panel and the condition that fluid flow existed in the panel. Representative panel mesh and fluid flow mesh is shown in Figure 4.12 to represent the meshing scheme used for panel section and fluid flow of a module.

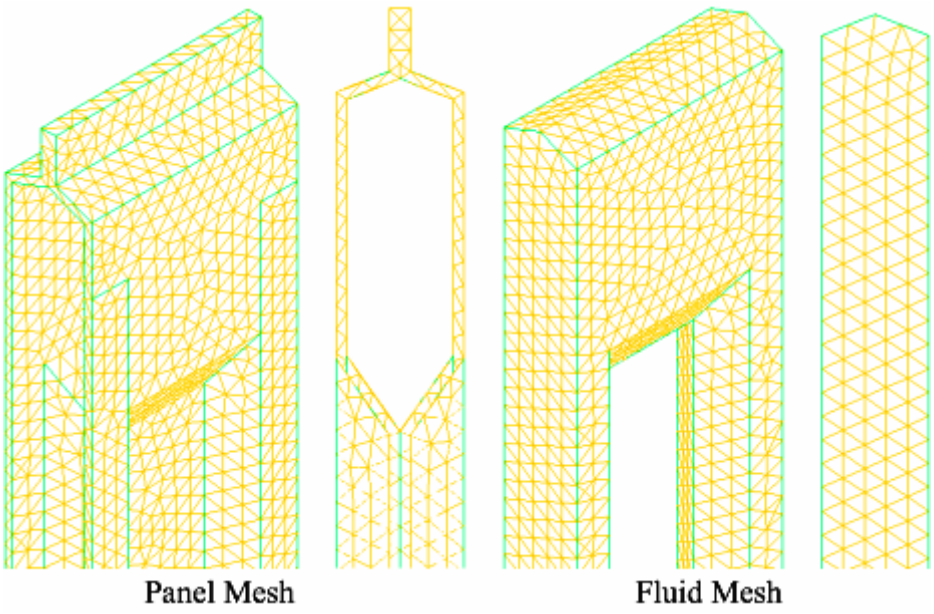


Figure 4.12 Partial views of panel mesh and fluid mesh

Fluid flow section was modeled as a continuum. By the help of boundary conditions and continuum type sections, fluid flow section is analyzed by processing program as fluid flow occurs at this continuum. Tetrahedral meshing scheme with four nodes was used for volume meshing. Figure 4.12 is representative for the reason that interval size of meshing scheme changes depending on the convector design and this yields changes at the interval size of the mesh used for panel and fluid flow sections. The contact face between panel and convector is seen as rectangle in Figure 4.12. Two boundary conditions were specified for the panel and the fluid flow section of the module. Faces at the right and left of the module is the contact faces with another module. Therefore, faces at the right and left of the panel and fluid flow sections were specified as symmetry boundary condition. Panel was specified as solid and fluid flow was specified as fluid.

Partial views of meshed convector designs are shown in Figure 4.13, 4.14 and 4.15. Tetrahedral meshing scheme with four nodes was used for volume meshing in order to provide unity at the meshing scheme for the whole model. The mesh densities differ from design to design due to the implementation of different interval size of tetrahedral meshing scheme. The discrepancies at the mesh densities are arisen from the design of the convectors. Small rectangle faces at the right and left of the convectors are the contact faces with another convector. Two boundary conditions were specified as symmetry for convectors.

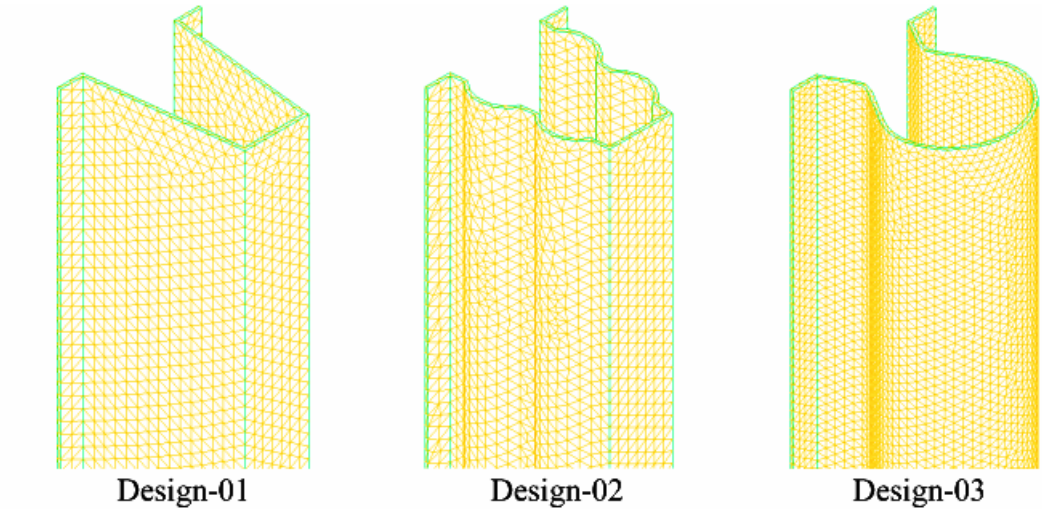


Figure 4.13 Partial views of Design-01, -02 and -03 mesh

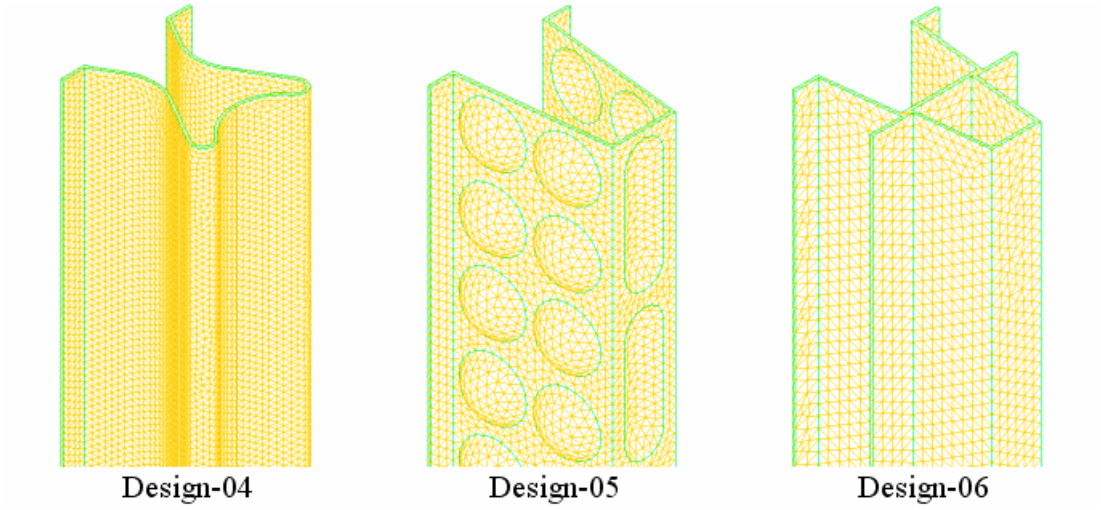


Figure 4.14 Partial views of Design-04, -05 and -06 mesh

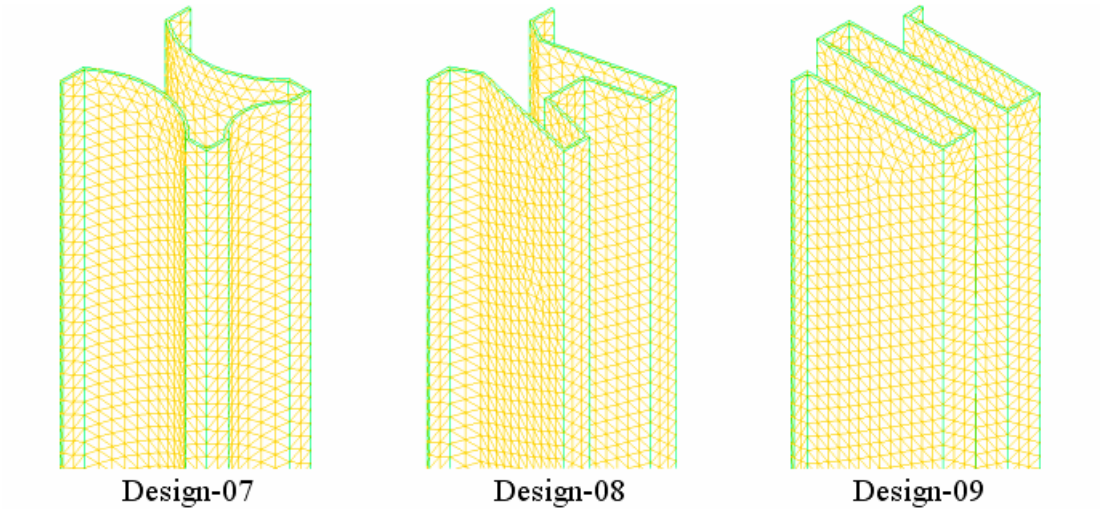


Figure 4.15 Partial views of Design-07, -08 and -09 mesh

First six convector designs (Design-01, -02, -03, -04, -05 and -06) were aimed to be used for analyses that fluid flow existed at the inner surface of the module. Due to the complexity of the numerical model going to be used for analyses that fluid flow existed at the inner surface of the module, Design-02, -03, -04 and -05 could not be used. For this reason, Design-07, -08 and -09 were designed in addition to six convector designs. Design-07 and -08 are the modified versions of Design-04 as seen Figure 4.14. Major change takes effect at top corners for Design-07 and at depth of the top arc and top corners for Design-08. The utilization of three contact faces rather than two contact faces forms the major change for Design-09. Half of numerical model used for fluid flow inside the module is shown in Figure 4.16.

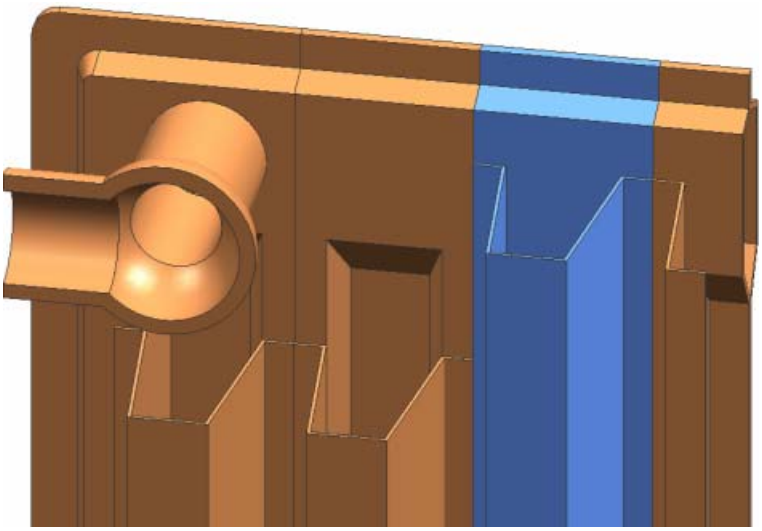


Figure 4.16 Model used for fluid flow inside the module

Half of the numerical model is the combination of four modules with short convectors, two modules with normal height convectors (blue region seen in Figure 4.16) and two half modules with normal height convectors. By this way, thermal output of the modules with short convectors can be computed whilst processing the numerical model. Numerical models were created for Design-01, -06, -07, -08 and -09. The amount of nodes and elements for convector designs are listed in Table 4.3. The smallest interval size was used for Design-04. Design-03, -04 and -05 whose interval sizes are smaller than two among the first six convector designs could not be used for the analyses that fluid flow existed inside the module. For this reason, Design-07 -08 and -09 were created.

Table 4.3 Amount of nodes and elements for convector designs

Numerical model	Interval size	Panel		Convector	
		nodes	elements	nodes	elements
Design-01	2.60	15311	44984	18393	53667
Design-02	2.45	16008	47724	22885	66948
Design-03	1.75	29367	86858	42387	125798
Design-04	1.46	43349	129324	69442	208267
Design-05	1.85	27621	81640	43397	127851
Design-06	2.42	17081	49955	28688	86365
Design-07	2.96	12017	35489	17250	50431
Design-08	3.05	10457	30534	18990	55578
Design-09	3.00	12459	36757	23836	70122

4.2.2 Processing

Numerical models prepared as modules with new convector designs were processed in computational fluid dynamics (CFD) program FLUENT in order to compute the thermal output of the modules. The numerical models were used for two different analyses. One of the analyses is to compute the thermal output of the modules against the fix wall temperature at the inner surface of panel section. Specified inner wall temperature was taken from the previous numerical study in which 75°C inlet and 65°C outlet water temperatures was obtained against the ambient convective heat transfer coefficient of 6 W/m^{2}K. The specified temperature for the inner surface of the panel section was the average temperature at the inner surface of panel section at the previous study. For this reason, there is no fluid flow existed in the modules.

Three-dimensional, segregated, implicit, steady solver was used with laminar viscous model. Energy equation was turned on because of the thermal analysis. The outer surface region of the panel section and convector section were in contact with an ambient at 20ºC. Forced convection model was used for computations. Boundary conditions specified for computations are listed in Table 4.4.

Table 4.4 Boundary conditions for fix inner surface temperature of modules

Zone	Type	Properties	Inputs
Sym. Panel and Convector	Symmetry	----------	No input
Inner surface of Panel	Wall	Thermal condition	temperature
		Temperature	340.6 K
		Material	steel
Outer surface of Panel	Wall	Thermal condition	convection
		Heat transfer coefficient	6 W/m^{2}K
		Free stream temperature	20ºC
		Material	steel
Outer surface of Convector	Wall	Thermal condition	convection
		Heat transfer coefficient	6 W/m^{2}K
		Free stream temperature	20ºC
		Material	steel

The numerical model shown in Figure 4.16 was used instead of the modeling whole radiator with fluid flow inside in order to decrease the computation time. Thermal outputs of two different modules were computed against 75°C inlet water temperature. Outlet of fluid flow was specified at the uncovered section of the module with normal convector as seen in Figure 4.16. Three-dimensional, segregated, implicit, steady solver was used with laminar viscous model. Energy equation was turned on because of the thermal analysis. The outer surface region of the panel section and convector section were in contact with an ambient at 20ºC. Forced convection model was used for computations. Boundary conditions specified for computations are listed in Table 4.5. Material properties are not given due to the usage of same materials that are listed in Table 4.2.

Table 4.5 Boundary conditions for fluid flow inside the modules

Zone	Type	Properties	Inputs
Inlet	Mass Flow Inlet	Mass flow rate	0.0245 kg/s
		Total temperature	75ºC
		Direction type	normal to the boundary
Outlet	Outflow	----------	No input
Adiabatic	Wall	Heat flux	0
		Material	steel
		Position	T-Fitting and panel
Outer surface of Water	Wall	Thermal condition	coupled
		Material	liquid water
Outer surface of Panel	Wall	Thermal condition	convection
		Heat transfer coefficient	6 W/m^2K
		Free stream temperature	20ºC
		Material	steel
Outer surface of convectors	Wall	Thermal condition	convection
		Heat transfer coefficient	6 W/m^2K
		Free stream temperature	20ºC
		Material	steel

CHAPTER FIVE
NUMERICAL RESULTS

5.1 Effects of Variation at Ambient Convective Heat Transfer Coefficient

By means of the numerical model of the panel radiator that was described in previous chapter, the effects of variation at ambient heat transfer coefficient to the thermal output of the panel radiator is represented in this section. According to the default values of under relaxation factors, value of energy under relaxation coefficient was changed from 1 to 0.5 in order to obtain convergence in energy equation. Although this change yielded to increase at the computation time, this case could only be converged at this value of energy under relaxation. Pressure-velocity coupling method was chosen as SIMPLE. Pressure equation discretisation scheme was chosen as standard. Both momentum and energy equation discretisation scheme was chosen as first order upwind. At the end of nearly 45000 iterations with 522428 nodes, outlet water temperature of 65ºC could be obtained at ambient convective heat transfer coefficient of 6 W/m^2K. Static temperature distribution of panel radiator is given in Figure 5.1 with the usage of front and isometric view together.

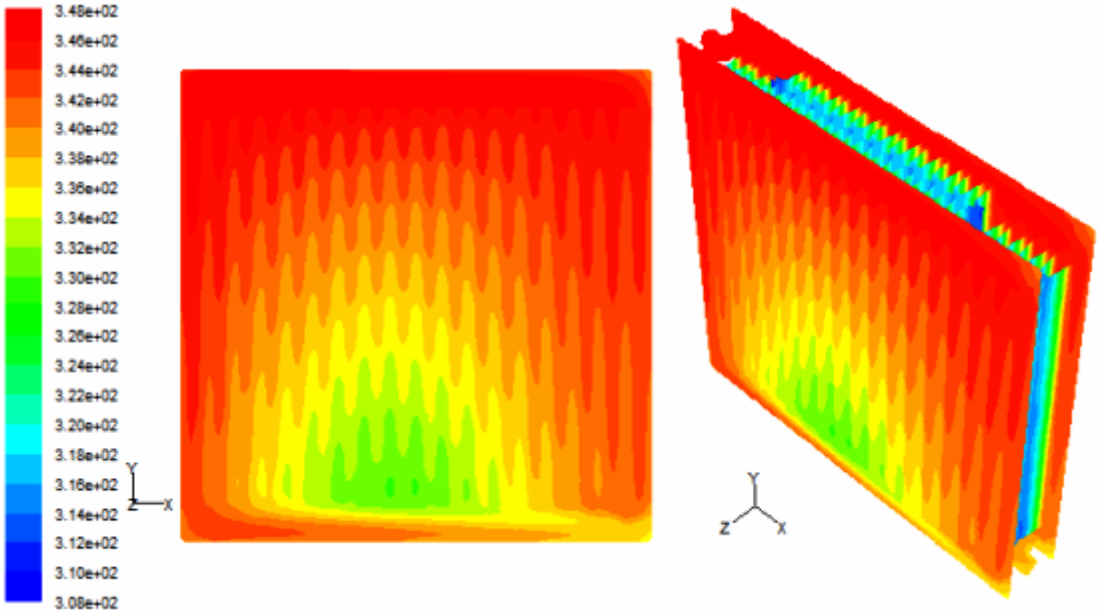


Figure 5.1 Static temperature distribution of the panel radiator

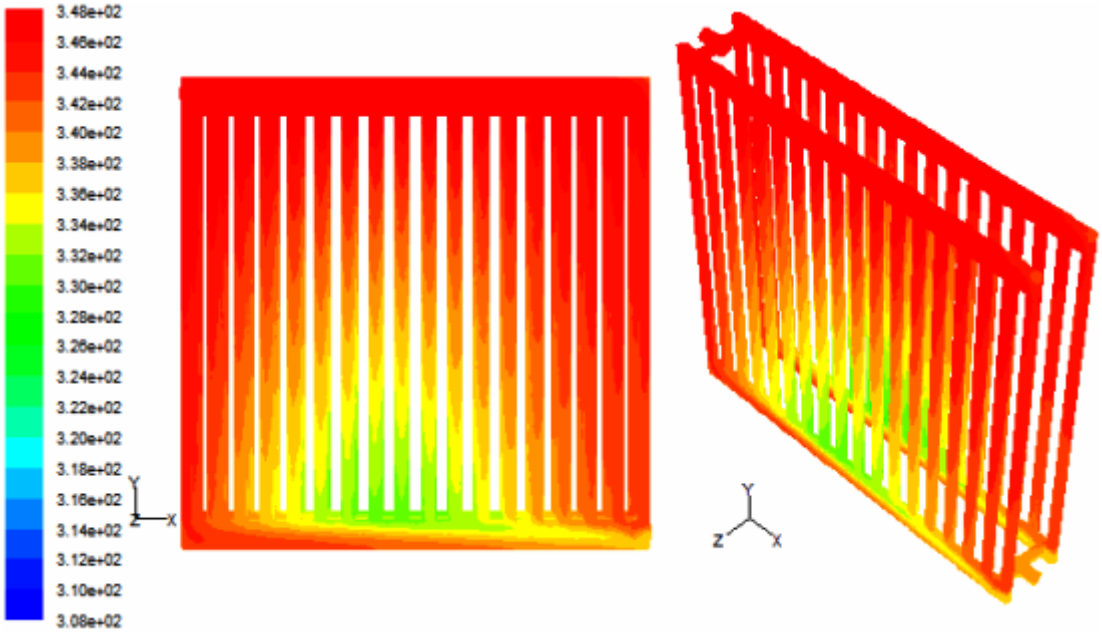


Figure 5.2 Static temperature distribution of fluid flow

Front and isometric view of static temperature distribution of fluid flow and convector is shown in Figure 5.2 and 5.3. In Figure 5.1 and 5.2, high temperature gradients are easily seen at the bottom-middle section of panel and fluid flow. This high gradient is arisen from distinct values of mass flow rates at vertical ducts.

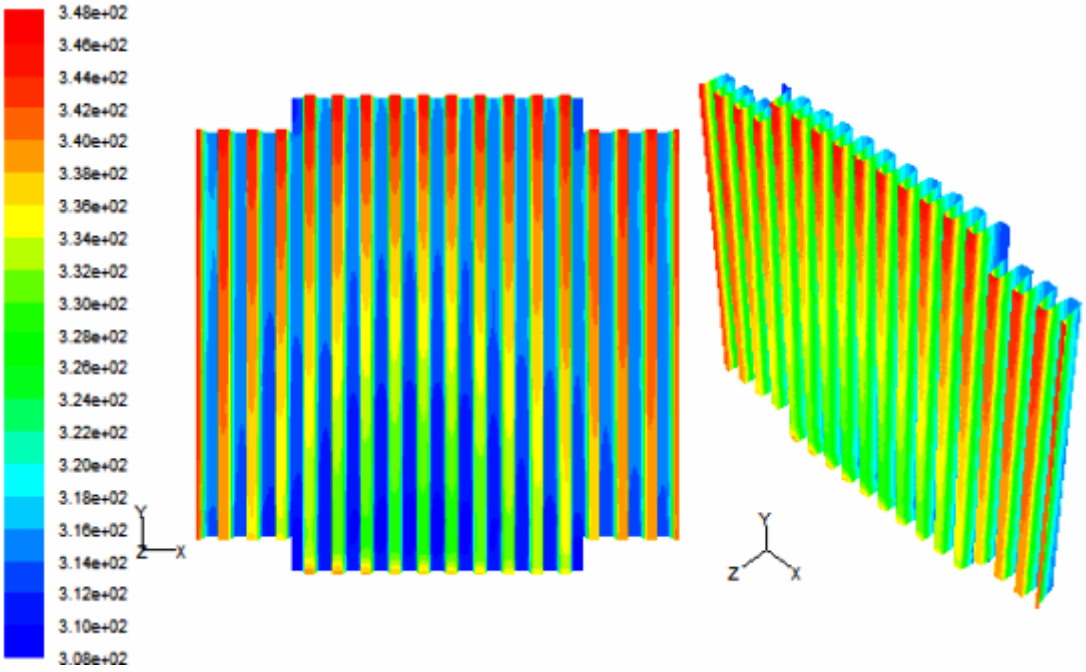


Figure 5.3 Static temperature distribution of convector

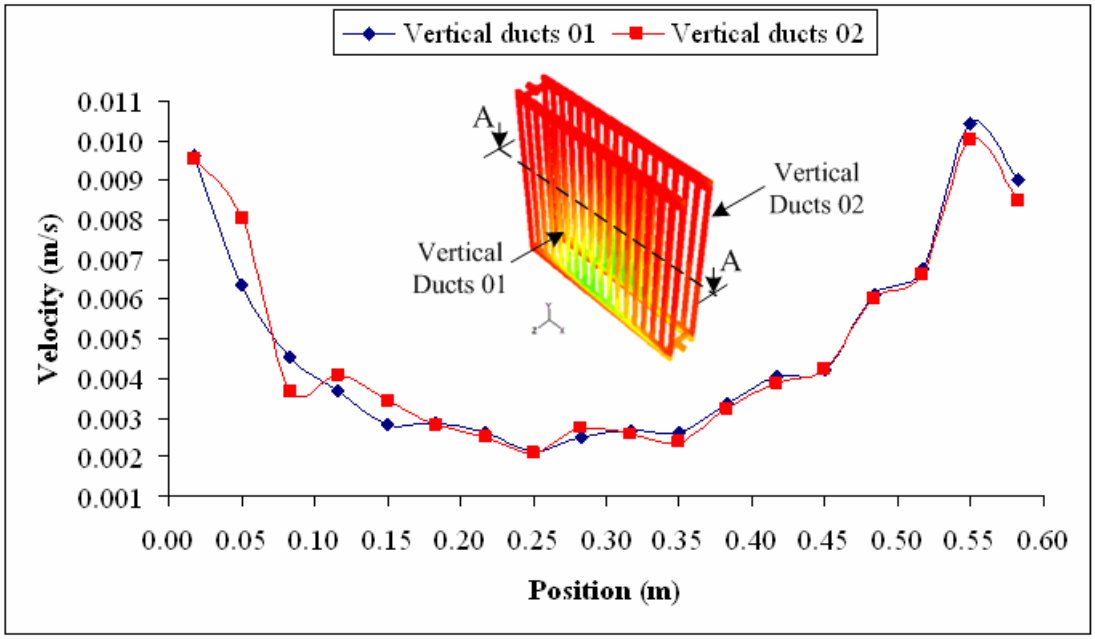


Figure 5.4 Velocity magnitudes of fluid flow along the radiator at vertical ducts (A-A)

Distinct values of mass flow rates at vertical ducts are shown in Figure 5.4. There are two strings in Figure 5.4 to represent the two vertical duct groups that are located on the arms of T-Fittings. This can be easily seen in Figure 5.5.

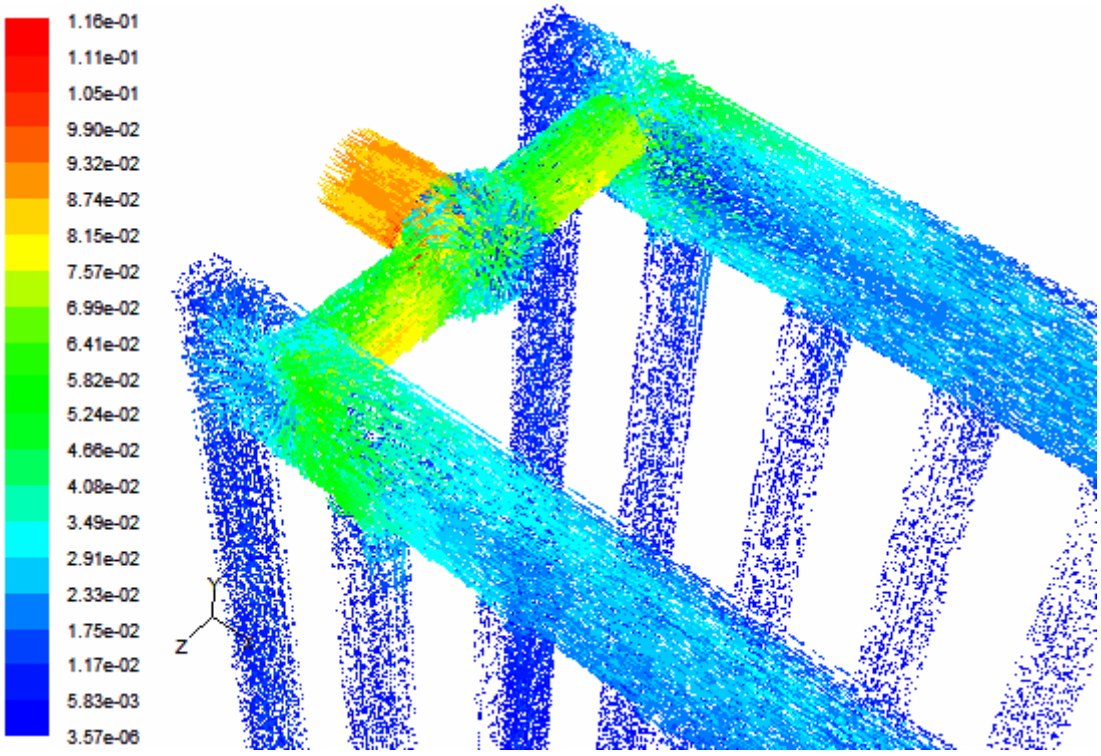


Figure 5.5 Partial view of vector form of velocity magnitudes at inlet T-Fitting and vertical ducts

Mass flow rates at the middle section of vertical ducts along the radiator are smaller than the regions towards inlet and outlet fittings. When water exits from the arms of inlet T-Fitting, water impinges the inner walls of panels. After the impingement, water moves along the upper horizontal water duct of radiator in opposite directions. One side of movement just crosses through the vertical ducts nearest to the inlet T-Fitting. Other one continues its movement along the horizontal water duct with separations to the vertical ducts. This separations form more resistance than the resistance that is formed by friction along the flow through the upper vertical ducts so this yields the distinct mass flow rates along the vertical ducts of the panel radiator and also yields the high temperature gradients at the middle bottom region of panel radiator.

The scarcity of velocity magnitudes at the middle vertical ducts affects the temperature distributions at all zones especially panel and convectors as shown in Figure 5.1, 5.2 and 5.3. The numerical results depending on the thermal output of the radiator at various shell-side convective heat transfer coefficients are listed in Table 5.1. For the fix inlet temperature of 75 ºC, outlet temperature of 65ºC that is related about the radiators in accordance with TS EN442 could be obtained at shell-side convective heat transfer coefficient of 6 W/m^2K. Symbols related with the specifications were taken from the experimental report of the radiator in order to get along with the symbols used whilst representing numerical results.

Table 5.1 Numerical results at various convective heat transfer coefficients

Specifications	Symbol	Heat transfer coefficient, h (W/m^2K)			
		6	8	9	10
Water flow rate (kg/h)	q_m	147	147	147	147
Inlet water temperature (ºC)	t_1	75.0	75.0	75.0	75.0
Outlet water temperature (ºC)	t_2	65.1	63.0	62.0	61.1
Temperature drop (ºC)	t_1- t_2	9.9	12.0	13.0	13.9
Enthalpy difference (kJ/kg)	Δh	40.5	49.0	53.0	56.8
Reference air temperature (ºC)	t_r	20.0	20.0	20.0	20.0
Mean water temperature (ºC)	t_m	69.1	67.8	67.0	66.5
Excess temperature (ºC)	ΔT	49.1	47.8	47	46.5
Thermal output (W)	Φ_{me}	1664.7	2038.3	2199.2	2350.4

Convective heat transfer coefficient of shell-side is directly proportional to the thermal output of the radiator. The increase at the convective heat transfer coefficient of shell-side leads to the increase at the thermal output of the radiator. The variation also affects the thermal output of the convectors. These variations at the thermal output of the components of the numerical model are listed in Table 5.2. There are two convectors in a panel radiator. In order to show their heat transfer rates separately in Table 5.2, convectors are respectively named as "Convector-01" and "Convector-02".

Table 5.2 Heat transfer rates from zones

Zone name	Heat transfer rates (W)			
	h = 6 W/m^{2}K	h = 8 W/m^{2}K	h = 9 W/m^{2}K	h = 10 W/m^{2}K
Water	998.7	1199.8	1297.7	1389.7
Panel	431.4	558.6	617.5	674.6
Convector-01	282.1	332.0	350.7	367.4
Convector-02	282.2	332.5	351.3	368.2

* Given capacities belong to 600mm radiator.

Cross-section view of static temperature distributions at the inlet and outlet T-Fittings is shown in Figure 5.6

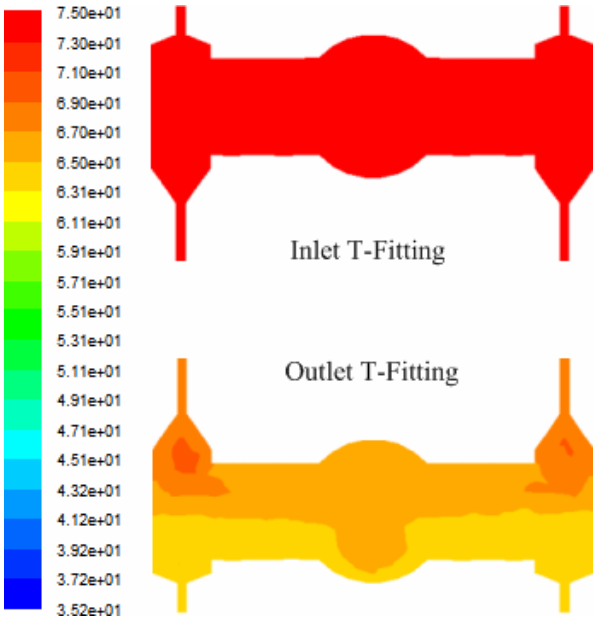


Figure 5.6 Static temperature distributions at inlet and outlet T-Fittings

Temperature distribution at the inlet T-Fitting is more homogenous than the distribution at the outlet T-Fitting. The homogenous distribution at inlet T-Fitting is arisen from the fix inlet water temperature of 75ºC. Temperature distribution at the outlet T-Fitting is showing variations at the arms of the fitting. They are not similar as shown in Figure 5.6. This irregularity is arisen from the variations at the mesh density at the arms of the T-Fitting. But temperature distributions generally show same tendency. The temperatures at upper regions of the outlet fitting arms are bigger due to the fact that these regions are in relation with the vertical duct nearest to the fitting. Temperatures at the vertical ducts are bigger than temperatures at bottom horizontal duct. In the middle region of the outlet T-Fitting, temperature distribution is becoming more homogenous than the distribution at arms for the condition that this region is the mixing point for the flows at arms.

Static temperature distribution at the axis of outlet T-Fitting arms depending on the variation of the ambient convective heat transfer coefficient is shown in Figure 5.7. Outlet water temperatures are decreasing whilst ambient convective heat transfer coefficient is increasing .This also yields the increase at the thermal output.

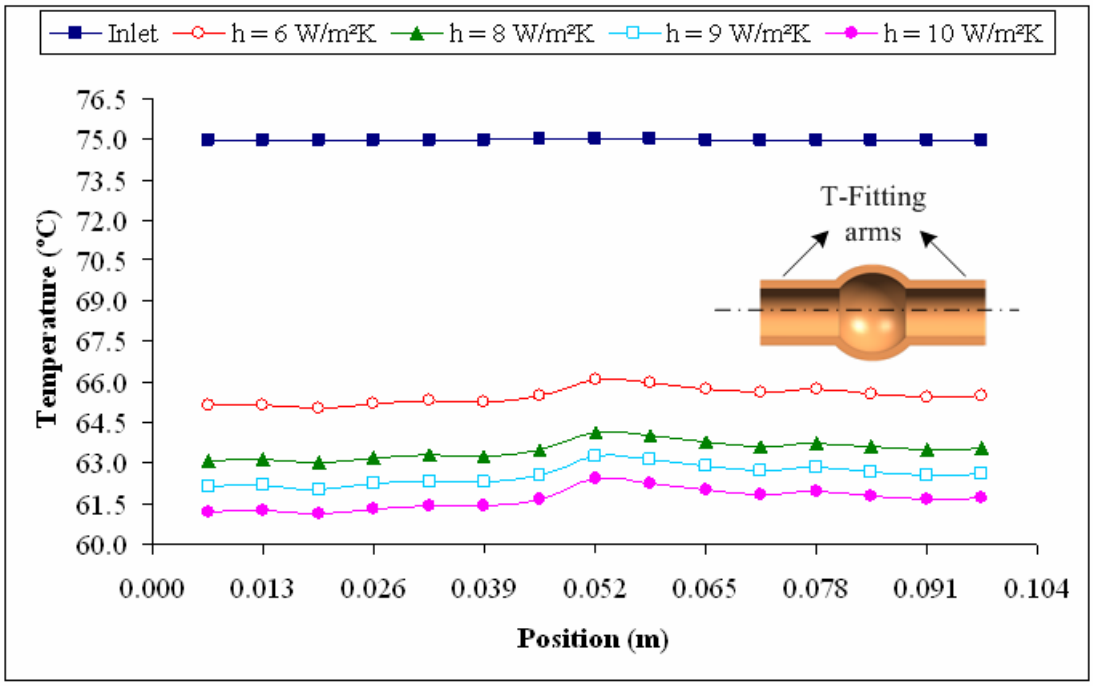


Figure 5.7 Temperature distributions at the axis of arms of the outlet T-Fitting

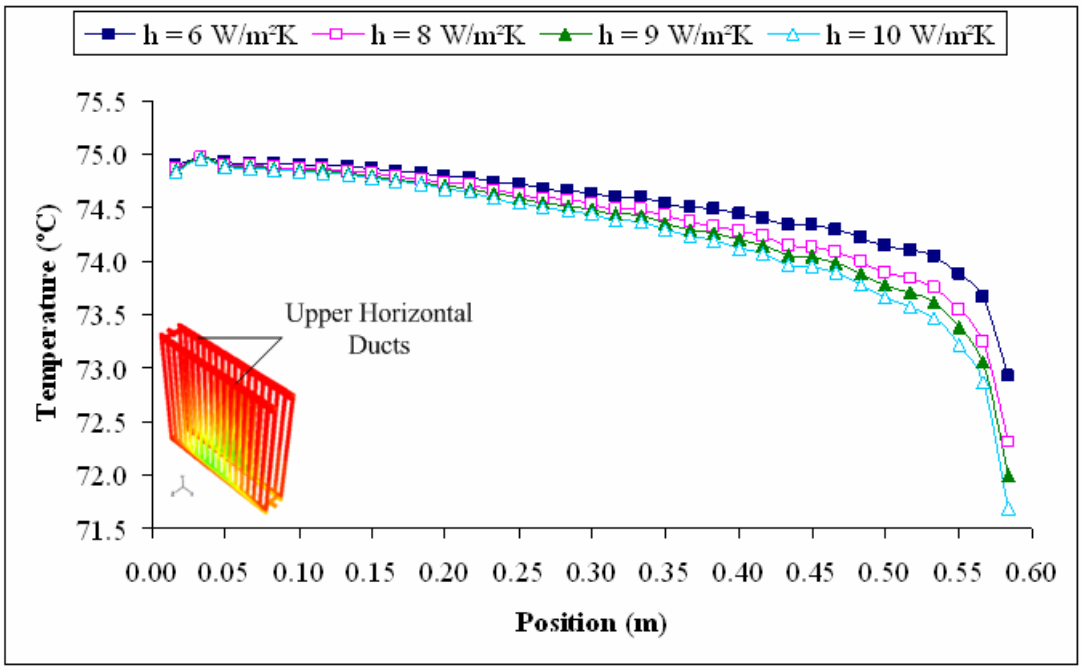


Figure 5.8 Static temperature distributions along the upper horizontal duct

Static temperature distribution at the upper horizontal duct represents a negative gradient as fluid flows along the upper horizontal duct. For the fix inlet temperature of 75ºC at four curves, last value of temperature distribution curves are getting smaller as the convective heat transfer coefficient increases.

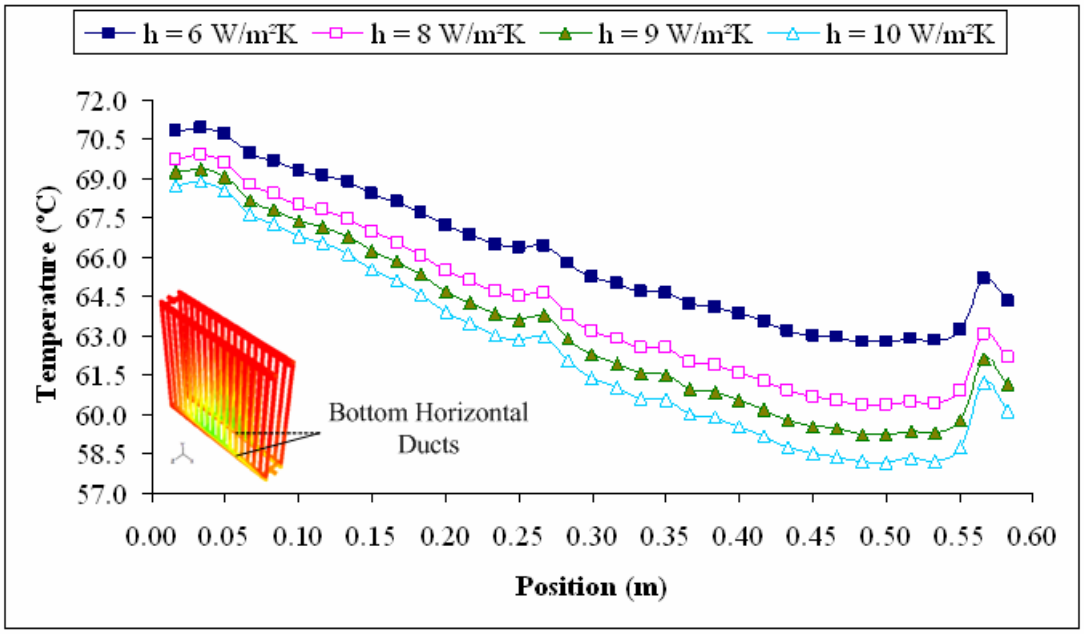


Figure 5.9 Static temperature distributions along the bottom horizontal duct

Towards the end of curves shown in Figure 5.8, temperature distributions represent higher gradient than other regions because of the separations to the vertical ducts. This yields the decrease at mass flow rates along the upper horizontal duct. This decrease yields fluid to loose more energy so temperature values are becoming smaller towards the end of the duct.

The temperature distribution curves shown in Figure 5.9 are inversely proportional with the variation at the convective heat transfer coefficient of ambient as temperature distribution curves shown in Figure 5.8. Temperature distribution curves at the bottom horizontal duct represent negative gradient until fluid flow reaches outlet fitting. Temperature values increases towards the outlet fitting. Towards the end of curves shown in Figure 5.9, a peak point is seen. This peak point is the inlet of outlet fitting. At the right-hand side of the peak point, curves show a negative gradient again. This negative gradient is arisen from last vertical duct. The assembly of the outlet fitting is between the last vertical duct and the duct before the last vertical duct. Last points of curves seen in Figure 5.9 represent the outlet of the last vertical duct. The flow direction at the left hand side of the peak point is in the opposite direction of flow that occurs on the right hand side. The temperature value seen at the last point of curves is the temperature of fluid at the outlet of the last vertical duct. This flow only mixes with other flows in the arms of outlet T-Fitting. The reason for temperature augmentation at the left hand side of the peak point is the addition of the hotter water at the vertical ducts towards the outlet fitting and the decrease at the convectors height.

Table 5.3 Mean water temperatures at the horizontal ducts

Zone type	Convective heat transfer coefficient, h (W/m^2K)			
	6	8	9	10
Upper horizontal duct (ºC)	74.52	74.38	74.31	74.25
Bottom horizontal duct (ºC)	66.02	64.14	63.25	62.41
Temperature difference (ºC)	8.5	10.24	11.06	11.84

Mean water temperatures at the upper horizontal duct do not represents big discrepancies as the mean water temperatures at bottom vertical ducts. Variation of

convective heat transfer coefficient completely shows its effect at the bottom horizontal duct due to heat transfer areas below the upper horizontal duct.

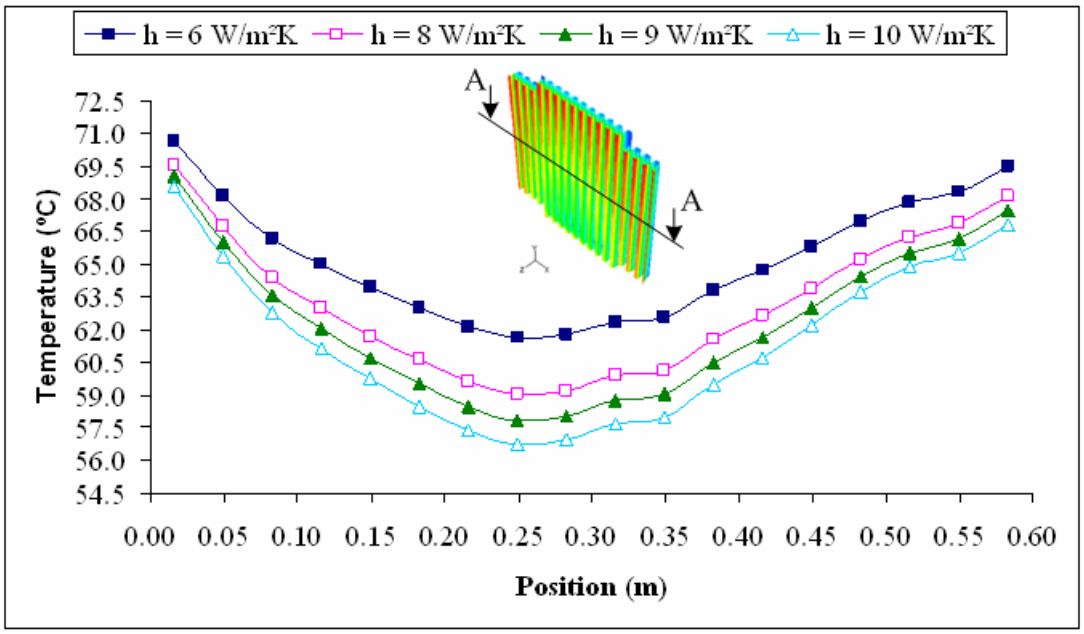


Figure 5.10 Static temperature distributions in the middle of the fin bases along the radiator.

Fin base temperatures are shown in Figure 5.10 depending on the convective heat transfer coefficients. The discrepancies at the mass flow rates of vertical ducts also affect the fin base temperature distribution.

5.2 Evaluation of Experimental Data with Numerical Data

The radiator used in previous section was manufactured in accordance with TS EN442. Thermal output of the radiator was obtained by means of an experimental facility in accordance with TS EN 442-2. According to TS EN442-2, radiator must be tested at three excess temperatures (ΔT) in order to obtain the characteristic equation of the radiator. Excess temperature (ΔT) is the difference between the mean water temperature (t_m) and the reference air temperature (t_r). For this reason, radiator is respectively tested for excess temperatures of 30±2.5°C, 50±2.5°C and 60±2.5°C. Inlet temperatures of 52.6°C, 75°C and 86.3°C are obtained whilst maintaining excess temperatures of 30±2.5°C, 50±2.5°C and 60±2.5°C.

75°C inlet and 65°C outlet conditions were obtained with the ambient convective heat transfer coefficient of 6 W/m^{2}K. In order to evaluate the experimental data with the numerical data, numerical studies were made for the fix inlet temperatures of 52.6°C, 75°C and 86.3°C under the influence of the fix ambient convective heat transfer coefficient of 6 W/m^{2}K. The numerical model used for this study is similar to the numerical model used in previous section. Material properties and boundary conditions are similar to the specifications respectively listed in Table 4.1 and 4.2. Forced convection model was used for computations. Pressure-velocity coupling method was chosen as SIMPLE. Pressure equation discretisation scheme was chosen as standard. Both momentum and energy equation discretisation scheme was chosen as first order upwind. Energy under relaxation factor was changed from 1 to 0.5 according to the default values of under relaxations.

In case of 75°C inlet temperature and 6 W/m^{2}K ambient convective heat transfer coefficient, outlet temperature of 65.1°C is obtained for the radiator in accordance with TS EN442 as a consequence of the numerical study. The specifications of experimental and numerical data are listed together in Table 5.4. In order to compare the discrepancies between the numerical and experimental data, there is a ratio exists in Table 5.4 and this is shown as "Num. / Exp.".

Table 5.4 Experimental and numerical data at 75°C inlet water temperature

Specifications	Symbol	Results		Num. / Exp.
		Experimental	Numerical	
Water flow rate (kg/h)	q_m	146.7	147.0	1.002
Inlet water temperature (ºC)	t_1	75.0	75.0	1.000
Inlet water enthalpy (kJ/kg)	h_1	314.0	209.1	-
Outlet water temperature (ºC)	t_2	65.0	65.1	1.001
Outlet water enthalpy (kJ/kg)	h_2	272.3	168.6	-
Temperature drop (ºC)	t_1- t_2	10.0	9.9	0.990
Enthalpy difference (kJ/kg)	Δh	41.7	40.5	0.971
Reference air temperature (ºC)	t_r	20.0	20.0	1.000
Mean water temperature (ºC)	t_m	70.0	69.1	0.987
Excess temperature (ºC)	ΔT	50.0	49.1	0.982
Thermal output (W)	Φ_{me}	1699.4	1664.7	0.979

There is little discrepancy exists at water flow rates listed in Table 5.4. The discrepancy is arisen from the computation of water flow rate according to the data obtained from commercial catalog of the radiator. The ratio at the inlet and outlet enthalpies are not given in Table 5.4 for the reason that CFD program FLUENT uses a reference temperature of 25°C during the computation of enthalpy values. Numerical values listed in Table 5.4 directly given from the report section of CFD program FLUENT. Enthalpy for the pressure-based solver is computed as (Fluent version 6.3 user's guide, 2006),

$$h = \int_{T_{ref}}^{T} c_P dT \tag{5.1}$$

where T_{ref} = 298.15K. The reference temperature for the enthalpy computation at the experimental data is taken as 273.15K. Reference temperatures are different but this discrepancy does not affect the enthalpy difference. Enthalpy difference is independent from the reference temperature. Computed enthalpy difference indicates nearly 3% discrepancy with the experimental data. If experimental reference temperature is used for enthalpy computation, 0.1% discrepancy exists between the numerical and experimental data for the outlet water enthalpy.

Reference temperatures are same for both conditions but mean water temperatures are different from each other. The computed value for the mean water is the volume average of the whole fluid region at the numerical model. On the other hand, the given value for the experimental mean water temperature is computed as the average of inlet and outlet water temperatures. Computed mean water temperature indicates 1.3% discrepancy with the experimental mean water temperature. If the method for computation of experimental mean water temperature is used for the numerical data, experimental and numerical mean water temperatures indicates nearly no discrepancies. The discrepancy at the mean water temperatures also affects the excess temperatures. Excess temperature of 49.1°C is obtained as a consequence of the numerical study and this value is in the tolerance with 50±2.5°C that is necessary for the measuring points described in TS EN442-2.

Thermal output of the radiator is given from flux report section of the CFD program for heat transfer zones in contact with the ambient. Ambient convective heat transfer coefficient was specified as 6 W/m^2K. With this conditions, computed thermal output of the radiator manufactured in accordance with TS EN 442 indicates 2.1% discrepancy with the output obtained by means of experiments.

Radiator was tested at tree different excess temperatures. One of them is 50±2.5°C and evaluation of this condition with the experimental data is given above. Another tested excess temperature is 60±2.5°C. The inlet condition for this excess temperature is experimentally specified as 86.3°C. In case of 86.3°C inlet temperature and 6 W/m^2K ambient convective heat transfer coefficient, outlet temperature of 74.4°C was obtained for the radiator in accordance with TS EN442 as a consequence of the numerical study. The specifications of experimental and numerical data are listed together in Table 5.5. Computed outlet temperature of the radiator indicates 1.3% discrepancy with the experimental outlet temperature. In order to supply consistency at three different excess temperatures, numerical study was made for the fix ambient convective heat transfer of 6 W/m^2K. Depending on the increase at the excess temperature, increasing the ambient convective heat transfer coefficient may lead to obtain closer outlet temperature as supplied in experiments.

Table 5.5 Experimental and numerical data at 86.3°C inlet water temperature

Specifications	Symbol	Results		Num./Exp.
		Experimental	Numerical	
Water flow rate (kg/h)	q_m	146.6	147.0	1.002
Inlet water temperature (ºC)	t_1	86.3	86.3	1.000
Inlet water enthalpy (kJ/kg)	h_1	361.4	256.4	-
Outlet water temperature (ºC)	t_2	73.7	74.4	1.013
Outlet water enthalpy (kJ/kg)	h_2	308.5	207.5	-
Temperature drop (ºC)	t_1- t_2	12.6	12.0	0.952
Enthalpy difference (kJ/kg)	Δh	52.9	48.9	0.924
Reference air temperature (ºC)	t_r	20.1	20.0	0.995
Mean water temperature (ºC)	t_m	80.0	79.0	0.987
Excess temperature (ºC)	ΔT	59.9	59.0	0.985
Thermal output (W)	Φ_{me}	2156.0	2019.8	0.936

The discrepancy at the outlet water temperature also leads discrepancies in other specifications. Computed temperature drop indicates 4.8% discrepancy with the experimental temperature drop. The ratio at the inlet and outlet water enthalpy is not given because of the discrepancies at reference temperature used for enthalpy computations. Enthalpy difference indicates %7.6 discrepancy with the experimental enthalpy difference. For this excess temperature, reference air temperature used in experiments is 20.1ºC but this temperature is in tolerance with TS EN442-2 although reference air temperature used in numerical study is fixed to 20ºC for all conditions. Depending on the discrepancy at the outlet water temperature, computed mean water temperature indicates 1.3% discrepancy with the experimental mean water temperature that is obtained by taking the average of the inlet and outlet water temperatures. Excess temperature of 59ºC is in the tolerance with 60±2.5°C that is necessary for the measuring points described in TS EN442-2. Computed excess temperature also indicates 1.5% discrepancy with the experimental excess temperature. The computed outlet water temperature's being greater than experimental outlet temperature leads smaller amount of heat transfer than heat transfer occurred in experiments so this leads 6.4% discrepancy between the computed thermal output and experimental thermal output.

The third excess temperature that radiator was tested for is 30±2.5°C. In case of 52.6°C inlet temperature and 6 W/m^2K ambient convective heat transfer coefficient, outlet temperature of 46.8°C is obtained for the radiator in accordance with TS EN442 as a consequence of the numerical study. The specifications of experimental and numerical data are listed together in Table 5.6. Computed outlet temperature of the radiator indicates 1.5% discrepancy with the experimental outlet temperature for this case. Computed outlet temperature is smaller than the experimental outlet temperature due to the usage of 6 W/m^2K fix ambient convective heat transfer coefficient. Depending on the decrease at the excess temperature, decreasing the ambient convective heat transfer coefficient may lead to obtain closer outlet temperature as supplied in experiments. The discrepancy at the computed outlet temperature leads discrepancies at other features of this case according to the experimental data.

The ratio for the water inlet and outlet enthalpies is not given due to the usage of different reference temperatures at numerical study and experimental study. The computed enthalpy difference indicates 10% discrepancy with the experimental enthalpy difference. For this excess temperature, reference air temperature used in experiments is 19.9ºC but this temperature is in tolerance with TS EN442-2 although reference air temperature used in numerical study is fixed to 20ºC for all conditions. The discrepancy at the mean water temperature is 2.2%. Computed excess temperature of 29ºC is in the tolerance with 30±2.5°C that is necessary for the measuring points described in TS EN442-2. The discrepancy between the computed and the numerical outlet water temperature is 0.7°C. The computed mean water temperature is 49ºC. However, the difference between the experimental inlet and experimental outlet temperature is 5.1°C. Due to this small value of inlet and outlet water temperature difference, a small change at this difference makes a great effect on the thermal output of the radiator. The computed thermal output of the radiator indicates 11.6% discrepancy with the experimental thermal output.

Table 5.6 Experimental and numerical data at 52.6°C inlet water temperature

Specifications	Symbol	Results		Num./Exp.
		Experimental	Numerical	
Water flow rate (kg/h)	q_m	146.7	147.0	1.002
Inlet water temperature (ºC)	t_1	52.6	52.6	1
Inlet water enthalpy (kJ/kg)	h_1	220.4	115.4	-
Outlet water temperature (ºC)	t_2	47.5	46.8	0.985
Outlet water enthalpy (kJ/kg)	h_2	198.9	91.5	-
Temperature drop (ºC)	t_1- t_2	5.1	5.8	1.137
Enthalpy difference (kJ/kg)	Δh	21.5	23.9	1.112
Reference air temperature (ºC)	t_r	19.9	20.0	1.005
Mean water temperature (ºC)	t_m	50.1	49.0	0.978
Excess temperature (ºC)	ΔT	30.1	29.0	0.963
Thermal output (W)	Φ_{me}	876.3	990.5	1.130

The evaluation of the numerical data with the experimental data for three different excess temperatures is respectively listed in Table 5.4, 5.5 and 5.6. The most convergent data to the experimental data is obtained for the inlet temperature of 75ºC at the same time for the excess temperature of 50±2.5°C. The radiator manufactured

in accordance with TS EN442 must supply the inlet temperature of 75°C and outlet temperature of 65°C. The discrepancies at other excess temperatures are arisen from the fix ambient convective heat transfer coefficient of 6 W/m^{2}K. Small changes at the ambient convective heat transfer coefficient makes the computations more converged as computed for 50±2.5°C excess temperature.

Static temperature distributions along the radiator for three different inlet water temperatures are shown in Figure 5.11. "UHD" abbreviation is used for the flow at the upper horizontal duct and "BHD" abbreviation is used for the flow at the bottom horizontal duct as shown in Figure 5.11.

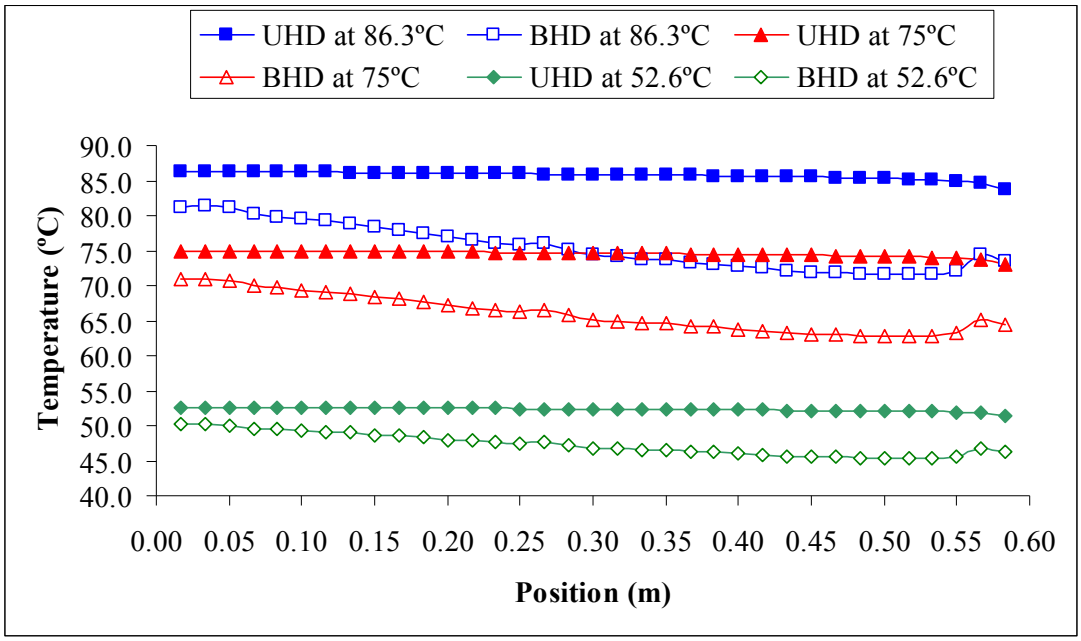


Figure 5.11 Static temperature distributions at upper and bottom horizontal ducts

The temperature distributions at the upper horizontal ducts for three inlet temperatures represent negative gradient towards the end of the horizontal ducts due to the heat transfer to the ambient. The magnitude of temperature change along the upper horizontal ducts is proportional to the temperature drop along the radiator so the gradient at the "UHD at 86.3°C" is bigger than other UHD strings shown in Figure 5.11. Temperature drop for 86.3ºC, 75ºC and 52.6 ºC is respectively 2.47 ºC, 2.05 ºC and 1.21 ºC. UHD strings getting flatter as the temperature drop decreases

along the radiator. This also affects the temperature distributions along the bottom horizontal ducts. Temperature drop at the bottom horizontal ducts is respectively 9.83ºC, 8.15ºC and 4.18ºC. According to the temperature drop at the upper horizontal ducts, temperature drop at the bottom horizontal ducts is bigger due to the increase at the mass flow rate along the duct with lower temperature than occurred at the upper horizontal duct. For the three BHD strings, strings make a peak towards the end of the strings. Peak points occurred at arms of the outlet T-Fitting. Peak heights change proportional to the temperature drop along the bottom horizontal duct. Maximum peak can be seen at "BHD at 86.3ºC" string.

Static temperature distributions along the vertical ducts for three excess temperatures are shown in Figure 5.12. The temperature distribution along the vertical ducts represents a parabolic form due to the discrepancies at the mass flow rates along the vertical ducts. The discrepancies at the mass flow rates are arisen from the resistances that occurred at the inlet of the vertical ducts whilst fluid flow occurs along the upper horizontal duct. The parabolic form can be easily seen for the temperature distribution at the 86.3°C. As the temperature drop along the radiator is getting lower, the parabolic form is becoming straighter like an arc.

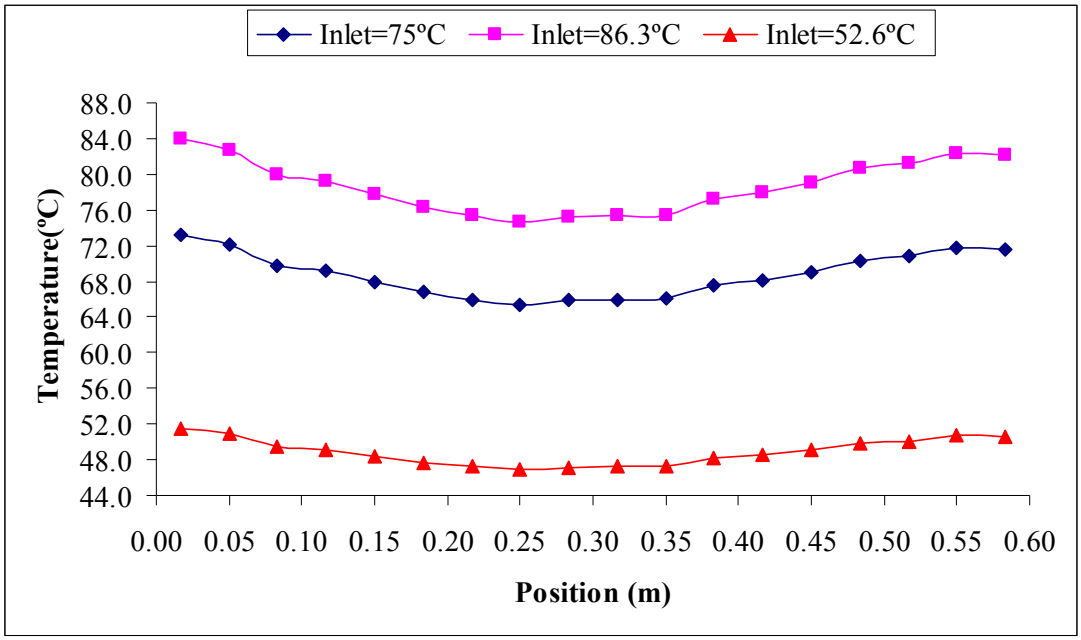


Figure 5.12 Static temperature distributions at vertical ducts along the radiator

Mean water temperatures at the upper and bottom horizontal ducts according to the three excess temperatures are listed together in Table 5.7. Temperature difference between UHD (upper horizontal duct) and BHD (bottom horizontal duct) must be lower than the temperature drop along the radiator due to the taking the average of temperature distribution along the horizontal duct. Temperature drop along the radiator is computed from the temperatures at the inlet and outlet of T-Fittings. For this reason, "$t_{m\text{-}uhd} - t_{m\text{-}bhd}$" is labeled as temperature difference.

Table 5.7 Mean water temperatures at UHD and BHD for three different excess temperatures

Specifications	Symbol	Excess Temperature (°C)		
		50±2.5	60±2.5	30±2.5
Mean water temperature at UHD (°C)	$t_{m\text{-}uhd}$	74.525	85.727	52.319
Temperature drop at UHD (°C)	$t_{d\text{-}uhd}$	2.043	2.465	1.209
Mean water temperature at BHD (°C)	$t_{m\text{-}bhd}$	66.022	75.473	47.308
Temperature drop at BHD (°C)	$t_{d\text{-}bhd}$	8.150	9.826	4.801
Temperature difference (°C)	$t_{m\text{-}uhd} - t_{m\text{-}bhd}$	9.503	10.254	5.011

5.3 Evaluation of Thermal Output with New Convector Designs

Thermal output of the new convector designs are computed in case of fix temperature at the inner surface of the module and fluid flow inside the module. Two different processing operations are generated in order to evaluate thermal output of the new convector designs. For this reason, evaluation is performed in two sections:

5.3.1 Fix Temperature at Inner Surfaces of Modules

Inner surface temperatures of modules (inner surfaces of panel sections) were fixed to an average temperature of 67.45°C (340.6K). The specified temperature for the inner surfaces was obtained from the analysis that satisfies the 75°C inlet and 65°C outlet conditions of the radiator in accordance with TS EN442. Pressure-velocity coupling method was chosen as SIMPLE. Pressure equation discretisation scheme was chosen as standard. Both momentum and energy equation discretisation scheme was chosen as first order upwind. Iterations were sustained until zero heat flux was obtained at the net heat flux monitor.

Table 5.8 Specifications of convector designs for fix temperature at inner surfaces

Specifications	 Design-01	 Design-02	 Design-03	 Design-04	 Design-05	 Design-06
Heat transfer surface area (m^2)	0.0995	0.1080	0.1070	0.1253	0.1146	0.1296
Surface ratio with Design-01	1.00	1.09	1.08	1.26	1.15	1.30
Thermal output of panel (W)	11.66	11.66	11.66	11.66	11.66	11.66
Thermal output of convector (W)	18.19	19.25	19.11	20.75	20.46	21.47
Convector Output ratio	1.00	1.06	1.05	1.14	1.13	1.18
Thermal output of module (W)	29.85	30.91	30.77	32.41	32.12	33.13
Module Output ratio	1.00	1.04	1.03	1.09	1.08	1.11

The most increase at the thermal output of modules was obtained for Design-06. The ratios listed in Table 5.8 are computed according to the value of Design-01(original design) with related specification. The increase at the thermal output of the module is 11% according to Design-01. Static temperature distributions of convector designs are given in Figure 5.13 and 5.14.

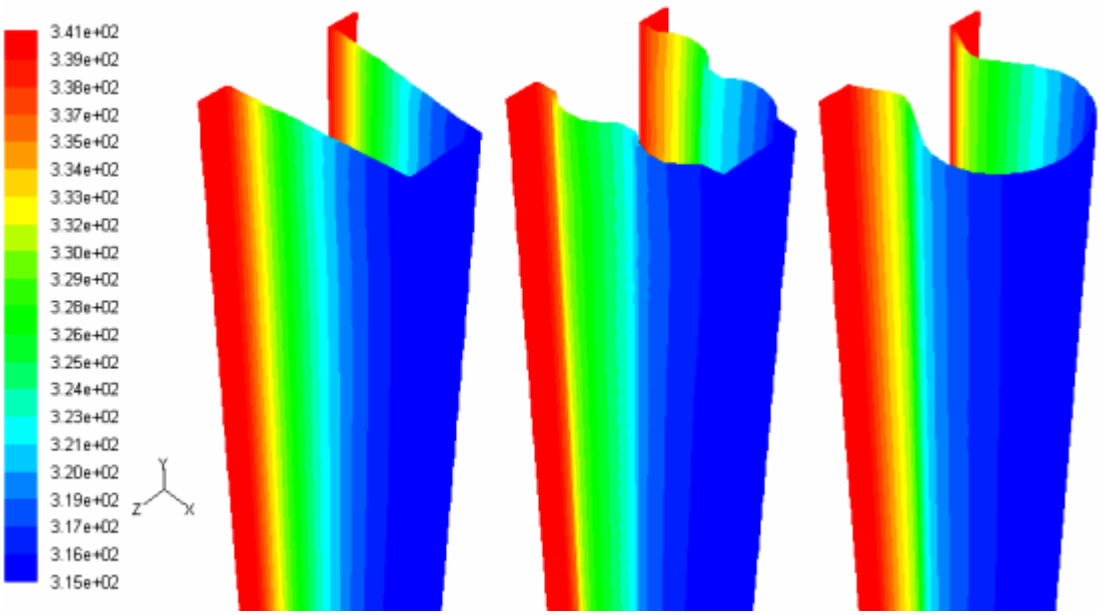


Figure 5.13 Static temperature distributions of Design-01, -02 and -03

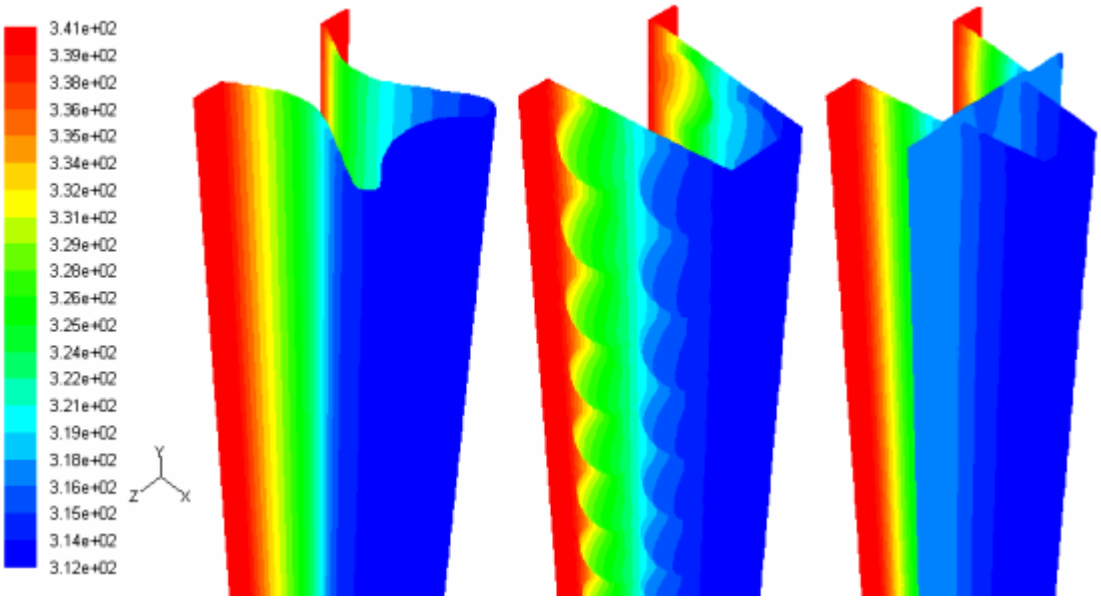


Figure 5.14 Static temperature distributions of Design-04, -05 and -06

Remarkable increases at thermal outputs were obtained for Design-04, -05 and -06. Minimum temperature values at the color maps manifest appreciable increases.

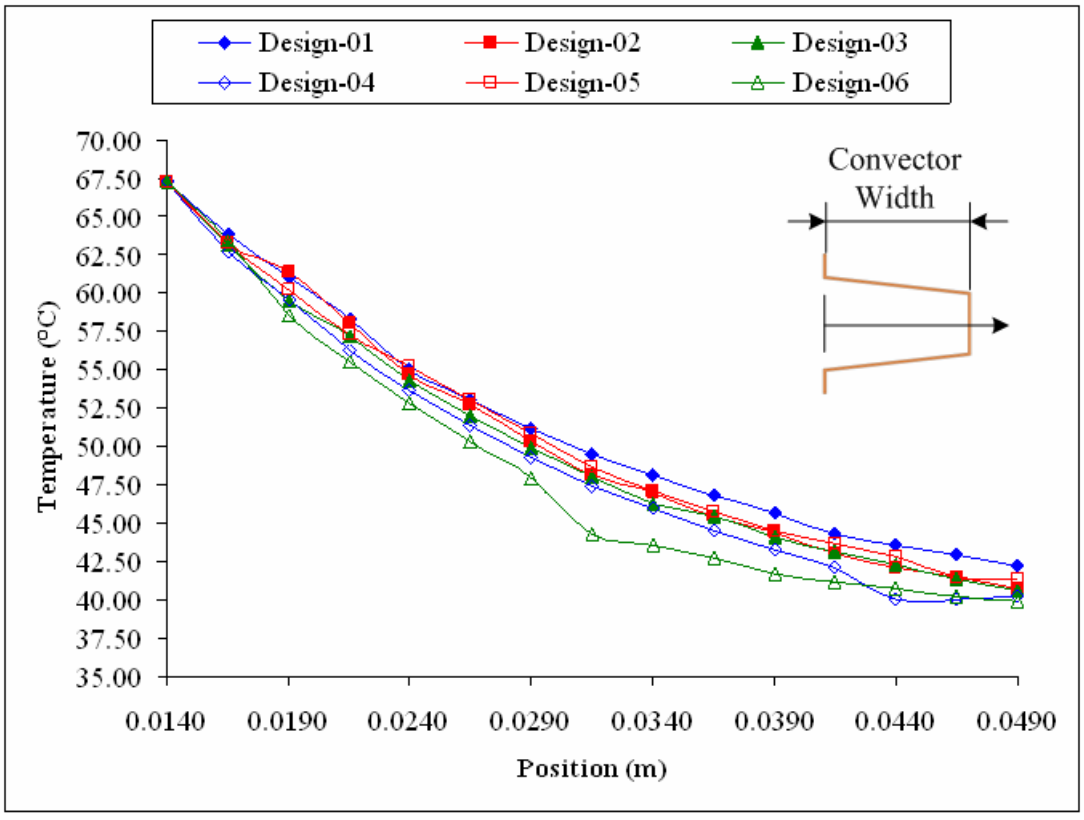


Figure 5.15 Static temperature distributions of convectors along convector width.

The heat transfer surface area of Design-06 is 30% greater than Design-01 according to Table 5.8. But the increase at thermal output is 11%. The reason why thermal output is not proportional to the heat transfer surface area is based on the gradients along the convector width shown in Figure 5.15. Thermal outputs of Design-04 and -05 are closer to each other. On the other hand, 11% discrepancy exists at the heat transfer surface areas of Design-04 and -05 according to Design-01. Increase at heat transfer surface of Design-05 at the high temperature gradient sections as seen in Figure 5.14 is more than Design-04. The major increase at the surface area of Design-04 was performed at the top of the convector where temperature gradients are becoming smaller and smaller.

Design-05 was created in order to investigate the effect of pops at the thermal output of original design. By means of pops, 15% increase at heat transfer surface area was obtained. This increase yields 8% increase at the thermal output. Similarities exist between Design-02 and Design-05 at cross-section areas of convectors. Cross-section area of Design-02 is extruded along the convector height. But pops area used at the side surfaces of Design-05. Extruded section leads only increase at cross-section area. On the other hand, pops lead also increase at cross-section area and along the height of convector. As a consequence of this, 6% discrepancy exists between heat transfer areas of Design-02 and -05.

Gradients of temperature distributions given in Figure 5.15 are proportional to the thermal output of the modules. A sudden temperature decrease occurs at the middle section of Design-06. This region is the crossing section of cascade convector design. After the middle section of convector, the changes at the gradients are becoming closer to each other according to the change before this section for all convectors. In order to obtain the same thermal output at the top region of convector as obtained at the bottom region for unit area, nearly 2.4 times of area at the bottom region is needed at the top region of Design-06. The major area increase at the convector designs, except Design-05, takes place at the regions towards the top of the convectors. For this reason, increase at thermal outputs of convectors is not as much as increase at heat transfer areas of convectors.

5.3.2 Fluid Flow Inside The Modules

The numerical models used for this computation differ from previous models. In order to model the fluid flow inside the modules, modules are used instead of one module as seen in Figure 5.16. Each numerical model consists of four short convectors, two and two half normal convectors, two partial panels and T-Fitting. By this way, thermal outputs of short convectors placed near the T-Fitting could be investigated according to the normal convectors.

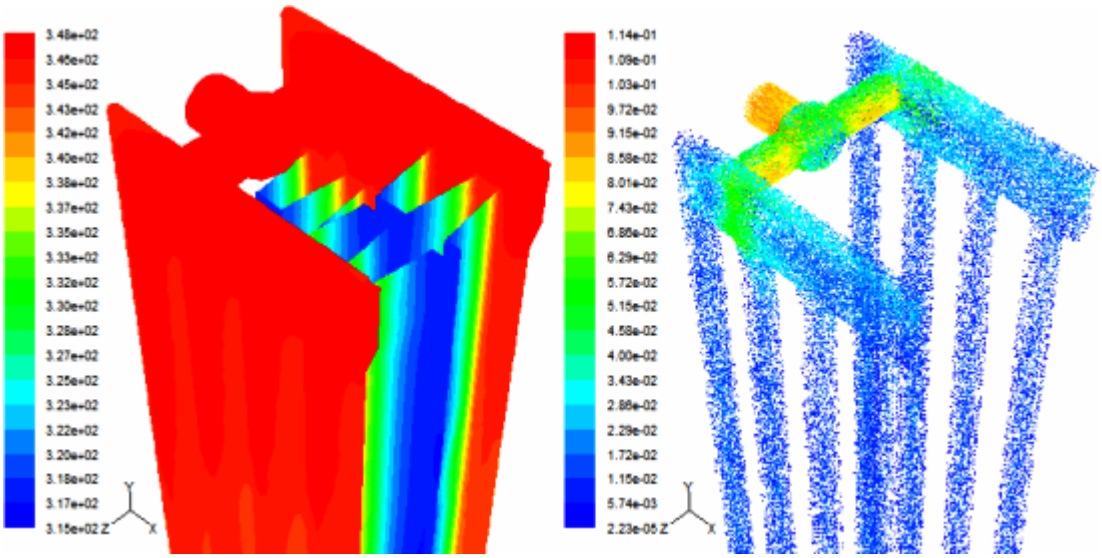


Figure 5.16 Temperature and velocity distributions of Design-01

Combination of modules and T-Fitting made the numerical model more complex than models used in previous section. Complexity of the model restricted the usage of some convector designs in the previous section. Design-01 (original design) and -06 (obtained best thermal output in previous section) were used for this computation. In addition to the usage of previous designs; Design-07, -08 and -09 were also created. Thermal outputs of the modules were computed for the condition that 75°C inlet water temperature is specified at T-Fitting. Pressure-velocity coupling method was chosen as SIMPLE. Pressure equation discretisation scheme was chosen as standard. Both momentum and energy equation discretisation scheme was chosen as first order upwind. Iterations were sustained until zero heat flux was obtained at the net heat flux monitor.

Thermal outputs and related specifications of convector designs are listed in Table 5.9. The most increase at the thermal output of convectors was obtained for Design-09 that differs from other convectors due to the existence of extra contact face between panel and convector. By means of Design-07 and -08, models similar to Design-04 were investigated.

Table 5.9 Specifications of convector designs for fluid flow inside the modules

Specifications		 Design-01	 Design-06	 Design-07	 Design-08	 Design-09
Heat transfer surface area (m^2)		0.0996	0.1298	0.1226	0.1448	0.1738
Surface ratio with Design-01		1.00	1.30	1.23	1.45	1.75
Short Convector (H = 480mm)	Average temp. inner surface (°C)	71.35	71.11	71.24	71.21	69.64
	Thermal output of panel (W)	12.96	12.90	12.95	12.93	11.60
	Thermal output of convector (W)	16.77	19.16	17.69	18.55	31.89
	Convector output ratio	1.00	1.14	1.05	1.11	1.90
	Thermal output of module (W)	29.73	32.06	30.64	31.48	43.49
	Module output ratio	1.00	1.08	1.03	1.06	1.46
Normal Convector (H = 560mm)	Average temp. inner surface (°C)	71.00	70.68	70.87	70.81	69.25
	Thermal output of panel (W)	12.58	12.50	12.56	12.55	11.51
	Thermal output of convector (W)	19.26	22.24	20.54	21.53	31.62
	Convector output ratio	1.00	1.15	1.07	1.12	1.64
	Thermal output of module (W)	31.84	34.74	33.10	34.08	43.13
	Module output ratio	1.00	1.09	1.04	1.07	1.35
Thermal output ratio of convectors		0.87	0.86	0.86	0.86	1.01
Thermal output ratio of modules		0.93	0.92	0.93	0.92	1.01

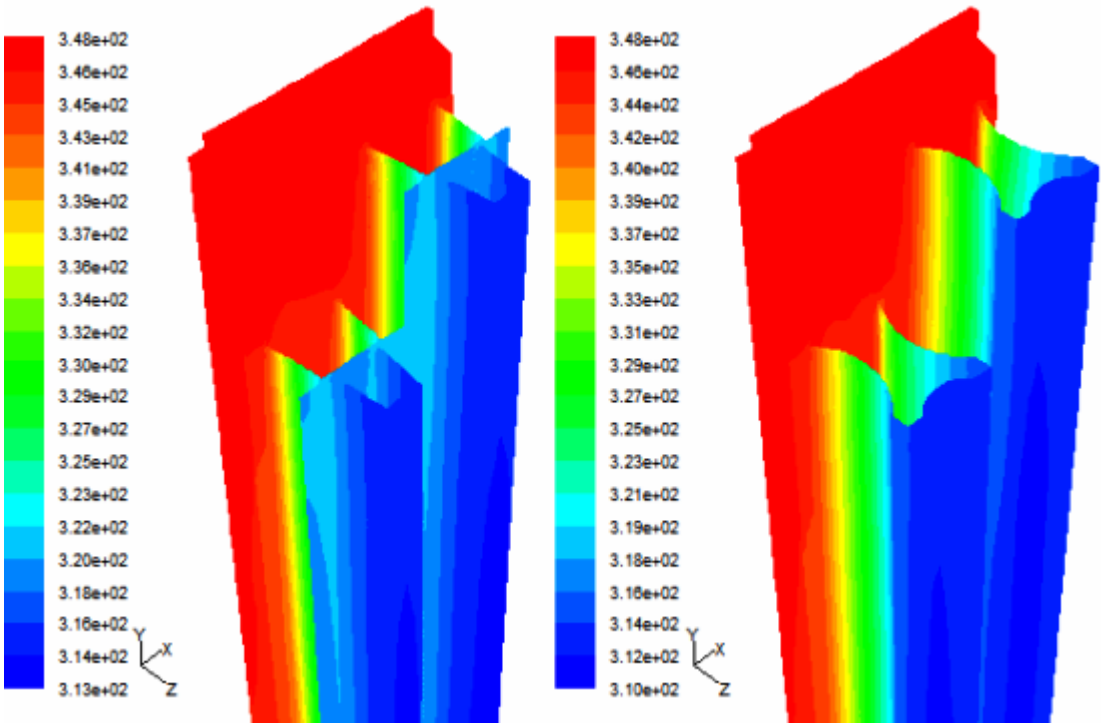


Figure 5.17 Static temperature distributions of Design-06 and -07

Convector heights are not uniform at Design-09 according to other designs as seen in Figure 5.18 due to the implementation of three contact faces.

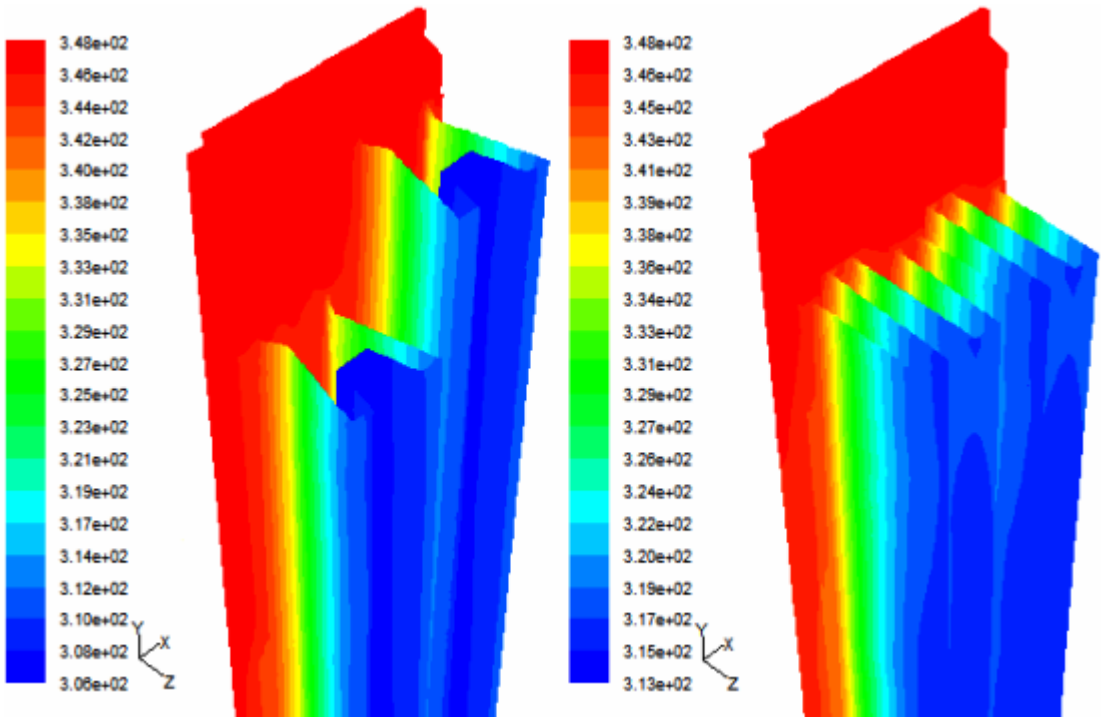


Figure 5.18 Static temperature distributions of Design-08 and -09

Remarkable increase at heat transfer area of convector design was obtained for Design-09. As a consequence of this, the most increase at thermal output of convectors was obtained for Design-09. 75% increase at heat transfer area and the implementation of three contact faces made major increase at thermal output of the module. Without the usage of third contact face (on dry duct) between panel and convector, %75 increase at heat transfer area would not make 35% increase at thermal output of module due to the fact that increase at heat transfer areas would be concentrated towards the top of the convector. But this increase towards top of the convector would not make same effect at thermal output of module as increase near the contact faces. Temperature gradients near the contact faces are bigger than towards top of the convector so more heat transfer area is needed to make the same effect as obtained near the contact faces. 45% increase at heat transfer area of Design-08 made 7% increase at thermal output of the module. 75% increase at heat transfer area of Design-09 without third contact face would not make same effect at thermal output as obtained with third contact face according to Design-08.

The increase at the heat transfer area of Design-08 is 15% more than Design-06. But thermal output of Design-06 is 2% more than Design-08 according to Design-01(original design). This is arisen from the increase at heat transfer areas near the contact regions as described for Design-09. Design-07 is the modified version of Design-04. Design-07 differs from Design-04 with the corners at the top of convector. The corners are sharpened in order to not yield mesh problems as formed at Design-04. Although 23% increase at heat transfer area was obtained for Design-07, increase at the thermal output was 4% depending on the position of formed increase at heat transfer area. The thermal output ratios of convectors depending on the convector height are almost equal to the heat transfer area ratios of short and normal convectors. The heat transfer area ratios for convectors, except Design-09, are 86%. Heights of the convectors are uniform at Design-09. 1% discrepancy at the thermal output ratio of convectors for Design-09 is arisen from hotter water temperature at first module according to other module. Average inner surface temperatures of the modules are inversely proportional to the thermal output of the modules.

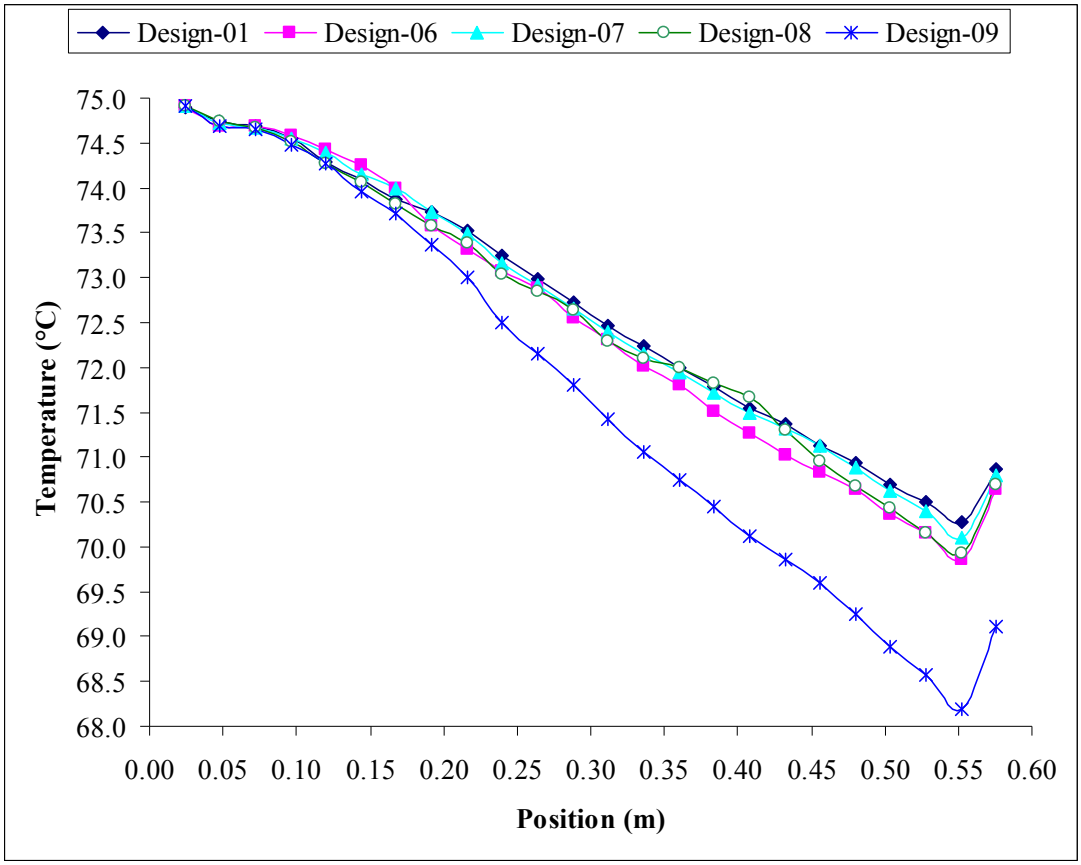


Figure 5.19 Total temperature distributions along the vertical ducts of modules

Temperature distribution along the vertical ducts is given from the middle region of upper horizontal duct at the inlet of vertical duct to middle region of bottom horizontal duct at the outlet of vertical duct. At the inlet section of the vertical ducts, water temperatures are nearly at the same value. As water flows through the vertical duct, temperature distribution strings, especially string for Design-09, diverge from each other. Gradients of temperature distribution strings increase towards the outlet region of vertical duct depending on the thermal output of modules. The peak at the end of the strings as seen in Figure 5.19 is arisen from the water flow at the bottom vertical duct.

CHAPTER SIX
CONCLUSION

Investigated panel radiator was manufactured in accordance with TS EN442. Experimental data, represented and compared in this study, was supplied by the producing company and was obtained at CETIAT laboratories in France. Catalogue data of Type-22 radiator was specified by means of experimental results. The expense of specifying the radiator thermal output at a reference experimental facility is so high-priced. Therefore, this numerical study was performed to asses that numerical method could be or not be an alternative for experimental method.

The aim of the study was to specify thermal outputs by means of forced convection model and then to create convector designs for enhancing thermal output. Thermal outputs of new convector designs were also aimed to be investigated by means of natural convection and radiation. Three-dimensional model of radiator was used for numerical study. Convergency problems were occurred at natural convection analysis due to existence of both turbulence and laminar boundary layers at the shell-side of the radiator. Laminar boundary layer was formed at rear face and the gap between panels at the same time turbulence boundary layer was formed at the front face of radiator. Therefore, computations were only performed by means of forced convection model.

The thermal output of the panel radiator for 75°C inlet and 65°C outlet conditions was computed with 2% discrepancy according to the test results. The discrepancy at the thermal output may lead to make accurate assumption about the thermal output of a radiator before radiator is sent to a reference experimental facility. In order to obtain 65°C outlet water temperature for 75°C inlet water temperature, thermal output of the radiator was investigated depending on the variation of ambient convective heat transfer coefficient. 65°C outlet water temperature was obtained for the ambient convective heat transfer coefficient of 6 W/m^2K.

In addition to 50°C excess temperature, thermal output was also investigated for 60°C and 30°C excess temperatures that were used to specify the characteristic equation of the radiator. The discrepancy for 60°C excess temperature is 7% and for 30°C excess temperature is 13%. For 60°C excess temperature, water left the radiator at a higher temperature than specified outlet temperature though experiments. On the other hand, water left the radiator at a lower temperature than specified outlet temperature for 30°C excess temperature though experiments. The reason for these is the implementation of fix ambient convective coefficient against the variation of excess temperature. Small modifications at the ambient convective heat transfer coefficients depending on the increase or decrease at the excess temperature according to 70°C excess temperature may lead to obtain more accurate thermal outputs.

Modifications at convector design were performed to enhance the thermal output of the radiator. Five convector designs were created in order to investigate their thermal output according to the original design. Thermal outputs of modules were computed with the implementation of fix surface temperature to the inner surface of panel. Among these convectors, maximum increase at heat transfer area could be obtained by the usage of cascade convector design. The increase at the thermal output of module with the usage of cascade convector was 11% in the event of 30% increase at heat transfer surface area of convector. The effect of pops at the convector surface was also investigated. By means of pops, the increase at thermal output is 8% in the event of 15% increase at the heat transfer surface area. According to the increase at the thermal output of cascade design, pops leads to obtain better thermal output since the amount of increase at the heat transfer surface area with the usage of pops was much more at the fin base than cascade design.

Thermal outputs of new designs were also computed for the water flow existed inside the modules in addition to fix surface temperature at the inner surface of panel. Constraints were occurred during the implementation of created convector designs to this analysis due to the usage of more complex model than fix temperature model. Only, original convector design and cascade convector design could be implemented

to this analysis. Three additional convectors were created. One of them differed from other convectors with the usage of three contact faces rather than two contact faces between panel and convector. Other convector designs were created as the modified version of a convector design used in previous analysis. According to 9% increase at the thermal output of the cascade convector design, 35% increase at thermal output of convector with three contact faces was occurred in the event of 75% increase at its heat transfer surface area.

During the production of convector with three contact faces, tears usually occur at the edges of the convectors at the pressing process due to the usage of very thin steel sheets. This may make no sense for the company that has its own foundry. But this is a problem for the other companies that make researches to enhance thermal output of their radiators. Therefore, cascade convector design may be a reliable alternative convector design for these companies. The implementations of both designs require new moldings to form convectors. An extra welding process must be added to the production line of cascade system to combine convector parts each other.

Obtained data as a result of the numerical study was supported by the experimental results. Nevertheless, the variable expense of an experiment is proportional to the number of conditions going to be investigated and number of configurations going to be tested. Though numerical study, extremely large volumes of results can be virtually produced with no added expense. In order to reduce lead times and cost of new designs, numerical study is a reliable alternative to the experimental study.

REFERENCES

Arslanturk C. (2006). Optimum design of space radiators with temperature dependent thermal conductivity. *Applied Thermal Engineering, 26* (11-12), 1149-1157.

Arslanturk C. & Ozguc, A. F. (2006). Optimization of a central-heating radiator. *Applied Energy, 83*, 1190–1197.

Beck, S. B. M., Blakey, S. G. & Chung M. C. (2001). The effect of wall emissivity on radiator heat output. *Building Services Engineering Research & Technology, 12* (3), 185–194.

Beck, S. M. B., Grinsted S. C., Blakey S. G. & Worden K. (2004). A novel design for panel radiators. *Applied Thermal Engineering, 24*, 1291-1300.

Chen, Q. (1990). Comfort and energy consumptions analysis in buildings with radiant panels. *Energy and Buildings, 14* (4), 287-297.

Fluent version 6.3 user's guide. Fluent Incorporated, 2006.

Gregory, P. D. (1986). Aluminuim radiators. *Technical Note TN-BSRIA (Building Services Research and Information Association)*, 17p.

Grétarsson, S. P., Valdimarsson, P. & Jónsson V. K. (1991). Heat transfer modeling of a plate radiator for district heating applications. *International Journal of Energy Research, 15*, 301-315.

Harlow, F. H. & Welch, J. E. (1965). Numerical calculation of time-dependent viscous incompressible flow of fluid with three surface. *Phys. Fluids, 8*, 2182-2189.

Huang, P. G., Launder, B. E. & Leschziner, M. A. (1985). Discretization of non-linear convection process: a broad-range comparison of four schemes. . *Comput. Methods Appl. Mech. Eng., 48*, 1-24.

Hayase, T., Humphery, J. A. C. & Greif R. (1992). A consistently formulated QUICK scheme for fast and stable convergence using finite-volume iterative calculation procedures. *J. Comput. Phys., 98*, 108-118.

Harris, D. J. (1995). Use of metallic foils as radiation barriers to reduce heat losses from buildings. *Applied Energy, 52* (4), 331-339.

Issa, R. I. (1986). Solution of implicity discretised fluid flow equations by operator-splitting. J. *Comput. Phys., 62*, 40-65.

Incropera, F. P. & DeWitt D. P. (1996). *Fundamentals of heat and mass transfer* (4th ed.). USA: John Wiley & Sons.

Inard, C., Meslem, A. & Depecker P. (1998). Energy consumption and thermal comfort in dwelling-cells: a zonal-modal approach. *Building and Environment, 33* (5), 279-291.

Leonard, B. P. (1979). A stable and accurate convective modelling procedure based on quadratic upstream interpolation. *Comput. Methods Appl. Mech. Eng., 19*, 59-98.

Leschziner, M. A. (1980). Practical evaluation of three finite difference schemes for the computation of steady-state recirculating flows. *Comput. Methods Appl. Mech. Eng., 23*, 293-312.

Lu, W., Howart A. T. & Jeary A. P. (1997). Prediction of airflow and temperature field in a room with convective heat source. *Building and Environment, 32* (6), 541-550.

Oliet, C., Oliva, A., Castro, J. & Pérez-Segarra, C. D. (2007). Parametric studies on automotive radiators. *Applied Thermal Engineering, 27*, 2033–2043.

Patankar, S. V. & Spalding, D. B. (1972). A calculation Procedure for heat, mass and momentum transfer in three dimensional parabolic flows. *Int. J. Heat Mass Transfer, 15*, 1787.

Spalding, D. B. (1972). A novel finite-difference formulation for differential expressions involving both first and second derivates. *Int. J. Numer. Methods Eng., 4*, 551.

Patankar, S.V. (1980). *Numerical heat transfer and fluid flow*. New York: Hemisphere Publishing Corporation, Taylor & Francis Group.

Probert, S. D., Chester, P. H. & Hobday, R. A. (1989). Optimisation of "radiator" shelf design in order to achieve energy thrift. *Applied Energy, 32* (1), 71-82.

Radiator standard BSEN442. (n.d.). Retrieved June 20, 2006, from *http://www.plumbingpages.com/featurepages/BSEN442.cfm*

Scarborough, J. B. (1958). *Numerical mathematical analysis* (4th ed.). Baltimore: John Hopkins University Press.

Van Doormal, J. P. & Raithby, G. D. (1984). Enhancements of the SIMPLE method for predicting incompressible fluid flows. Numer. *Heat Transfer, 7*, 147-163.

Versteeg, H. K. & Malalasekera W. (1995). *An Introduction to computational fluid dynamics: the finite volume method*, London: Prentice Hall.

Ward, I. C. (1991). Domestic radiators: performance at lower mass flow rates and lower temperature differentials than those specified in standard performance tests. *Building Services Engineering Research & Technology, 12* (3), 87-94.

Wendt, J. F. (Ed.). (1995). *Computational fluid dynamics: an introduction* (2nd ed.). Germany: Springer.

Wallentén, P. (2001). Convective heat transfer coefficients in a full-scale room with and without furniture. *Building and Environment, 36*, 743-751.

Witry, A., Al-Hajeri M. H. & Bondok, Ali A. (2005). Thermal performance of automotive aluminium plate radiator. *Applied Thermal Engineering, 25*, 1207–1218.

Zhai, Z. & Chen Q. (2004). Numerical determination and treatment of convective heat transfer coefficient in the coupled building energy and CFD simulation. *Building and Environment, 39*, 1001-1009.

Zhai, Z. J. & Chen Q. Y. (2005). Performance of coupled building energy and CFD simulations. *Energy and Buildings, 37*, 333–344.